Mutational analysis of ribosomal DNA and maturation-scheme analysis of ribosomal RNA in *A. thaliana*

Dissertation

zur Erlangung des Doktorgrades

der Naturwissenschaften

vorgelegt beim

Fachbereich Biowissenschaften der

Goethe-Universität Frankfurt am Main

von

Thiruvenkadam Shanmugam

aus Thanjavur, Indien

Frankfurt am Main 2022

(D30)

vom Fachbereich Biowissenschaften der Goethe Universität als Dissertation angenommen.

Dekan: Prof. Dr. Sven Klimpel

Erster Gutachter: Prof. Dr. Enrico Schleiff

Zweiter Gutachter: Prof. Dr. Michaela Müller-McNicoll

Datum der Disputation: .....

Dedicated to my late brother, Karthi Shanmugam.

ABSTRACT

Ribosome biogenesis is a fundamental cellular process beginning with long precursor rRNA transcription from multi-copies of repetitive 45S ribosomal DNAs. At the subunit level, the primary pre-rRNA transcript encapsuled in 90S protein-RNA complex undergoes decisive splitting in two chief ways for further maturation into large (LSU) and small (SSU) ribosomal subunit. The usage of specific rDNA copies from defined chromosomes and their selective role during growth and development have been a topic of interest owing to its contribution to specialized ribosome theory which proposes non-monolithic functions for ribosomes and thereby their mRNA translation potential. Dual-guide CRISPR/Cas9 mediated disruption of rDNA regions resulted in stable disruption of up to 2.5% and 5% of all rDNA copies in hetero- and homozygous (*ploop KD*) conditions, respectively. At the RNA level, the mutation excised a critical structural element, P-loop on the LSU 25S rRNA. Mutation caused a dosage dependent defect with homozygosity leading to severe developmental defects through vegetative and reproductive growth phases which is manifested in their proteome by means of disregulation through both increase and decrease of several gene ontological categories of proteins in mutants. Interestingly, the mutation on chromosome 4 triggered dosage compensation through rRNA expression from chromosome 2 further compounded by ectopic rRNA biogenesis defects. The mutated copies however are not incorporated in the translating ribosomes and as a direct or indirect consequence led to elevated basal autophagic levels in the mutants.

The primary 35S transcript is known to undergo two modes of initial cleavages at the pre-rRNA level that aid in their subsequent maturation. Root cell culture (RCC) studies shows that these cells contain a novel ITS2-first cleaved precursor even under control growth conditions, P-C_2 adding a third maturation means for the 35S pre-rRNA. This maturation path is further known to be triggered under elevated growth temperature forming a novel adaptive response in Arabidopsis and two other crop plants, tomato, and rice. Taken together, the pulse-chase labeling analysis of control and stressed tissues uncovers the fine-tuned pre-rRNA schematics with crossovers between multiple maturation paths.

Table of Contents

ABSTRACT ..... **I**

INDEX OF FIGURES ..... **V**

INDEX OF TABLES ..... **VI**

ABBREVIATIONS ..... **VII**

ZUSAMMENFASSUNG ..... **X**

INTRODUCTION **1**

1.1 Ribosome Biogenesis 1
1.1.1 Nucleolus and rDNA Organization 3
1.1.2. Pre-rRNA synthesis 5
1.1.3 Emerging concepts of ribosomal heterogeneity 6
1.2 CRISPR and its application in plants 8
1.3 Pre-rRNA processing in Eukaryotes 10
1.4 Factors controlling ribosome biogenesis 12

2 OBJECTIVES **14**

3 MATERIAL **15**

3.1 Oligonucleotides 15
3.2 Chemicals and Enzymes 16
3.3 Media 17
3.4 Bacterial Strains 17
3.5 Plasmids 17
3.6 Plants - Wildtype, mutants and stable transgenics 18
3.7 Antibodies 18

4 METHODS **19**

4.1 Molecular biological methods 19
4.1.1 Golden gate cloning 19
4.1.2 Purification of DNA 19
4.1.3 Heteroduplex PCR 20
4.1.4 High resolution DNA gel electrophoresis 20
4.1.5 RNA-sequencing and SNP analysis 20
4.1.6 Proteomic analysis 21
4.1.7 Metabolic pulse chase labeling of RNA 21

4.1.8 Reverse Transcription of RNA 22
4.1.9 Circular Reverse Transcription PCR 22
4.1.10 RNA Gel electrophoresis 22
4.1.11 Gel Drying 23
4.1.12 Northern Blotting and Hybridization 23
4.1.13 Ribosomal subunit profiling 24
4.1.14 SDS-PAGE, Western blotting, and Hybridization 24
4.1.15 Quantification 25

4.2 Plant Methods 26

4.2.1 Growth and maintenance of root cell culture (RCC) 26
4.2.2 Growth and maintenance of plants 26
4.2.3 Stress treatments of plants 27
4.2.4 Arabidopsis floral transformation 27
4.2.5 Plant crossing 27
4.2.6 Fractionation of root cell culture (RCC) 28
4.2.7 RNA Purification 28
4.2.8 Confocal Laser Scanning Microscopy 28

5 RESULTS 29

5.1 Cas9 editing of rDNA and its effect in plant development 29

5.1.1 Cas9 targeted the P-loop region of 25S rDNA 29
5.1.2 Mutation led to 5% alteration of all rDNA copies 30
5.1.3 Mutation caused dosage dependent phenotypic effects 32
5.1.4 Severe mutation class exhibited global proteome defects 33
5.1.5 Mutated copies are linked to NOR regions of Chr 4 36
5.1.6 NOR4 mutation led to compensation from NOR2 copies 38
5.1.7 Mutants displayed pre-rRNA maturation defects 40
5.1.8 Mutated copies are not incorporated in polysomes 41
5.1.9 Autophagic flux is elevated in the severe mutant class 43
5.1.10 Small RNAs associated with P-loop region are unaffected 45

5.2 Redefining of pre-rRNA maturation schematics in plants 47

5.2.1 RCC contains ITS2-derived precursor in control conditions 47
5.2.2 Viable RRP5 mutant display ITS2-derived pre-RNA defects 49

5.3 Dynamics and thermal susceptibility of rRNA maturation in plants 52

5.3.1 Pulse labeling reveals rate limiting steps in rRNA production 52
5.3.2 High growth temperature alters pre-rRNA levels 54
5.3.3 Heat-induced maturation schemes are conserved in tomato and rice 58
5.3.4 High growth temperature induced response in quick and reversible 60
5.3.5 High growth temperature alters the pre-rRNA intermediate composition 63
5.3.6 Acute heat stress affects the assembly and overall precursor levels 65
5.3.7 Heat Stress affects pre-rRNA maturation in *hot* mutants 68

6 DISCUSSION 70

6.1 Cas9 editing of ribosomal DNA copies 70

6.1.1 A case for selective role of ribosomal DNA copies 70
6.1.2 Growth manifestation due to mutation 71
6.1.3 Ectopic rRNA expression and dosage compensation 72
6.1.4 Overarching consequence of ribosomal DNA mutations 73

6.2 Revised schematics of Arabidopsis pre-rRNA splitting 75

6.3 The dynamics of maturation schemes 76

6.3.1 RNA maturation schemes are sensitive to heat 78
6.3.2 Novel precursor formation under heat 79
6.3.3 A path for the ITS2-first maturation schemes under heat 79
6.3.4 Fine tuning the maturation schemes based on temperature 80

7 REFERENCES 83

8. APPENDIX 93

ACKNOWLEDGEMENTS ..... Error! Bookmark not defined.

PUBLICATIONS i

CURRICULUM VITAE ..... Error! Bookmark not defined.

ERKLÄRUNG ii

EIDESSTATTLICHE VERSICHERUNG ii

INDEX OF FIGURES

Figure 1. Snapshot of ribosome biogenesis in Eukaryotes
Figure 2. Ribosomal DNA organization in model plant, *A. thaliana*.
Figure 3. Factors contributing to ribosomal heterogeneity
Figure 4. Mechanism of CRISPR-Cas9 editing
Figure 5. Precursor rRNA cleavage conservation in 3 model species
Figure 6. CRISPR-Cas9 mutagenesis of 25S rDNA copies and screening
Figure 7. Analysis of proportion of mutated copies
Figure 8. Phenotypical aberrations of resulting 25S rRNA mutation
Figure 9. Global proteomic changes in the mutant
Figure 10. Mapping of mutational locus and its phenotypic correlation
Figure 11. Ribosomal RNA dosage compensation and its related defects
Figure 12. Analysis of pre-rRNA maturation defects in *ploop KD* mutants
Figure 13. Analysis of mutational copies distribution in ribosomal complexes
Figure 14. Status of autophagic flux in *ploop KD* mutants
Figure 15. Trans and cis-derived snoRNAs on the P-loop region
Figure 16. Identification and fine mapping of ITS2-first cleavage precursors
Figure 17. Characterization of a factor controlling ITS2-first maturation path
Figure 18. Pulse-labeling analysis of pre-rRNA synthesis in RCC and seedlings
Figure 19. Role of growth temperatures in Arabidopsis pre-rRNA maturation
Figure 20. Identities of heat-induced pre-rRNA precursors
Figure 21. Pattern conservation of HS induced effects in Tomato and Rice
Figure 22. The alteration of maturation scheme is quick and reversible
Figure 23. Pulse-chase pre-rRNA analysis under increased growth temperature
Figure 24. Characterization of novel heat-induced precursor in RCC
Figure 25. Polysomal reduction and subunit pre-rRNA distribution under HS
Figure 26. Pre-rRNA perturbations in heat sensitive mutants
Figure 27. Proposed model of defects in *ploop KD* mutants
Figure 28. Pre-rRNA maturation dynamics in root cell culture and seedlings
Figure 29. Pre-rRNA maturation paths controlled by temperature

INDEX OF TABLES

Table 1. Cloning, Screening, RT-PCR analyses of CRISPR-Cas9 mutants

Table 2. Northern Hybridization

Table 3. Circular RT-PCR and ABI sequencing

Table 4. Plasmids used and constructed in this dissertation

Table 5. Arabidopsis mutant and transgenic lines used in this dissertation

Table 6. List of antibodies used in this dissertation

Table 7. List of proteins distinctly present in BG seedlings

Table 8. Rate constants of control and heat stressed pre-rRNA synthesis

Table 9. IC_{50} and EC_{50} values of pre-rRNAs during high growth temperature

ABBREVIATIONS

Non-standard abbreviations

A. thaliana, At	Arabidopsis thaliana	EtBr	ethidium bromide
aa	amino acid	ETS	external transcribed spacer
ARPF2	Arabidopsis ribosome production factor 2	FC	fibrillarin center
ATG8e	autophagy related 8e protein	GC	granular center
ATP	adenosine triphosphate	GFP	green fluorescent protein
BG	background	GO	gene ontology
Bis-Tris	bis-(2-hydroxy-ethyl)-amino-tris(hydroxymethyl)-methane	gRNA	guide RNA
bp	base pair	HCl	hydrogen chloride
BRIX	biogenesis of ribosomes in Xenopus homolog 1	HDR	homology directed repair
Cas	caspase	HMW	high molecular weight
cDNA	complimentary DNA	HS	heat stress
CEVd	citrus excortis viroid	HSP	heat shock protein
Chr	chromosome	IC	induction
CID	collision-induced dissociation	IGS	intergenic spacer
Col-0	Columbia-0	IPTG	isopropyl b-D-1-thiogalactopyranoside
CRISPR	clustered regularly interspaced short palindromic repeats	IRP	involved in rRNA processing
crRNA	CRISPR RNAs	ITS	internal transcribed spacer
cRT	circular RT	KD	knock down
Cy	cytoplasmic	KH_2PO_4	potassium dihydrogen phosphate
DAS	days after stratification	K_p	processing rate constant
ddH20	double distilled water	K_s	synthesis rate constant
DFC	dense fibrillar center	LB	lysogeny broth
Dig-Lig	Digestion Ligation	LEA	late embryogenesis abundant
DMSO	dimethyl sulfoxide	LMW	low molecular weight
DNA	deoxyribonucleic acid	LSU	large ribosomal subunit
dNTP	deoxyribonucleotide	max	maximal
DTT	dithiothreitol	MB	molecular biological
E. coli	*Escherichia coli*	Me	methylation
EC	inhibition	MgCl2	magnesium chloride
EDTA	ethylene diamine tetra acetic acid	min	minimal
EF1Bβ	elongation factor 1B-beta	MLS	malate synthase
Enp1	essential nuclear protein 1	MS	Mass Spectrometry
Eq	equation	MS	Murashige-Skoog

Mtr4	defective in mRNA transport 4
m/z	mass to charge ratio
NaCl	sodium chloride
NAD	nucleolar associated domains
NaOH	sodium hydroxide
Na_2HPO_4	disodium hydrogen phosphate
NASC	Nottingham Arabidopsis Stock Center
NC	non-treated control
nESI	nano-electrospray ionization
No	nucleolar
Nob1	nin one binding protein 1
Nop10	nucleolar protein 10
NOR	nucleolar organizing region
NP-40	nonidet P-40
NSAF	normalized spectral abundance factor
nt	nucleotide
Nu	nucleoplasmic
N-term	amino terminal
OD	optical density
OD254	optical density measured at wavelength of 254 nm
O/N	overnight
Os	*Oryza sativa*
P	phosphorylation
PAGE	polyacrylamide gel electrophoresis
PAM	protospacer adjacent motif
PARP	poly (ADP)-ribose polymerase
PCR	polymerase chain reaction
PIPES	piperazine-N,N'-bis(ethanesulfonic acid)
PMSF	phenylmethanesulfonylfluoride-fluoride
PNK	polynucleotide kinase
Pol	Polymerase
PO_4	phosphate
pre-rRNA	precursor rRNA
prmt3	protein arginine methyltransferase 3
PSRP6	plastid-specific ribosomal protein 6 precursor
PTC	peptidyl transferase center
PVDF	polyvinylidene difluoride
RBF	ribosome biogenesis factor
RNP	ribonucleoprotein
RNA	ribonucleic acid
RNAP	RNA polymerase (bacterial)
RNase	ribonuclease
RP	ribosomal protein
RPL	ribosomal protein L
RPS	ribosomal protein S
rRNA	ribosomal RNA
Rrp5	ribosomal RNA processing 5
RT	reverse transcription
RT-PCR	reverse transcription PCR
S	svedberg unit
SAM	S-adenosylmethionine
SDS	sodium dodecyl sulphate
sgRNA	single guide RNA
Sl	*Solanum lycopersicum*
SNP	single nucleotide polymorphism
snoRNA	small nucleolar RNA
snoRNP	small nucleolar ribonucleoproteins
SOD	superoxide dismutase
Sp	*Streptomyces pyogenes*
SSC	saline-sodium citrate
SSU	small ribosomal subunit
T	transgeneration
TAIR	The Arabidopsis Information Resource
Taq	*Thermus aquaticus*
TBE	Tris Borate EDTA
TIF-IA	Transcription initiation factor I
TOR	target of rapamycin
tracrRNA	transactivating crRNA
tRNA	transfer RNA
T7	bacteriophage T7

UBF	upstream binding factor	X-Gal	5-bromo-4-chloro-3-indolyl-β-D-galactopyranoside
UV	ultraviolet	*xrn*	exoribonuclease
VAR	variant	^{32}P	Phosphorus-32
VRC	ribonucleoside-vanadyl-complex	[γ-^{32}P]	gamma phosphate group with ^{32}P
WT	wildtype	∑I	Summation of Intensity

Standard abbreviations

µCi	microcurrie	min	minute
µg	microgram	mL	milliliter
µL	microliter	mm	millimetre
µM	micromolar	mM	millimolar
°C	degree Celsius	ng	nanogram
d	day old	nL	nano litre
g	relative centrifugal force	nm	nanometre
h	hour	pH	potential of hydrogen
kDa	kilo Dalton	pmol	picomolar
knt	kilo nucleotide	rpm	revolution per minute
m^2	square metre	sec	second
M	molar	V	voltage
mA	milliampere	v/v	volume per volume
MDa	mega dalton	w/v	weight per volume
mg	milligram		

ZUSAMMENFASSUNG

Die Ribosomenbiogenese ist ein mehrstufiger und multikompartimenteller Reifungsprozess, der sich über drei wichtige Organellen erstreckt. Er beginnt im Nukleolus und setzt sich im Nukleoplasma und im Zytoplasma fort. Für diesen Prozess sind die Aktivitäten aller drei großen RNA-Polymerasen erforderlich. So ist beispielsweise die Aktivität von RNA pol II für die Transkription von Hunderten von mRNAs erforderlich, die für die Bestandteile der ribosomalen Proteine (RP) und mehrere andere Proteine kodieren, die am Ribosombiogeneseprozess beteiligt sind und als ribosomale Biogenesefaktoren (RBFs) bezeichnet werden. Da die Ribosomenproduktion die gesamte Transkriptionsleistung dominiert und je nach Wachstumsstadium bis zu 80 % der gesamten Transkription einer bestimmten Zelle ausmacht, werden die genomischen DNA-Regionen (ribosomale DNA, rDNA), die für ribosomale RNAs kodieren, in der Regel durch mehrere Kopien repetitiver Regionen kodiert, die im Fall der Modellpflanze Arabidopsis Hunderte von Kopien umfassen. Je nach Organismus sind diese Kopien in der Regel tandemförmig auf einem oder mehreren Chromosomen angeordnet. Der Prozess der Biogenese selbst beginnt mit der Transkription dieser rDNA-Kopien durch eine spezielle Polymerase, RNA Pol I, in den nukleolär organisierenden Regionen (NORs). In Arabidopsis sind die rDNA-Kopien in den NOR-Regionen der Chromosomen 2 und 4 verteilt, die als NOR2 und NOR4 bezeichnet werden. Während diese rDNA-Kopien im Prinzip als analog zueinander bezeichnet werden, gibt es innerhalb der rDNA-Kopien selbst Polymorphismen in Bezug auf die Länge der 3'-Transkriptionsbereiche (3'-ETS), durch die sie in die Untervarianten 1-4 (Var1-Var4) eingeteilt werden. Diese NORs können in Abhängigkeit des Entwicklungsstadiums einzigartige Chromatin-Konfigurationen aufweisen, die durch Chromatin-Aktivierungs- oder Silencing-Markierungen auf Histonen und DNA-Sequenzen vermittelt werden. Dies führt zu einer variablen Transkription von rDNA-Kopien mit für Entwicklungsstadien spezifischen Variantenprofilen.

Nach der Transkription der rDNA-Kopien enthält der transkribierte Vorläufer der ribosomalen RNA (rRNA) unreife Regionen zwischen reifen rRNA-Arten, und bildet den so genannten 90S-Komplex. In Arabidopsis werden die reifen rRNA-Regionen, 18S, 5.8S und 25S, auf beiden Seiten von *external transcribed sequences* (5'-ETS und 3'-ETS) flankiert, während sie intern durch *internal transcribed sequences* (ITS1

und ITS2) getrennt sind. Die Reifung dieses 90S-Komplexes, der die primäre 35S-Transkript-prä-rRNA enthält, wurde hauptsächlich durch erste Spaltungsschritte entweder an ITS1 oder 5'-ETS beschrieben. Abhängig von der Menge der resultierenden Transkripte im ausgewogenen Gleichgewicht (*steady-state*) wurden diese Wege als *Major-Pathway* ("*major ITS1-first*") und *Minor-Pathway* ("*minor 5'-ETS-first*") charakterisiert, wobei der *Major-Pathway* zu P-A3 und der *Minor-Pathway* zu 32S-Transkripten führt. Die resultierenden Transkripte dienen als diagnostische Vorläufer für die entsprechenden Reifungswege. Diese deterministischen Stellen sind das Resultat der endonukleolytischen Spaltung und des exonukleolytischen Trimmens konservierter Stellen der unreifen prä-rRNA-Regionen.

Verteilung der rDNA-Kopien und ihre spezifische Rolle bei der Pflanzenentwicklung

In Arabidopsis gibt es Hunderte von rDNA-Kopien in NOR2 und NOR4. Die selektive funktionelle Rolle der beiden chromosomalen Kopien ist noch nicht vollständig geklärt, da die auf den zwei Chromosomen verteilten Varianten unterschiedliche Expressionsmuster während der Pflanzenentwicklung aufweisen. Darüber hinaus führt die genomweite Unterbrechung von rDNA-Kopien durch potente CRISPR/Cas9-Enzyme zu einer verminderten Überlebensfähigkeit der Transformanten, während die keimbahnspezifische Expression von Cas9, die zu einer Reduktion von bis zu 80 % der rDNA-Kopien führt, keine Auswirkungen auf das Pflanzenwachstum und die Entwicklung hat. In dieser Studie wird hingegen das konstitutiv exprimierte, im Vergleich weniger potente SpCas9 verwendet, das mit Hilfe eines Dual-Guides 25 bp der 3'-Seite der 25S rDNA-Regionen ausschneidet. Auf RNA-Ebene enthielt die herausgeschnittene Region die *P-loop*- und die Helix-82-Regionen der 25S rRNA. Die Mutation führte zu einer stabilen Vererbung des Exzisionsmusters in etwa 2.5 % bis 5 % aller rDNA-Kopien, in Abhängigkeit des heterozygoten bzw. homozygoten Zustands der diploiden Arabidopsis-Pflanzen, wobei eine große Anzahl von Kopien intakt blieb. Die daraus resultierenden Mutationen zeigten mosaikartige Mutationsereignisse von Exzisionen, die aus dem Doppelstrangbruch (DSB) an den beiden PAM-Stellen hervorgehen, indem die Enden des DSB direkt ligiert wurden, wobei der klassische Reparaturmechanismus der Nicht-homologen Endverbindung zum Einsatz kam. Auffallend ist, dass die PCR-basierte Indizierung der chromosomalen Positionen der Mutationen zeigte, dass die Mutationen mit dem genetischen Locus NOR4 auf Chromosom 4 korreliert sind, wobei Genotyp und Phänotyp als einzelner Locus segregieren, wobei das mendelsche Segregationsverhältnis von 1:2:1 in

rückgekreuzten Nachkommen eingehalten wird, was ein Beweis für die Cas9-Aktivität in Chromosom 4, aber nicht in Chromosom 2 ist.

Noch wichtiger ist, dass die Mutationen mit geringer Kopienzahl ausreichten, um die Fitness des Pflanzenwachstums und der Pflanzenentwicklung zu beeinträchtigen, wobei die Dosis der Mutation eine Rolle für die Schwere der daraus resultierenden Phänotypen spielte. Sowohl heterozygote als auch homozygote Keimlinge bildeten keine Seitenwurzeln aus. Während die Größe der Primärwurzel bei heterozygoten Keimlingen mit der des Wildtyps vergleichbar war, wiesen die homozygoten Keimlinge eine stark reduzierte Größe auf. Spätere Wachstumsstadien waren dadurch gekennzeichnet, dass die heterozygoten Mutantenpflanzen die Rosettengröße des Wildtyps erreichten, während die homozygoten sich nicht erholten und in ihrer reproduktiven Fitness stark beeinträchtigt waren. Noch wichtiger ist, dass die Phänotypen der Mutanten jenen bereits bekannter Mutanten ähnlich waren, in denen ribosomale Proteine und ribosomale Biogenesefaktoren fehlten, und zwar in Bezug auf die erhöhte Verzahnungsrate des Rosettenblatts, was auf Gemeinsamkeiten bei defekten Ribosomenfunktionen hinweist. Die Proteomanalyse der stark verkümmerten homozygoten Keimlinge wies auf großflächige Veränderungen des Proteoms in mehreren genontologischen Kategorien hin, darunter Photosynthese, Proteinsynthese und -Assemblierung, DNA-Synthese und RNA-Verarbeitung, die in den Mutanten deutlich verringert waren. Insgesamt fehlten von 3050 allgemein identifizierten Proteinen etwa 53 Proteine in den Mutanten und mindestens fünf Proteine wurden in den Mutanten, nicht aber im Wildtyp, identifiziert. Interessanterweise wurde festgestellt, dass AtPARP2, ein negativer Regulator des Seitenwurzelwachstums, in den Mutanten im Vergleich zum Wildtyp ektopisch vorhanden ist, was eine direkte phänotypische Korrelation zwischen dem fehlenden Seitenwurzelwachstum in den Mutanten und dem veränderten Proteom herstellt.

Ein weiterer deutlicher Effekt der Mutation ist der resultierende Dosisausgleichsmechanismus, der durch die Mutation der von NOR4 kodierten Kopien ausgelöst wird. Die Expressionsmuster von Var1-4 deuten darauf hin, dass Var1, das zu NOR2 auf Chromosom 2 gehört, in den Mutanten dereprimiert ist, was zu erhöhten Expressionsniveaus führt, die auch in späteren Wachstumsstadien fortbestehen. Außerdem ist die zeitliche Verarbeitung von prä-rRNAs in der homozygoten Mutante stark beeinträchtigt. Insbesondere die für den *Minor-Pathway* charakteristische Vorstufe, 32S, scheint in der Mutante auf ein verdoppeltes

Expressionsniveau zu akkumulieren, was auf Nebenwirkungen der ektopischen Var1-Expression oder auf eine Beeinträchtigung der Funktion der pathwayspezifischen Ribosomen-Biogenese-Faktoren hindeutet. Diese Effekte spiegeln sich auch in den allgemeinen Eigenschaften der exprimierten prä-rRNAs wider, die auf Basis ihrer Einzelnukleotid-Polymorphismen (SNP) analysiert wurden. Im Vergleich zum Wildtyp wiesen mehrere Nukleotide der prä-rRNAs in der Mutante eine unverhältnismäßig hohe Häufigkeit von Polymorphismen im Vergleich zur Referenz-rDNA-Sequenz auf. Dies stellt zusätzliche Konsequenzen für effiziente ribosomale Translation dar, da SNPs die Hauptquelle für die ribosomale Heterogenität in Eukaryoten sind. Es ist erwähnenswert, dass die Mutation keine Auswirkungen auf das Niveau der *cis*- und *trans*-wirkenden snoRNAs in der mutierten Region hatte, was darauf hindeutet, dass der Phänotyp eher durch eine defekte ribosomale Funktion verursacht wurde.

Die zelluläre Fraktionierung auf der Grundlage von Sedimentations-koeffizienten und die anschließende PCR-Analyse zeigten, dass diese mutierten Kopien von prä-rRNAs in der Mutante im Allgemeinen nur in sehr geringen Mengen exprimiert werden. Darüber hinaus sind sie in reifenden Untereinheiten aus dem freien Pool und bis hin zu 50S-, und in geringerem Maße auch in 80S-Fraktionen vorhanden, nicht jedoch in translatierenden Polysomen. Dies deutet darauf hin, dass es entweder zelluläre Qualitätskontrollmechanismen gibt, die diese defekten Kopien reparieren und aus dem translatierenden Pool eliminieren, oder dass die Exzision wichtiger struktureller rRNA Elemente die Assemblierung ribosomaler Proteine und Biogenese-faktoren mit einem 90S-Komplex, der die defekte rRNA enthält, behindert. In Übereinstimmung damit zeigten die Mutanten eine erhöhte Autophagie-Umsatzrate, die mittels ATG8e, einem Marker für die Bildung von Autophagosomen, analysiert wurde.

<u>Neudefinition der prä-rRNA-Reifungswege und ihre Rolle bei der Pflanzen-akklimatisierung</u>

Nachdem bisher zwei Arten von prä-rRNA-Verarbeitungspfaden in Pflanzen beschrieben wurden, scheinen Pflanzenwurzelzellkulturen (RCC) eine zusätzliche Art der primären Transkriptspaltung zu besitzen, welche eine "*ITS2-first cleavage*" beinhaltet. Im Gegensatz zu den reifen Enden der *Major*- und *Minor-Pathways* scheinen diese Vorläufer an der 3'-Seite heterogen zu sein, während sie eine deterministische 5'-Stelle besitzen, was zu P-C2-ähnlichen Vorläufern führt. Diese Vorläufer akkumulieren zudem unter Kontrollbedingungen in einer nicht-tödlichen

Mutante des Rrp6-Proteins, was auf die Rolle dieses bedeutenden Biogeneseproteins bei der Verarbeitung der prä-rRNA hinweist. In Hinblick auf die drei beschriebenen Reifungspfade für primäre prä-rRNA zeigen Puls-Chase-Analysen in RCC und jungen Keimlingen, dass es zwischen den Gewebetypen Variationen hinsichtlich der Verarbeitungs- und Syntheseraten gibt, sowohl von intermediären Vorläufern als auch von endgültigen reifen rRNA-Spezies. Vor allem die Synthese der 35S prä-rRNA variierte zwischen den beiden analysierten Gewebetypen, wobei RCC schnellere Raten aufwies. Während die Raten der *Major*- und *Minor*-Vorläufer in den nachfolgenden Schritten in der RCC vergleichbar waren, war die Synthese der 32S-*Minor*-RNA in Keimlingen erhöht. Die Bedeutung zusätzlicher Reifungsmodi im Verhältnis zu den bestehenden Reifungswegen wurde als Reaktion auf hohe Temperaturen untersucht. Es ist von Bedeutung, verschiedene Arten der Reaktion von Pflanzen auf hohe Temperaturen aufzuklären, da die steigenden globalen Temperaturen eine große Herausforderung für die Aufrechterhaltung der globalen Produktivität der wichtigsten Kulturpflanzen darstellen. Bei den reifen rRNA-Arten waren die Syntheseraten der 25S rRNA vergleichbar, während die 18S-rRNA-Produktion in der RCC deutlich höher war.

Die prä-rRNA-Prozesse reagierten auf Temperaturen zwischen 36°C und 42°C, bei denen die Konzentrationen der charakteristischen Vorstufen der *Major*- und *Minor-Pathways* zusätzlich zu ihren nachgeschalteten Vorstufen stark abfielen. Diese Bedingungen führten jedoch zur Akkumulation der ITS2-abhängigen P-C2-Vorläufer, vor allem zwischen 36°C und 39°C. Außerdem schwankten die primären Transkriptmengen unter diesen Bedingungen, was eher auf den Einfluss der Transkription als auf die Verarbeitung selbst hindeutet. Die hitzeinduzierten P-C2-ähnlichen Vorläufer, waren überwiegend polyadenyliert und von heterogener Natur mit mindestens vier deterministischen Stellen. Die Polyadenylierung konzentrierte sich jedoch auf zwei deterministische in ITS2, nämlich C2 und E. Es wurde festgestellt, dass dieses hitzeinduzierte ITS2-Reifungsschema in einer sowohl in einer dikotylen Modellart, der Tomate, als auch einer monokotylen Art, dem Reis, konserviert ist, was auf eine breitere Konservierung dieses Mechanismus bei Kulturpflanzen hinweist. Es wurde gezeigt, dass diese Reaktionen zeitlich korreliert sind, wobei längere Expositionszeiträume zu höheren Konzentrationen von P-C2-Vorläufern führen und die Rückkehr zur normalen Wachstumstemperatur die Verarbeitungsschemata in nur sechs Stunden wieder auf die ursprünglichen

Vorläuferniveaus zurückführt. Die zelltypspezifischen hitzeinduzierten Effekte zeigten sich in der RCC, wo die Exposition gegenüber hohen Temperaturen zur Produktion neuartiger Vorläufer führte, die kleiner waren als des charakteristischen Vorläufers des *Major-Pathways*, P-A3. Diese <P-A3-Vorläufer wurden in der RCC sowohl unter Puls-Chase- als auch unter *Steady-State*-Analysebedingungen kontinuierlich induziert, und ihre Identität entsprach der deterministischen P-Stelle von 5'-ETS am 5'-Terminus und den heterogenen Enden, die näher an der A2-Stelle von ITS1 am 3'-Terminus liegen. Die Fraktionsanalyse der Vorläuferstufen bei extremen Temperaturen von 42°C zeigt die Abnahme unreifer Vorläufer beider Reifungswege, während die allgemeine Translationskapazität unter diesen Bedingungen stark reduziert ist. Die Analyse von prä-rRNAs in Mutanten, die in ihrer Reaktion auf Hitzestress beeinträchtigt sind, gibt jedoch keinen Aufschluss über ihre erhöhte Empfindlichkeit, außer im Falle der Mutante für HSP101, bei der die P-C2-Konzentrationen leicht erhöht waren, auch nach Rückkehr zur Kontrolltemperatur.

Die Art und Weise der wachstumstemperaturabhängigen ribosomalen Reifung in Pflanzen lässt sich grob in drei Modi unterteilen. Bei einer kontrollierten Wachstumstemperatur von 22°C-36°C sind der *major* ITS1-abhängige Weg und der *minor* 5'ETS-abhängige Weg für die korrekte 40S- und 60S-Reifung am wichtigsten. Bei mäßig hohen Temperaturen von 36°C-39°C kommt es jedoch zu einer Nonsens-Aufspaltung der Untereinheiten, so dass die prä-40S-Untereinheit die 18S-5.8S enthält und die prä-60S-Untereinheit ohne eine entsprechende 5.8S-Spezies der rRNA entsteht. Während die prä-40S zu einer funktionalen 40S-Untereinheit reifen kann mit einer korrekt abgespaltenen 5.8S-Region, könnte die Funktion der prä-60S eine externe Beladung mit der 5.8S rRNA erfordern, vergleichbar mit der Beladung der 60S-Untereinheit mit der 5S rRNA. Möglicherweise sind diese Untereinheiten aber auch das Ziel von Mechanismen des *non-sense ribosome degradation*-Mechanismus (NRD). Bei erhöhten Temperaturen von 42°C werden die Verarbeitungsmodi des primären Transkripts durch *major*, *minor* und ITS2-abhängige Schemata aufgegeben. Dies resultiert aus Defekten bei der Reifung und der daraus folgenden Anhäufung von Vorläufern höherer Ordnung, $35SA^{123}B$ und 35S, die intakte 3'ETS enthalten, was auf einen Mangel an Exonukleaseaktivität bei diesen Temperaturen hinweist.

1 INTRODUCTION

Ribosomes are macromolecular machines that essentially performs genetic decoding functions for translating the intermediate RNAs to corresponding functional and structural proteins in living cells. They are ribonucleoprotein (RNP) complexes majorly composed or ribosomal proteins (RP) and ribosomal RNA (rRNA) with sizes varying from 2.3 MDa in E. coli up to 4.3 MDa in humans (Melnikov *et al.*, 2012). A functional unit of ribosomes typically consists of varying size of large and small subunit with the measurements of rRNAs and subunits named after their sedimentation coefficient, S, in svedberg units. For example, in model eukaryote yeast, the smaller subunit (40S) is comprised of 18S rRNA with 33 RPs, while large subunit (60S) is made up of three species of 5S, 5.8S and 25S rRNA in addition to 46 RPs. Structurally, the 40S subunit possess a head, body, and platform while the large crown-like subunit maintains a central protuberance, ridge and unique stalks characterized by specific RPs (Yusupova and Yusupov, 2017). Defined by the chemical nature of tRNA that binds, the subunit intersection is manifested by three functional sites, A-site (binds aminoacylated tRNA), P-site (binds peptidyl-tRNA) and E-site (binds deacylated tRNA) (Nürenberg-Goloub and Tampé, 2019). Catalytic activity of ribosome is mediated through 25S rRNA component mediated by the peptidyl transfer center (PTC) while the small subunit is critical for mRNA insertion inside the head structure thereby ensuring associated dependent translation (Nissen *et al.*, 2000).

The synthesis of ribosomes is highly coordinated in proportion to fluctuating cellular demand with cells dedicating up to 60% of all cellular ATP currency (Zhou *et al.*, 2015). These interventions are mainly mediated through signaling pathways impacting nuclear architecture (Cerqueira and Lemos, 2019). Despite their membrane less nature, nucleolus remains the primary site of onset of ribosome biogenesis. Majority of events, including precursor rRNA synthesis and initial splitting into pre-40S and pre-60S occurs in nucleolus after which maturation proceeds in nucleoplasm and cytoplasm.

1.1 Ribosome Biogenesis

The mature subunits of ribosomes are predated by relatively short-lived larger pre-ribosomal subunits before leading to maturation through multistep pathways. In eukaryotes, the ribosomal DNA is transcribed in the spatially restricted nuclear domain

called Nucleolus to form a large 90S super complex, which traverses through nucleoplasm while exiting through nuclear pore complex into cytoplasm (Nissan et al., 2002). The RNA component of 90S complex is composed of long ribosomal RNA (rRNA) transcript encompassing mature 18S, 5.8S and 25S rRNA sandwiched in between two external transcribed sequences (5'ETS, 3'ETS) and internal transcribed sequences (ITS1, ITS2). These sequences do not form part of mature ribosomes, they however must be spliced and trimmed in the pre-ribosomal subunits. To accomplish this, the 90S complex and subsequently split pre-40S (Small Subunit, SSU) and pre-60S (Large Subunit, LSU) processomes are swarmed by either common or subunit specific proteins that can bind to ribosomal RNA regions themselves or by binding to the pre-bound proteins. These proteins however are distinguished from Ribosomal Proteins (RPs) in that they do not form the part of mature ribosome itself. These group of proteins merely conduit the conversion of immature to mature ribosomes aiding in the biogenesis, hence the name Ribosome Biogenesis Factors (RBFs) (Grandi et al., 2002) and they in addition to RPs make up for the protein component of 90S complex and subsequently splitted in to pre-60S and pre-40S complexes (Woolford and Baserga, 2013; de La Cruz et al., 2015) (Figure 1). In eukaryotes, the RBFs chiefly accumulate in nucleolus and in nucleoplasm wherein they are readily available for rRNA binding and therefore nucleolus forms the first site of ribosomal RNA biogenesis (Nissan et al., 2002).

The 90S complex formation begins with the transcription of rDNA copies often simultaneously as observed by the Miller spread experiments (Miller and Beatty, 1969) by RNA Polymerase I that contains 14 subunits in addition to specific initiation factors of its own. The transcribed RNA is subjected two main classes of chemical modifications through separate complexes: 2'-O-Methylation (Kiss-László et al., 1996) on any of 4 Nucleotides and pseudouridylation of Uridines (Ganot et al., 1997). These modifications are carried out by separate complexes termed C/D snoRNPs or H/ACA snoRNPs that are guided by base-pairing of plethora of available small nucleolar RNAs (snoRNAs) for both classes termed C/D Box snoRNAs and H/ACA box snoRNAs, respectively. These modifications are known to occur in structurally relevant residues to aid either subunit RNA folding, ribosome function and specialization. In addition to these, there is also specialized U3 snoRNPs that does not result in methylation of specific rRNA residue but instead they are involved in structurally stabilizing the 5' ETS for cleavage on at least three known sites (Grandi et al., 2002).

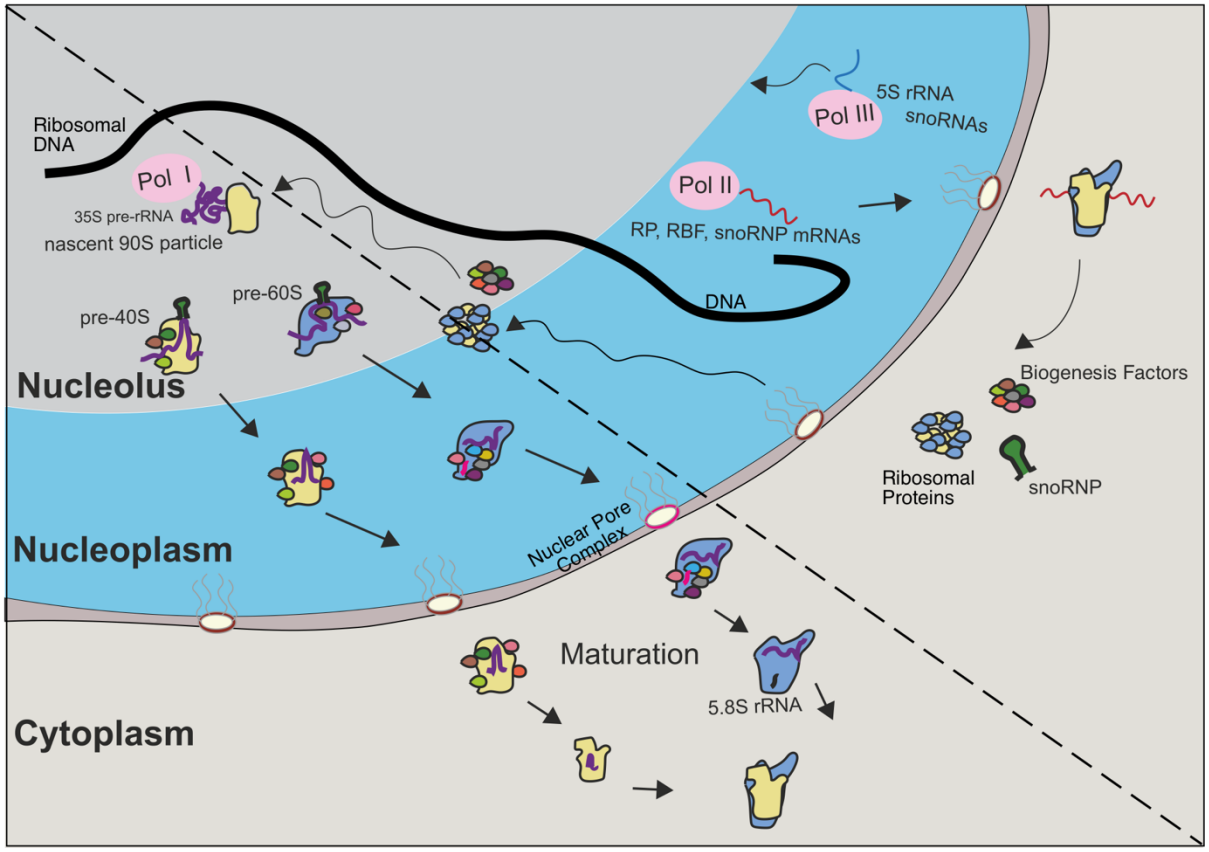

Figure 1. Snapshot of ribosome biogenesis in Eukaryotes

The whole biogenesis mechanism can be divided into two phases indicated by the diagonal dashed line. On the lower left, the schematics of 90S particle formation and it subsequent splitting through maturation steps in cell compartments. On the top right side, the involvement of RNA Pol II and III for the biogenesis mechanism in terms of its production of components are highlighted. Adapted from Greber, 2016.

1.1.1 Nucleolus and rDNA Organization

Ribosomal DNA organization is inextricably linked to the nucleolar architecture and thus has direct consequence for efficient ribosome biogenesis. rDNA copies as repetitive arrays on chromosomes forms the elemental basis for nucleolar organizing regions (NORs) (Manuelidis and Borden, 1988). These rRNA encoding transcriptional units are separated by intergenic spacer (IGS) regions possessing RNA Pol II activity and other regulatory motifs (Lindström et al., 2018). Nucleolar layers are briefly classified as larger granular center (GC) that encapsulates one or more dense fibrillar center (DFC) in which all of them further confine a dedicated fibrillarin center (FC). This membrane free arrangement is further encircled by heterochromatin thus forming a peri-nucleolar heterochromatin. More importantly, the NORs of specific

chromosomes can exhibit variable silent and active chromatin states depending on growth stages with chromatin strands of active NORs extending inside the dense fibrillarin center for transcription (Leitch et al., 1992). Multiple nucleolar proteins including RNA Pol I, fibrillarin and nucleophosmin contribute to the structural integrity of nucleolus, in addition to roughly 500 proteins constituting the nucleolar proteome (Andersen et al., 2005). In addition to earmarked NOR associations, several nucleolar associated domains (NAD) have been reported to include centromeres, 5S rDNA arrays of other chromosomes, imprinted genes, etc. (van Koningsbruggen et al., 2010).

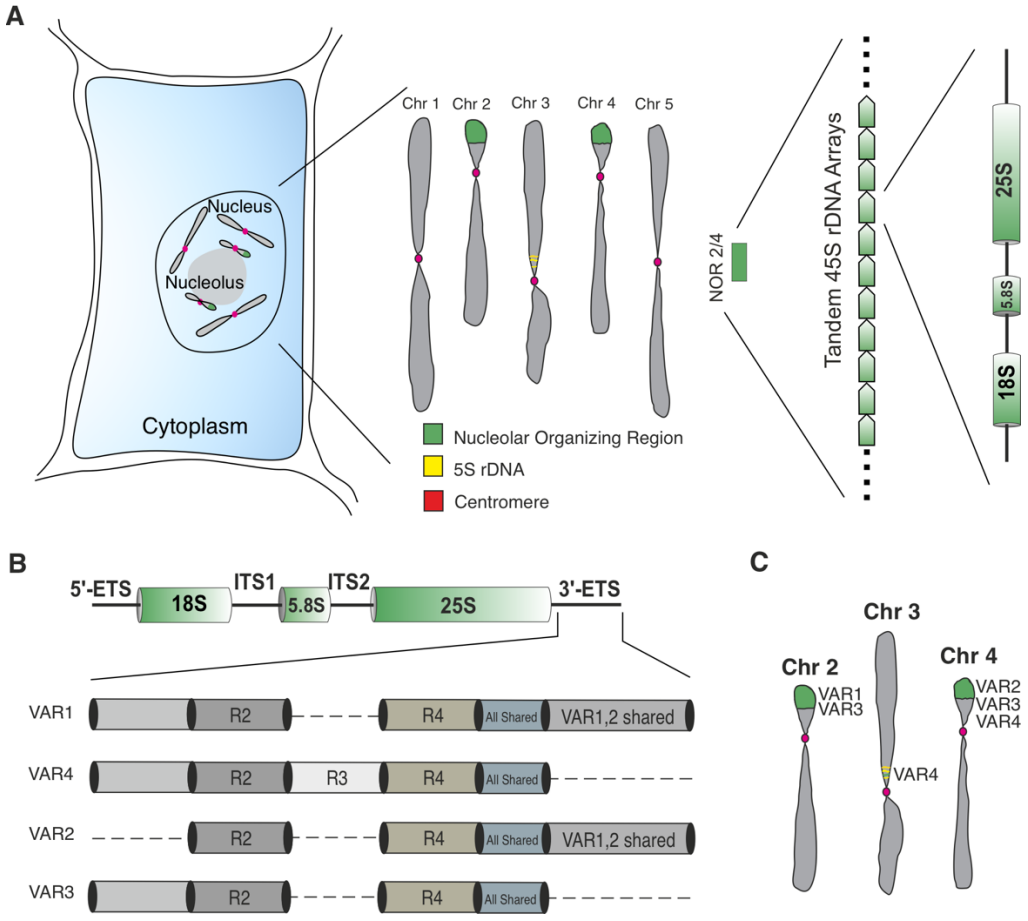

Figure 2. Ribosomal DNA organization in model plant, *A. thaliana*.

A. Arabidopsis contains five haploid chromosomes in which short arm telomeric regions are marked by their characteristic nucleolar organizing regions (NORs) of Chr 2 and Chr 4. The 5S repeats are encoded from the Chr 3 which are also found to contain few repeats of rDNAs. The NORs are tandem arrays of repetitive copies of rDNA. **B.** The 3' ETS region of rDNA copies possess polymorphism in terms of its length, and these are broadly classified into four sub types, VAR1-4 with shared and unique regions. **C.** The linkage analysis of variants to the locations on the chromosomes. Adapted from Chandrasekhara et al., 2016.

In *A. thaliana* Col-0 ecotype, ribosomal RNA encoding copies in genome are positioned at the telomeric regions of chromosome 2 and 4, designated as nucleolar NOR2 and NOR4 of chromosome 2 and 4, respectively. These 45S rDNA copies are arranged in tandem fashion with intermittent intergenic spacers separating each transcription unit (Figure 2A). Based on the length polymorphism at the 3' ETS regions of these rDNA copies, they are broadly classified into four types, VAR1, 2, 3 and 4 (Figure 2B). The characteristics of NOR2 and NOR4 based on distribution of each VAR has been genetically mapped in A. thaliana. For instance, NOR2 contains VAR1 type with VAR3 but on the other hand NOR4 contains VAR2, 3 and 4 with no copies of VAR1 (Pontvianne et al., 2010; Chandrasekhara et al., 2016). Few copies of VAR4 type rDNA copies are also associated within the 5S repeats of Chromosome 3 close to the centromeric region (Abou-Ellail et al., 2011)(Figure 2C).

While all rDNA copies were initially thought of as similar and inconsequential at the sequence level, recent evidence have emerged for the biased expression of population of specific rRNAs with skewed single nucleotide polymorphisms. The observation of unique expression profile of specific VARs in different stages of growth and development is associated with the chromatin mediated silencing of either NOR2 or NOR4. Notably, VAR1 type is expressed during early stages of seed and seedling stages and subsequently, the NOR2 is quickly silenced leading to lack of VAR1 type during adult growth stages (Pontvianne et al., 2010; Chandrasekhara et al., 2016; Sims et al., 2021).

1.1.2. Pre-rRNA synthesis

The activity of dedicated RNA Pol I that transcribe rDNA copies can lead to up to 70% of all RNA being transcribed in the cell (Warner, 1999) and its intervention is continually explored for cancer therapy. Pol I is a multi subunit polymerase as the other RNA Pol II and III. In yeast, Pol I contains 14 subunits while Pol II and III possess 12 and 17 subunits respectively with many conserved subunits among all. The synthesis rate of RNA pol I and its interdependence to processing is underscored on whether the structures of synthesized rRNA is crucial for assembly (Nomura, 1973). While the rRNA perform the basal catalytic functions of ribosomes, variably efficient ribosomes have been reconstituted from the individual proteins and rRNAs indicating the lack of necessity for assembly of proteins onto the synthesized rRNA (Wilson and Nierhaus,

2007). However, promoter replacement analysis of *E. coli* has shown that the increased pace of synthesis achieved by T7 promoter instead of RNAP (single bacterial RNA Pol) promoter leads to exacerbated rRNA processing defects (Lewicki et al., 1993). In eukaryotes, a point mutation on yeast RNA Pol I, conferring reduced elongation rate led to processing defects resulting in accumulation of primary transcript (Schneider et al., 2007). These observations have led to identification of factors that can directly influence the pol I activity and thereby many initiation factors such as upstream binding factor (UBF), Rrn3p and SL1 have been shown to dynamically control the pre-rRNA processing (Kong et al., 2011; Learned et al., 1985; Claypool et al., 2003). In addition subunits of RNA Pol I are variably phosphorylated similar to Pol II indicating a common mechanistic phenomenon to influence the pre-rRNA and mRNA synthesis (Fath et al., 2004). In addition to above mentioned factors, local chromatin configurations are also thought to influence the pre-rRNA synthesis. Two contrasting line of evidence exist for the role of histones: there are reports of largely histone-less local rDNA regions undergoing transcription (Wittner et al., 2011) as opposed to regions of rDNA possessing transcription-positive histone marks (Jones et al., 2007).

1.1.3 Emerging concepts of ribosomal heterogeneity

'One gene - one ribosome - one protein' principle was proposed as early as 1960s by Crick. This extrapolated complexity of ribosome machinery was set aside for an easier adopted 'monolithic machinery' to recognize the role of principal regulatory molecules they act upon, messenger RNAs (Martinez-Seidel et al., 2020). Soon after the rRNAs role in translation catalysis was established, the role of ribosomal proteins was chiefly ascribed to RNA folding and further evolved functions (Held et al., 1973; Röhl and Nierhaus, 1982). With the increased repertoire of RP and the associated factors of ribosomes and their differential expression, the specialized ribosome theory begin to set foot in the early 1990s (Norris et al., 2021). Evidence are increasingly presented for the multiple layers of regulatory aspects known to modulate the translation potential of messenger RNAs. From the ribosome's proteinaceous components, the presence or absence of constituent RPs on a ribosome (altered stoichiometry), dynamic association of ribosome associated proteins, compensatory RP paralogs, variable RP post-translational modifications (Ubiquitination, phosphorylation) can impart altered

translational capacity to ribosomes. At the RNA level, the sequence variations (single nucleotide polymorphisms), variable chemical base modifications (pseudouridylation, methylation, acetylation) are known to be contributing factors (Xue and Barna, 2012; Genuth and Barna, 2018.) (Figure 3)

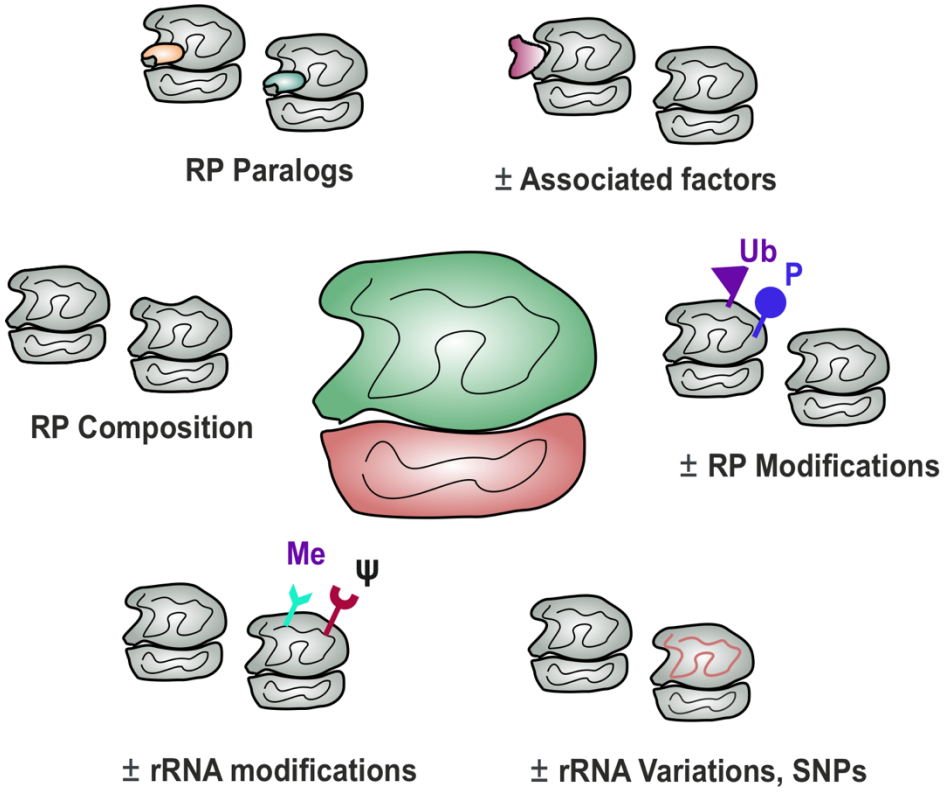

Figure 3. Factors contributing to ribosomal heterogeneity

The functional ribosomes and its translation potential can be modulated through its elemental RPs and rRNAs. In terms of RPs, their compositional stoichiometry, paralog distribution (variable colors), additional ribosome associated factors (extra colored factor), and variable ubiquitination and phosphorylation of RPs (indicated as Ub and P) can affect the activity. In terms of rRNA, the chemical modifications (indicated Me and ψ), variably encoded (orange colored) SNPs can affect the translation potential. Adapted from Norris et al., 2021.

Plant development is met with variable metabolic demands through embryonic, seedling, vegetative and floral development that can result in differing demands for ribosomes. The plethora of RNA and protein components expressed to produce plant ribosomes exhibit large scope for heterogeneity. Indeed, elevated heterogeneity at the ribosomal protein level has been documented for 80S ribosomes on Arabidopsis (Giavalisco et al., 2005). Many of the ribosomal proteins and factors are encoded by

multiple paralogs. These proteins are under differential promotor expression control in terms of growth stages, tissue specificity and hormonal control (Kovacevic et al., 2019). Moreover, the genetic diversity of RP gene families in plant kingdom is considerably higher than other model eukaryotes, by as much as ten-fold in the wake of genome duplication events. For example, in Arabidopsis, the 32 RPS and 48 RPL proteins are encoded by 102 and 146 RP genes, respectively (Carroll et al., 2008). In other eukaryotes, alongside the hallmark ribosomal proteins, the compositional variations are also seen in presence or absence of ribosomal associated factors (Xue and Barna, 2012). Furthermore, the RNA component of ribosomal RNAs exhibit sequence polymorphism at the level of primary sequence (Pontvianne et al., 2010; Sims et al., 2021). Moreover, the residues of rRNAs themselves are also endowed by differential chemical modifications (Azevedo-Favory et al., 2021; Streit and Schleiff, 2021) through presence or absence of 2'-O-methylation (Nm) (Wu et al., 2021)of ribose moiety and pseudouridylation (Ψ) of uridines (Sun et al., 2019), thus, adding more layers of rRNA based regulation of translation control (Sloan et al., 2017).

1.2 CRISPR and its application in plants

An adaptive immune mechanism, involving CRISPR (clustered interspaced short palindromic repeats)-Cas (CRISPR-associated protein) was originally discovered in bacteria as a natural defense mechanism against invading phages (Mojica et al., 2005; Barrangou et al., 2007). Accordingly, the host bacterium encodes for Cas9 protein complex alongside transactivating CRISPR RNAs (tracrRNA) (Bolotin et al., 2005; Deltcheva et al., 2011). The dedicated CRISPR locus can acquire and host specific spacer elements flanking CRISPR repeats that can code for pre-crRNA that can specifically mature to pathogen-specific crRNA. This crRNA in combination with tracrRNA is loaded onto the inactive Cas9 complex for the formation of potent active complex that can scan the invading genomes to introduce double strand breaks to inactivate them (Marraffini and Sontheimer, 2008).

Mechanistically, this scanning process entails the Cas9 scanning for complementarity of protospacer adjacent motif (PAM), example N(A/G/C/T)GG sequence on the genome and further melting of localized guide RNA onto the target DNA for increasing the specificity of target cut site (Figure 4). Bases on the structure determination and worked out model, the Cas9 protein contains six prominent

domains, RECI, RECII, PI (PAM interacting), Bridge helix, HNH and RuvC in which RECI is solely responsible for guide RNA binding, PI domain for PAM pseficity, bridge helix for target DNA binding. The nuclease domains HNH and RuvC performs the single-strand DNA nick on either side to introduce double strand break (Cavanagh and Garrity, 2014). This mechanism has quickly captured the imagination of the scientific community that adapted this technology as a powerful editing tool to introduce targeted double strand breaks in the genome of higher eukaryotes (Cong et al., 2013; Mali et al., 2013).

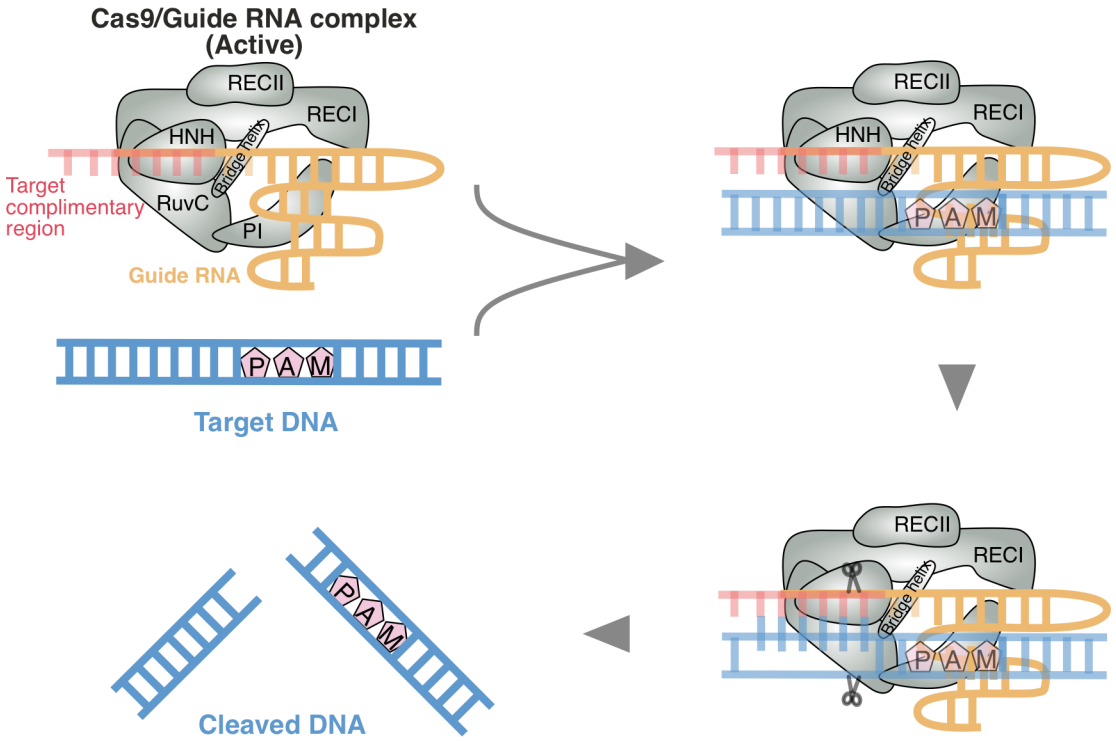

Figure 4. Mechanism of CRISPR-Cas9 editing

The proposed model of action of CRISPR Cas9 mutation begins with the formation of structurally rearranged active Cas9 complex upon binding to guide RNA containing complimentary region. This loaded complex then binds to the target DNA and localized to PAM region. Subsequent to complimentarity establishment, the HNH and RuvC domains nick the target single strand on both sides resulting in double strand break. Adapted from Cavanagh and Garrity, 2014.

In plants, heterologous expression of Cas proteins along with fused spacer and tracrRNA have been successfully utilized to edit the genomes of interest in model and crop species. Although Streptococcus pyogenes Cas9 has been the most used variant

thus far, iteratively developed SpCas9 variants, other species Cas9 variants and Cas12a variants have been successfully employed to diversify the PAM variations and specificity (Zhang et al., 2019).

1.3 Pre-rRNA processing in Eukaryotes

The processing of pre-rRNA transcript at the subunit level begins with simultaneous co-transcriptional processing of 5'ETS by coordinated cleavages on two specific sites, A0, A1 Yeast (Henras et al., 2015). Although the precise endonucleases responsible are unknown, the maturation steps involve the SSU processome complex comprising U3 and at least two snoRNAs in addition to RPS proteins. The other cotranscriptional processing event bears the B0 site cleavage by the Rnase III, Rnt1p to eliminate the 3'ETS (Kufel et al., 1999). The resulting 32S transcript forms the rate-limiting step in which it undergoes post-transcriptional processing cleavages at the ITS1 site for splitting into pre-40S and pre-60S subunits. This pre-40S subunit possess an endonucleolytic cleavage site A2 which is targeted by RNA cyclase protein Rcl1p (Horn et al., 2011) to produce 18S with short A2 fragment. The last step of 18S rRNA maturation of 40S subunit is performed in the cytoplasm through the terminal D-site cleavage of 18S by the RNA binding nuclease protein, Nob1 (Veith et al., 2012).

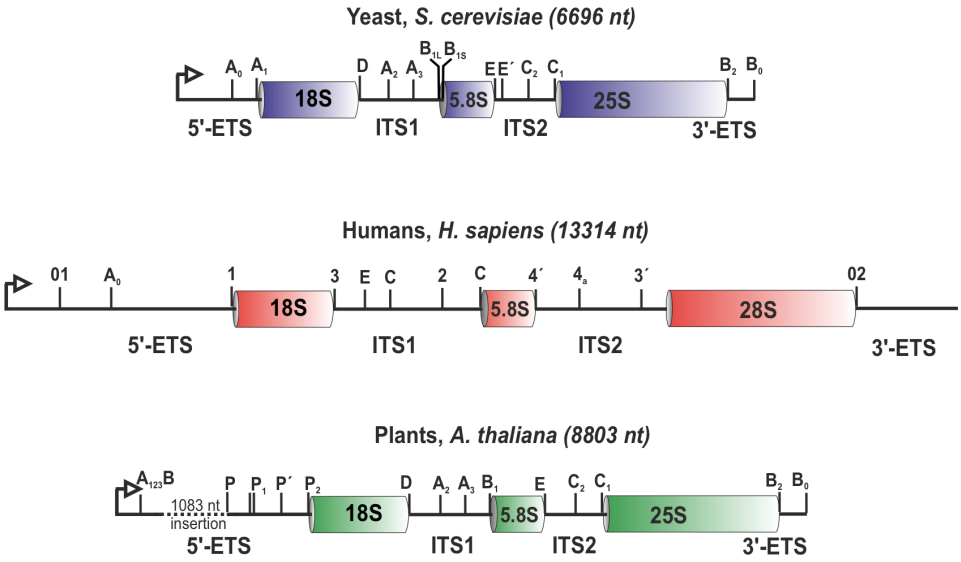

Figure 5. Primary rRNA structure and their cleavage conservation in 3 model species

Comparative primary structure of three model species, Yeast (Blue), Humans (Red) and Arabidopsis (Green) and their conserved cleavage sites during maturation of long precursor rRNA into three mature species of 18S, 5.8S and 25/28S. The right facing arrow denotes the transcription start site. Note that the common immature regions are broadly conserved even

while the length of primary transcript is double that of yeast in Human. The sites were adapted from Mullineux and Lafontaine, 2012 (Yeast and Human) and Weis, 2015 (Arabidopsis).

The immature pre-60S subunit after A2 cleavage can make use of two possible endonucleolytic cleavage sites in A3 and B1L. The predominant A3 containing former cleavage event further generate a smaller deterministic 27SB with cleavage at site B1 to generate overall 27SBs an 27SBL precursors with minor 6 nt differential isoforms (Lygerou et al., 1996; Oeffinger et al., 2009). After the 5' trimming of this fused 5.8S, the first endonucleolytic cleavage of C2 site in ITS2 give rise to 7SL and 7SS, which is again a rate-limiting step in 5.8S maturation. This precursor undergoes Mtr4 helicase dependent exonucleolytic trimming to two S and L forms of 6S and 5.8S. The 5' immature region of 25S containing C2 site of ITS2 is cleaved once again at C1 by Rat1p exonuclease (Geerlings et al., 2000) (Figure 5).

In mammalian cells, the ribosomal RNA encoding regions are twice that of yeast with similarly conserved cleavage sites with longer immature and mature regions (Mullineux and Lafontaine, 2012). The highlight of mammalian pre-rRNA processing however is subsequent to co-transcriptional processing events similar to yeast, the resulting 45S rRNA undergoes the first endonucleolytic cleavage majorly at site 2 of ITS1. This result in the pre-40S subunit with intact 5'ETS termed 30S precursor and pre-60S subunit with 32S (similar to yeast 27SA3) precursor rRNA (Bohnsack and Bohnsack, 2019). The resulting 30S undergoes undergoes 5' maturation on site A0 and 1 to generate 21S precursor. The resulting subunit undergoes exonuclease dependent trimming to generate 18S-A2 like precursor upon which E site is matured to site 3 of 18S rRNA in the cytoplasm (Henras et al., 2015). The remnant of primary transcript cleavage undergoes similar maturation of pre-60S dependent mechanism of yeast using with the largely conserved cleavage sites. This path is elucidated to be predominant in HeLa cells while minor levels of primary transcript undergo the cleavages in a manner similar to yeast (Figure 5).

Pulse-labeling experiments in Yeast have shown that most of the synthesized RNA chiefly undertakes the trimming of 5’ETS through concerted effort of exo- and endonucleases (Koš and Tollervey, 2010). This contrasts with humans where most of the observed precursors corresponded to a precursor containing intact 5’ETS with the first cleavage at A3 site of ITS1 (Zorbas et al., 2015). This delayed splitting of 90S processome into pre-60S and pre-40S has been shown to be characteristic feature of

yeast pre-rRNA processing pathways while the early splitting and thereafter the trimming into mature rRNAs has been known to be feature of mammalian rRNA processing pathways. Plants (Arabidopsis, Rice) however has been shown to process the pre-rRNA through both the pathways with Human-like path predominating the control growth conditions with a minority of longer 35S transcript processed via Yeast-like pathway (Weis, Kovacevic, et al., 2015; Hang et al., 2014). It is worth mentioning the conservation of processing sites are in general more similar to yeast than humans (Figure 5). It has never been shown in plants that ITS1-cleavage dominates through pulse-chase labeling experiments. This is even more crucial given that plants have been shown to possess additional ITS2-mediated cleavage paths albeit not in control conditions. The criteria so far have been to designate a pathway as ‘major’ depending on the intensity of the diagnostic intermediate upon northern hybridization and vice versa for ‘minor’ pathway. Pulse-chase labeling experiments are needed to decode the precise paths and for the determination of ratios of each path among the three to pinpoint the differences to other model system.

1.4 Factors controlling ribosome biogenesis

Major changes to biogenesis activity are attributed to nucleolus signaling. The nucleolus responds to external stimuli through modulation of one of many hundreds of nucleolar proteins to target the master regulators of rRNA transcription through manipulation of TIF-IA, UBF, SL1 or Pol I directly. The stimuli can span from bacterial and viral attack, oxidative stress, oncogene activation, DNA damage, and nutrient depletion (Chen and Stark, 2019).

Ribosome biogenesis is modulated according to the growth needs and this is largely modulated by TOR signaling pathways at the transcriptional level. In yeast, after the exponential growth phase resulting in depletion of carbon sources, the organism enters a quiescent state similar to depletion of cells starved of nitrogen and phosphate sources (Lillie and Pringle, 1980; Werner-Washburne et al., 1993). A group of kinases chiefly TOR1C, Snf1p (sucrose non-fermenting 1p) and Pho85p (phosphate metabolism 85) are involved in regulating these nutrient sources and phosphorylate downstream targets to achieve Pol I-dependent transcriptional response (Galdieri et al., 2010). The two chief targets of TORC1 includes the master regulator Sch9p, a kinase that directly affects the protein synthesizing capability and Tap42p (Urban et

al., 2007). The Sch9p phosphorylation modulates the activity of Pol I through recruitment of initiation factor Rrn3p, promotes Pol II activity of ribosome biogenesis genes and derepresses Pol III activity on 5S rRNA genes (Philippi et al., 2010).
Besides the transcriptional based control, TOR1C has recently been shown to promote an alternative switching of cleavage site from A2 to A3 under variety of growth limiting challenges such as limited nitrogen, heat, and oxidative stress conditions (Kos-Braun et al., 2017). This switch in processing schematics leads to dramatically less de-novo synthesized ribosome populations as a coping mechanism to control protein synthesis rate. In Tomato plants, the infection by a viroid CEVd (Citrus excortis viroid) leading to specific accumulation of P'-A3 precursor and thereby modulating the 40S subunit maturation (Cottilli et al., 2019).

2 OBJECTIVES

Our understanding of ribosome biogenesis based on the significance of specific rDNA copies at the chromosome levels is still poorly understood in all eukaryotes. In addition, the vulnerability of rDNA copies to the CRISPR/Cas9 machinery needs to be further explored to study their governing mechanisms. In this dissertation, attempt was made to utilize CRISPR-Cas9 machinery to target and excise a critical structural element for the integrity of ribosome assembly. This approach was mainly taken to evaluate the efficiency of Cas9 machinery on inducing mutation on variable chromatin targets that can in turn signify their importance for plant development. Overall, although there are roughly 1000 copies of rDNAs in the Arabidopsis genome, the critical copies required for fitness and as such whether such mutation can be compensated by the intact copies remains unknown. Hence, the main objective was to utilize Cas9 machinery to deduce the fitness costs on plant development.

Th other objective of this thesis is to explore novel maturation means in plants and to identify their correlative factors. Furthermore, the nomenclature of major and minor pathways based on their observed steady state levels were challenged by employing pulse-chase labeling analysis of plant pre-rRNA maturation. While the cell culture model was initially used to establish the schematics, conditional factors were used to further envisage their role in normal plant growth. Given plants are sessile organisms, they encounter unique abiotic stress factors and as such their effect on cells predominant RNA's metabolism remains largely elusive. Hence, the second core objective of this dissertation was to give an account of variations in pre-rRNA maturation schemes and their significance for mature rRNA production under unfavorable growth conditions.

3 MATERIAL

3.1 Oligonucleotides

All oligonucleotides used in this study were procured from Eurofins Genomics (Ebersberg, DE) at 100 uM stock and used at 10 uM working concentration.

Table 1. Cloning, Screening, RT-PCR analyses of CRISPR-Cas9 mutants

Name	Sequence (5'-3')
CRISPR_g1F	TGTGGTCTCAATTGGTGGGGAGTTTGGCTGGGGGTTTTAGAGCTAGAAATAGCAAG
CRISPR_g2F	TGTGGTCTCAATTGCATCTGTTAAAAGATAACGCGTTTTAGAGCTAGAAATAGCAAG
CRISPR_R	TGTGGTCTCAAGCGACAAAAAAGCACCGACTCG
CRISPR_seq	GAACCCTGTGGTTGGC ATGCACATAC
Cas9-F	CTTCGACCTGGCCGAAGATG
Cas9-R	CGTATTTGACCTTGGTGAGC
Flanking-F	CAACCCCTGTTTTTGGTCCCAAG
Flanking-R	GATTTCTGTTCTCGTTGAGC
Mut-F	GTCAGGTGGGGAGTTTGGCTAC
25S-R	CGCGACGCGGGCATCAGTAGGG
ETS-F	GACAGACTTGTCCAAAACGCCCAC
ETS-R	CCTGGTCGAGGAATCCTGGACGATT

Table 2. Northern Hybridization

Name	Sequence (5'-3')
p1	CCTAGGCGGATCCATGCTTTCCAAC
p2	ACGGCAATTCCCCGCCACATCC
p3	GGTCGTTCTGTTTTGGACAGGTATC
p4	CGTTTTAGACTTCAGTTCGCAG
p5	GGATGGTGAGGGACGACGATTTGTG
p6	CGTTAAGGAGCTGTTGCTTTGTTAGTGTAG
p22	CTTTGGCGGGACTGAATCACTTCG
p23	GTTCCAACTAATCTACCGAAGTAC
p42	CCACGGATCCGGCGGGCAAGG
25S	CGCGACGCGGGCATCAGTAGGG
7SL	ACTGGGCAGCCCAGAAACATGC

SnRn5	GTTTGGCTGGGGCGGCACATCTGTT
SnoR35	TGTCAGACGGTTCAGGGAGGACGTTTACTTCTTC
U31a	TTTGAGAGAATCAGACAAAAATAGTCAATCACCATG
SnoR27	ATTGGATCTCAGGTTTTTCATGATTTGTCTTC
SnoR68Y	GCAGACACTAAACAGAAAACGCTGAGATCTG
U3.5	CCAGGGTAAAAGGCCTGTCTCT
Sl_p3	CGGGTCGTTCTGCTGTGCAGGTTTC
Sl_p4	CGTTTGTGTTAACAGAGCAGCG
Sl_p5	GAGGGGGCGACGCGATGCGTG
Os_p3 (S7A)	TGTTTTGGTCAGGGTCACGACAATGATCCT
Os_p3(S7B)	GCGGTCTGTTTTGGTCAGGGTCACG
Os_p4	CGTGTGGATTTAACTCGTGGTATC
p3'ITS1	CGAGGTCGATTTGGCGAGGGC
p5'ITS2	CCGGGGCGATTGATCGGCAAGCGAC

Table 3. Circular RT-PCR and sanger sequencing

Name	**Sequence (5'-3')**
cRT	ATCATTCAATCGGTAGGAGCGAC
cRT-F1	CTGCGAACTGAAGTCTAAAACG
cRT-R1	CTATCCGATCACCACTCATACGC
cRT-F2	GATACCTGTCCAAAACAGAACGACC
cRT-R2	CTTTGGCGGGACTGAATCACTTCG
M13(-20)F	TGTAAAACGACGGCCAGT
M13(-20)R	CAGGAAACAGCTATGAC

3.2 Chemicals and Enzymes

The chemicals were purchased from VWR (Darmstadt, DE) and Carl-Roth (Karlsruhe, DE). Plant growth media chemicals were purchased from Duchefa Biochemie (Haarlem, Netherlands). Plant DNA and RNA purification kits were purchased from QIAGEN (Dusseldörf, DE) and E.Z.N.A (Omega Bio-Tek, USA) respectively. For Northern blotting and hybridization high purity chemicals were sourced from Sigma-Aldrich (Steinheim, DE) and Invitrogen (Waltham, USA). Restriction enzymes were

purchased from Thermo Scientific (Waltham, USA), New England Biolabs (Ipswich, USA). Accustart II PCR were purchased from QuantaBio (Beverly, USA). Radionuclides were purchased from Hartmann Analytic (Braunschweig, DE).

3.3 Media

Plants were cultivated in full strength MS (Murashige-Skoog) media supplemented with 1% w/v sucrose and 0.8% w/v of phytoagar (pH 5.8). Root Cell Culture (RCC) were maintained in the media prescribed for YG1 cell line, rpc00050 (RIKEN, Japan). Phosphate starvation media for RCC contained 10 µM KH2PO4 in place of 1.25 mM KH2PO4 of final strength MS media. Liquid and solid agar LB media for growing bacteria (*E. coli* DH5α), Agrobacterium tumefaciens *GV3101*) were described before (Sambrook and Russell, 2001).

3.4 Bacterial Strains

CRISPR expression clones were constructed in *E. coli* strain, DH5α (Life Technologies). The binary vectors were maintained in *Agrobacterium tumefaciens* strain, GV3101.

3.5 Plasmids

CRISPR expression clones were constructed using Level 1 and Level 2 (Golden Gate System) vectors. For building Level 1 clones carrying guide RNAs in pICH47732 and pICH47742, AtU6.26 promotor sequence was supplied by pICSL01009 template plasmid #46968 sourced from Addgene (Watertown, USA). pICH41744 acted as an end linker for further mobilization into Level 2 vector, pICSL02208. (Dr. Nicola Patron, Earlham Institute, UK).

Table 4. Plasmids used and constructed in this dissertation

Plasmid Name	ID[1]	Golden Gate - Level
pICSL01009::AtU6p		Level 0
pICH47732		Level 1
pICH47732-guide1	S05-1048	Level 1
pICH47742		Level 1
pICH47742-guide2	S05-1049	Level 1

pICH41744		Level 1
pICSL02208	S02-227	Level 2 - Binary
pICSL02208-g1-g2	S05-1069	Level 2 - Binary

[1]ID denotes the stock number given after construction of clones in AK Schleiff Plasmid list.

3.6 Plants - Wildtype, mutants and stable transgenics

Arabidopsis wild type accession, Col-0 was used as standard practice in this study. CRISPR mutagenesis of Col-0 wild type led to creation of stable mutants. In addition, mutants of *Arabidopsis* of specified gene locus (Table 5) were sourced from varying origins as listed. Rice seeds, *Oryza sativa* (*japonica*) used in study were kind gift from Prof. Folkard Asch (Universität Hohenheim) and Tomato seeds used in this study belong to Moneymaker variety.

Table 5. Arabidopsis mutant and transgenic lines used in this dissertation

Mutant name	**ID[1]**	**Souce**
ploop KD	S05-309	This Dissertation
xrn2	S05-141	NASC
hot1-3	S05-180	NASC
hot3-1	S05-158	NASC
hot3-2	S05-159	NASC
rrp5Δ10	S05-413	Gift from Dr. Christian Wenzl (Uni-Heidelberg)
Transgenic name	**ID**	**Source**
GFP-ATG8e	S05-361	Gift from Dr. Yasin Dagdas (GMI, Vienna)
GFP-ATG8e/ *ploop KD* +/-	S05-388	This Dissertation

[1]ID denotes the stock number given after generation of stable transgenics in AK Schleiff Seed list.

3.7 Antibodies

Antibodies used in this dissertation are either commercially procured or developed elsewhere with the source given in Table 6. The secondary antibodies, Anti-Rabbit

(A9169) and Anti-Mouse (A9044) were purchased from Sigma Aldrich (Taufkirchen, DE).

Table 6. List of antibodies used in this dissertation

Primary Antibodies	Source	Secondary Antibody
RPL5	Weis et al 2015	Anti-Rabbit
RPL10	Jelena Kovacevic	Anti-Rabbit
RPS3-2	Jelena Kovacevic	Anti-Rabbit
EF1Bβ	Agrisera	Anti-Rabbit
ENP1	Weis et al	Anti-Rabbit
NOB1	Weis et al	Anti-Rabbit
GFP	#11814460001, Roche	Anti-Mouse
HSC70	SPA-817 Enzo Life Sciences	Anti-Mouse

4 METHODS

4.1 Molecular biological methods

4.1.1 Golden gate cloning

A PCR product of length 134-135bp was amplified using guide sequence (g1/g2) containing forward oligo and common reverse oligo (Table 1) with the template plasmid (Addgene: 46968) that supplies sgRNA sequence. The resulting PCR product (gRNA-sgRNA) was combined with AtU6p donor, pICSL01009 in a Level 1 Dig-Lig reaction using Bsa I and T4 DNA Ligase (Thermo Scientific, DE) with pICH47732 and pICH47742 acting as acceptors according to published protocol (Weber et al., 2011). The resulting Level 1 donor clones containing AtU6p::g1RNA:sgRNA, AtU6p::g2RNA::sgRNA were end-linked with pICH41744 into a Level 2 acceptor plasmid, pICSL002208 using Level 2 Dig-Lig reaction mediated by BpiI and T4 DNA Ligase described as earlier.

4.1.2 Purification of DNA

For crude purification of genomic DNA from plants for routine genotyping, 3 mm disc of expanding leaf was excised and briefly crushed using green pestles in 400 µL

extraction buffer (200 mM Tris pH 7.5, 250 mM NaCl, 25 mM EDTA, 0.5% SDS). 300 After full speed centrifugation for 15 min at RT, 300 µL of lysate was mixed with equal volume of isopropanol and centrifuged at 4°C further to pellet the genomic DNA. The pellet was washed further with 70% ethanol, dried at RT for 30 min, dissolved up to 50 µL ddH20, saved at 4°C and can be used for up to 2 years. For high quality quantitative genomic DNA PCR, Plant DNEasy kit (QIAGEN) was used according to manufacturer's instructions.

4.1.3 Heteroduplex PCR

Heteroduplex PCR protocol was adapted from (Zhu et al., 2014). Essentially, 20 µL of PCR reaction volume contained genomic DNA template, 1X Taq buffer, 2.5 mM dNTPs, forward and reverse oligos and Taq polymerase. The reaction was programmed with normal PCR programs with following modification: after the final extension of 72°C for 5 min, the PCR products were denatured at 95°C for 10 min and followed by reannealing to 25°C with linear 1°C / min reduction program.

4.1.4 High resolution DNA gel electrophoresis

Heteroduplex PCR products were resolved on 15% (w/v) acrylamide concentration containing TBE (90 mM Tris, 90 mM Boric acid, 2 mM EDTA, pH 8.0) gels. The gels were pre-run at 100V for 30 min. Samples were loader after, electrophoresed at 150V and the gels were stained with ethidium bromide.

4.1.5 RNA-sequencing and SNP analysis

The RNA-seq library preparation was performed on total RNA from 14d old BG and *ploop KD* seedlings without rRNA depletion. Sequencing was performed on NovaSeq 6000 at the Novogene Sequencing Facility (Beijing, China). The sequencing analysis was performed by Dr. Stefan Simm (Uni-Medizin Greifswald). Accordingly, the paired end reads of lengths of 2*150 bp were mapped specifically against the annotated *A. thaliana* precursor rDNA repeat (Sims et al., 2021) using Bowtie2 (Langmead and Salzberg, 2012). As a result, 35 million reads were properly mapped onto rRNA in BG and *ploop KD* from a sum of 63 and 60 million reads respectively. SNP calling was conducted using LoFreq (Wilm et al., 2012) with default parameter settings.

4.1.6 Proteomic analysis

For proteomic analysis, 20 mg fresh weight of 10d old seedlings from four biological replicates of BG and *ploop KD* were finely ground with liquid nitrogen. The mass spectrometric measurements were conducted at MOSYS, Uni-Vienna by Dr. Palak Chaturvedi. Accordingly, the purified proteins were pre-fractionated by 1D SDS-PAGE, trypsin digested and desalted using shotgun proteomics method as described earlier (Chaturvedi et al., 2013; Ghatak et al., 2020). For sample loading, one µg / replicate was introduced on to C18 reverse-phase column (EASY-Spray 500 mm / 2 µm particle size, Thermo Scientific). For separation, following conditions were used: a 90 min gradient with 98% solution A (0.1% formic acid) and 2% solution B (90% acetonitrile, 0.1% formic acid) at 0 min to 40% solution B again at 90 min with a flow rate of 300 nL/min. The nESI-MS/MS measurements with Orbitrap QExative (Thermo Scientific, Bremen, DE) were conducted with following settings: Full scan range 350^{-1},800 m/z resolution 120,000 max. 20 MS2 scans (activation type CID), repeat count 1, repeat duration 30 sec, exclusion list size 500, exclusion duration 30 sec, charge state screening enabled with the rejection of unassigned and +1 charge states, minimum signal threshold 500. The generated raw data was processed with SEQUEST algorithm in Proteome Discoverer Program (v 1.3) as described earlier (Chaturvedi et al., 2013; Zhang et al., 2021). The proteins were identified from the fasta protein sequences contained within the TAIR 10. The proteins were quantified based on the total ion count and further normalized using NSAF approach (Paoletti et al., 2006).

4.1.7 Metabolic pulse chase labeling of RNA

The protocol was adapted from Nover et al., 1986. The RCC maintained at cell culture medium or *A. thaliana* seedlings maintained at hydroponic MS media without supplied agar were maintained overnight on fresh media containing minimal phosphate source (10 µM instead of 1250 µM KH_2PO_4) for starvation. The culture flasks or petri dishes were pulsed for indicated min with ^{32}P labeled orthophosphoric acid (P-RB-1-L Hartmann Analytic, Germany) at 5 µCi/mL of media. Pulsing was followed by multiple washes with PO_4 free media in case of Pulse-only conditions. For chasing, the washed RCC cells were supplemented with 100X original phosphate concentration containing

MS media for indicated time. The cells were withdrawn, excess media removed, frozen at liquid nitrogen and stored at -80°C until RNA purification.

4.1.8 Reverse Transcription of RNA

Reverse transcription in this dissertation was performed with either of two RT kits: SuperScript III RT system (Thermo Fisher, Germany) and RevertAid RT system (Thermo Fisher, Germany). Briefly, 100 ng - 5 µg RNA was used as template for 20 µL reaction with gene-specific oligo to synthesize cDNAs according to manufacturer's instructions. The cDNA was diluted further up to 50-100 µL before using 2 µL for RT-PCR reactions.

4.1.9 Circular Reverse Transcription PCR

Circularization of RNAs were performed according to Shanmugam et al 2017. Briefly, 5 µg of total or 0.5 µg of poly(A) RNA was circularized using T4 RNA Ligase I (NEB, USA) and incubated at 37°C for 2 h. The ligase was deactivated at 65°C for 5 min and the RNA was precipitated using 3M Sodium acetate and 100% Ethanol for overnight. The RNA pellet was washed and dissolved in nuclease free water for RT reactions as described above with specific oligos.

4.1.10 RNA Gel electrophoresis

For HMW RNA, a 1.2% high purity agarose containing gel was prepared for electrophoresis in 1X BPTE (10 mM PIPES, 30 mM Bis-Tris, 1 mM EDTA pH 6.5) buffer. The RNA samples (in 10 µL) were mixed with equal volume of Glyoxal loading buffer (60% v/v DMSO, 20% v/v deionized glyoxal, 12% v/v 10X BPTE buffer, 0.6% w/v of 80% glycerol, 2% of 10 mg/mL ethidium bromide) and denatured for 55°C for 1 h. The samples were cooled on ice and added with 2.5 µL of formamide loading buffer (95% formamide; 0.025% each of bromophenol blue, xylene cyanol FF and SDS; 5 mM EDTA), mixed, loaded onto the casted gel and electrophoresed at 60V for up to 16 h. For LMW RNA, a 6% -8% polyacrylamide gel containing 7M urea was prepared in 1X TBE (90 mM Tris-Borate, 2 mM EDTA). The RNA samples (in 5 µL) were mixed with equal volume of formamide loading buffer, denatured at 85°C for 5 min, snap-frozen on ice for 5 min and loaded onto the pre-run PAGE gels at 150 V.

4.1.11 Gel Drying

For drying agarose gels (up to 8 mm of thickness), a gel dryer (Savant SGD4050, USA fitted with a cooling unit was used. The mesh surface of the dryer was pre-heated up to 60°C and the cooling unit temperature was set at 4°C. The gel was placed carefully on a Whatman filter paper and covered with saran wrap without any air bubbles. The vacuum was pulled so that the rubber cover is properly pulled to the mesh in place.

4.1.12 Northern Blotting and Hybridization

For blotting RNA from agarose gels, the gels were photographed and pre-treated with following steps before vacuum blotting: once washed with ddH20, then treated with 0.1 M NaOH for 30 min, washed with water, followed by two treatments with Tris-Cl (0.5 M Tris, 1.5 M NaCl, pH 7.5) for 30 min each and allowed to equilibrate at 6X SSC (900 mM NaCl, 90 mM Trisodium citrate, pH 7.0) buffer for 10 min. The membranes were pre-treated for the same time with 6X SSC and the set up with membranes below the gel were vacuum blotted for up to 3h.

In case of denaturing PAGE gels, the gels were washed and stained with ethidium bromide. The equilibrated gels were set up for overnight electroblotting at 15 V in 4°C cold room mounted on a stirrer. The blotted membranes were UV-cross linked twice at auto cross link settings (UV Stratalinker 2400, Stratagene, USA)

For Northern hybridization, the membranes were washed with hybridization buffer (6X SSC; 0.1% w/v SDS; 2% v/v 100X Denhardt's solution (2% bovine serum albumin, 2% ficoll 400, 2% polyvinylpyrrolidone) and 0.05 mg/mL MB-grade DNA) for 30 min followed by addition of radio labeled northern oligoprobes. For radio end labeling, 50 pmol of oligo were labeled in a 20 µL of labeling reaction containing T4 Polynucleotide kinase (Thermo Fisher, Germany) and PNK Buffer A according to manufacturer's instruction. The [γ-32^{P}]-ATP (SRP201, Hartmann Analytic, Germany) for this reaction was added at the dedicated isotope handling facility. The radiolabeled probes containing buffer and membranes were allowed to hybridize O/N at 37°C. The membranes were washed for 30 min each with low-stringency wash buffer (6X SSC) and high-stringency wash buffer (2X SSC, 0.1% SDS) at 37°C. Post-washing, membranes were allowed to dry and exposed to storage phosphor-imaging screen depending on signal strength for duration of 2 h - 5 d. The screens were excited, and

the auto-radiography signals were recorded using Typhoon scanner 9400 (GE Healthcare, USA).

4.1.13 Ribosomal subunit profiling

Two different extraction buffers were used for ribosomal sub-unit profiling in this dissertation. Cell lysates from RCC were dissolved in extraction buffer (50 mM Tris-HCl pH 7.5, 50 mM NaCl, 1.5 mM $MgCl_2$, 1 mM DTT, 1% NP-40, 100 µg/mL cycloheximide, 10 mM ribonucleoside-vanadyl-complex (VRC) mix, 1% plant protease inhibitor cocktail) and the lysates were rotated end-to end and further clarified with subsequent centrifugations steps; 5000 g for 5 min and 14000 g for 10 min at 4°C. The lysates were loaded onto a sucrose cushion containing a linear gradient of 10-50% sucrose concentration in extraction buffer without detergents and inhibitors. The complexes were allowed to be separated based on their density using SORVALL Discovery 90SE ultracentrifuge (Kendro Laboratory Products, USA) at 98,900 g for 16 hours with TST41.14 rotor. The absorption profile at 254 nm of fractionated samples were measured by using density-gradient fractionation set up (Teledyne ISCO, USA) fitted with a gradient pump fractionator. Another extraction buffer utilized a recently published ribosome extraction buffer, REB (Firmino et al., 2020). Accordingly, 300 mg of liquid nitrogen ground fresh weight tissues were dissolved in up to 400 µL of REB buffer and the thawed mixture clarified as stated above except with a single centrifugation step of 20,000 g for 2 min. The cleared lysate was loaded onto 15-60% sucrose gradient and ultracentrifuged as earlier. The collected fractions with both methods were processed for RNA and protein purification as published earlier in Missbach et al., 2013.

4.1.14 SDS-PAGE, Western blotting, and Hybridization

SDS-PAGE in this dissertation was performed using apparatus from either Hoefer (Holliston, USA) or BIO-RAD Mini-PROTEAN Tetra electrophoresis system (Hercules, USA). A resolving gel with 12% and stacking gel with 4% polyacrylamide concentration was prepared using 1.5 M Tris pH 8.8 and 0.5 M Tris pH 6.8 respectively. The samples for electrophoresis were denatured with 2X Laemmli buffer (65.8 mM Tris-HCl pH 6.8, 26.3% w/v Glycerol, 2.1% SDS and 0.91% bromophenol blue) at 95°C for 5 min.

Denatured protein samples were loaded onto polymerized gels in gel running buffer (25 mM Tris pH 8.3, 192 mM Glycine, 0.1% SDS) and electrophoresed at 150 V.
For transferring to PVDF membranes, electroblotting was performed with transfer buffer (25 mM Tris pH 8.3, 192 mM Glycine, 20% methanol) in semi-dry conditions using TE 77 ECL semi-dry transfer unit (Amersham, UK).
After blotting, the membranes were blocked with 5% non-fat milk powder containing 1X PBS-T (137 mM NaCl, 2.7 mM KCl, 10 mM Na_2HPO_4,1.8 mM KH_2PO_4 and 0.05% w/v Tween-20) for 1 h. For probing of specific protein levels, the membranes were incubated with primary antibodies in 1X PBS-T at 4°C for O/N. After washing unbound primary antibodies and further incubation wih secondary antibodies coupled with horseradish peroxidase conjugates, ECL substrates (Thermo Fisher) were used to detect the chemiluminescent signals using ECL Chemostar (INTAS, Germany).

4.1.15 Quantification

Quantification (Chapter 5.3) were performed with average values of signal intensities of each precursor after background subtraction in Image J (Schindelin et al., 2012). The values were transferred to SigmaPlot for calculating each precursor intensities and the rate constants for the regimes presented in Figure 18B.
Accordingly, in control growth conditions of RCC and seedlings, the intensity of each precursor was normalized to the number of nucleotides with total production being ∑I. Based on the reaction scheme, the sum intensity of 35S was calculated by sum intensities of I_{32S}, $I_{P\text{-}A3}$, $I_{18S}*I_{P\text{-}A3}/(I_{P\text{-}A3}+I_{32S})$, $I_{27SB}*I_{32S}/(I_{P\text{-}A3}+I_{32S})$ and $I_{25S}*I_{32S}/(I_{P\text{-}A3}+I_{32S})$. With the calculated intensities, least square fit method was used to analyze the rate constants using following equation 1 for 35S and equation 2 for other precursors.

$$[A] \xrightarrow{k_s} [C] \quad \text{(Eq 1)}$$

$$[A] \xrightarrow{k_s} [B] \xrightarrow{k_p} [C] \quad \text{(Eq 2)}$$

where k_s denotes rate constant for synthesis and k_p the rate constant for processing in C, the analyzed precursor. In case of two origin for a denoted precursor, the analysis was either performed with a.) partial fraction of precursor production using one path (e.g. I_{27SB} (32S) = $I_{27SB}*I_{32S}/(I_{P\text{-}A3}+I_{32S})$ + $I_{25S}*I_{32S}/(I_{P\text{-}A3}+I_{32S})$ or I_{27SB} (35S) = I_{27SB} - $I_{27SB}*I_{32S}/(I_{P\text{-}A3}+I_{32S})$ + I_{25S} - $I_{25S}*I_{32S}/(I_{P\text{-}A3}+I_{32S})$) or b.) using the full value in unavoidable circumstances (I_{27SB} (T) = I_{27SB} + I_{25S}).

For stress chase conditions, the precursor intensity was normalized to initial density of 35S. The least square fit method was used to calculate the precursor synthesis and processing rates using equation 3 for 35S, 32S, 27SA, 27SB and 18S-A3 from heat-stressed samples (Figure 22, 23) and 35S and 32S precursors from the chase samples. For the rest of intermediates, equation 4 and mature 18S and 25S rRNAs, equation 2 was used.

$[C] –k_p–> [S]$ (Eq 3)

$[A] –k_s–> [C] –k_p–> [S]$ (Eq 4)

with same notations represented as before. The analysis did not include the subsequent precursor production from the major path precursor P-A3 and hence all values are only estimates. Equation 3 and 4 are similar to Equation 1 and 2 in these analyses.

For calculating the precursor abundance corresponding to the growth temperature, the intensities of each precursor were calculated relative to the maximal intensity observed for each precursor. These intensity values were further used by least square fit method using dose response hill equation as follows

$$I = I_{min} + (I_{max} - I_{min}) / (1 + 10^{[(\log[EC50]-T)*h]}) \quad \text{(Eq 5)}$$

in which EC_{50} denotes 50% inhibition (EC) or induction (IC). I_{min} denoted the background signal intensity whereas I_{max} the maximal signal observed. T being the logarithm of temperature and h is the Hill coefficient (no units). This section was adapted from Shanmugam et al., 2021.

4.2 Plant Methods

4.2.1 Growth and maintenance of root cell culture (RCC)

Arabidopsis root cell culture (RCC) used in this study is a kind gift from A. Batschauer (Philips Universität, Marburg)

4.2.2 Growth and maintenance of plants

For sterile growth of Arabidopsis in MS media containing plates - the seeds were surface sterilized using 0.1% Triton X-100 for 1 h, followed by 60 sec of 70% ethanol wash and subsequently five times washing steps to remove excess residual ethanol. The washed seeds were either carefully placed on the solid media or randomly spread on the media containing plates. The plates were stratified for 2-3 d at 4°C in dark. Then

the seeds were allowed to germinate and grow at 22°C with 16h / 8h light (120 µmol/m^2) dark conditions. For hydroponic growth conditions in liquid MS media, the sterilized seeds were added to the MS media containing flasks and maintained at shakers in walk-in plant growth chambers. For tomato and rice seeds, similar surface sterilization steps were followed by carefully placing in sterile media containing magenta plant culture boxes.

4.2.3 Stress treatments of plants

Heat stress treatments in this dissertation was adapted from Larkindale et al., 2005. Briefly, well grown Arabidopsis plants (16d old) growing inside 100 x 20 mm petri-dishes were floated on a water bath set at a given growth temperature (30°C-42°C) and time for imparting heat stress regimes. In case of magenta boxes, they were submerged and kept wholly inside the set water bath temperature for stress treatments.

4.2.4 Arabidopsis floral transformation

Arabidopsis floral transformation was adapted from Clough and Bent, 1998. The Arabidopsis plants exhibiting maximal floral growth stages were chosen for agrobacterium infection and any visibly fertilized flowers and siliques were clipped away. Secondary Agrobacterium culture containing desired expression cassettes were pelleted and resuspended to OD_{600} = 0.8 in 5% Sucrose solution containing 0.05% Silwet L-77 (Bio-world, USA). The floral tissues were dipped in agrobacterium suspension until visible film appears on the tissues. The plants were covered with black polybags for up to 16 h and later allowed to set seeds under normal growth conditions.

4.2.5 Plant crossing

For crossing of Arabidopsis transgenics or mutants, the pollen grain receiving flowers were emasculated by removing sepals, petals, and stamens to ensure avoidance of self fertilization. The male donor pollen grains containing anthers were excised with stamen structure and gently scratched on the pistil surface to dust the pollen grains

for fertilization to ensue. The plants were kept secluded, allowed for silique elongation to ensue and F1 seeds were later harvested.

4.2.6 Fractionation of root cell culture (RCC)

Fractionation of cell culture to three compartments (Palm, 2017) and subsequent purification of RNA was performed as described earlier (Streit et al., 2020).

4.2.7 RNA Purification

For total RNA purification of all plant tissues and cell culture, the E.Z.N.A kit was primarily used in this dissertation with 100 mg of finely ground powder using liquid nitrogen. In case of radiolabeled RNA purification of RCC and seedlings, the liquid nitrogen step was omitted to avoid disposing of radioactive substances. Instead, the tissues were ground with pestle and mortar containing lysis buffer atop ice to keep the mortar cool.

4.2.8 Confocal Laser Scanning Microscopy

For recording of GFP fluorescence with LSM780 Confocal Laser Scanning Microscope (Carl Zeiss, Germany), an excitation wavelength of 488 nm was used, and the emission was recorded between 505-525 nm.

5 RESULTS

5.1 Cas9 editing of rDNA and its effect in plant development

5.1.1 Cas9 targeted the P-loop region of 25S rDNA

To deduce the effect of rDNA mutation on phenotypic fitness, CRISPR-Cas9 machinery was employed to target 25S rDNA and excision of -20 bp region using dual guide RNAs. Due to multi copies on the genome, the chosen guide RNAs were poised to target the corresponding complementary sequence of hundreds of copies of ribosomal DNA regions (Figure 6A).

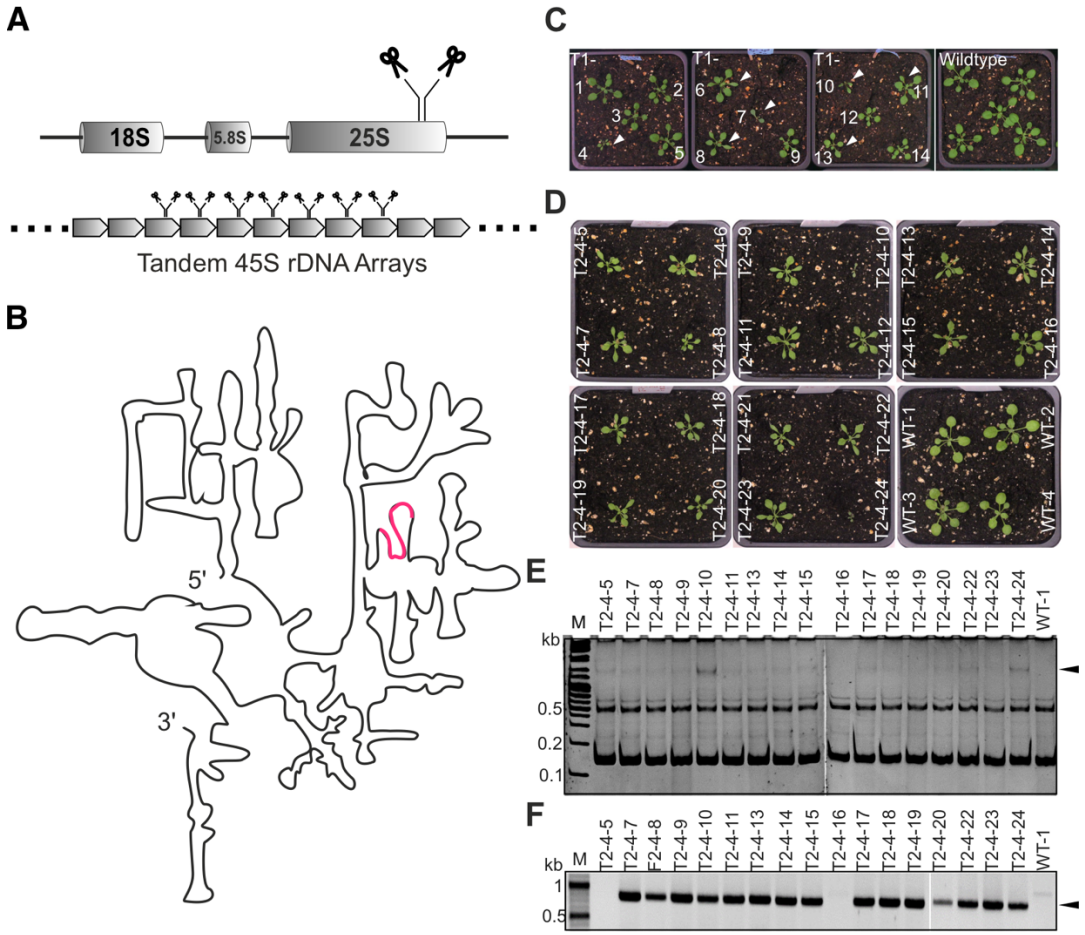

Figure 6. CRISPR-Cas9 mutagenesis of 25S rDNA copies and screening

A. Location of guide RNA regions targeting the 3' side of 25S rDNA region **B.** Location of P-loop region on secondary structure of 3' half of LSU ribosomal RNA. **C.** 23d old T1 plants transplanted after growing in selection media containing kanamycin. **D.** T2 plants grown from T1-4 containing the inheritable pointy-leaf phenotype **E.** Heteroduplex PCR conducted on genomic DNA of indicated plants using oligonucleotides (Flanking-F/R) to detect the mutation. Note the absence of heteroduplex band on T2-4-16 and its WT-like phenotype on panel B. **F.** The same plants were used to test the absence of Cas9 expression cassette using specific oligos (Cas9-F/R).

Based on the secondary structure of 25S rRNA, the excised region corresponded to a critical structural element termed P-loop embedded near the E/P/A site of translating ribosomes and crystal structure studies of 60S subunit shows P-loop (Figure 6B) in the vicinity of N-term of eukaryotic RPL29 alongside RPL10.

The floral transformation of CRISPR Cas9 cassettes were followed by T1 plants screening using the commonality on characterized ribosomal defects phenotypes. Accordingly, 7/14 plants exhibited altered morphology during the rosette development (Figure 6C, white arrowheads). These phenotype exhibiting plants were further propagated in T2 generation and accordingly T1-4 progenies were selected for their sex-cells carry over of the phenotype (Figure 6D). The T2 plants arising from T1 were biasedly segregated for screening the mutational genotype using heteroduplex PCR (Figure 6E). Accordingly, all the altered morphology displaying plants possessed heteroduplex band arising through re-annealing of wild-type and mutated copies marked by their higher order mobility under native PAGE conditions. Interestingly, T2-4-16 that displayed WT-like phenotype did not contain the mutational heteroduplex PCR allele, alongside WT-1 thus ensuring the specificity of the technique. These plants were further screened for the presence of Cas9 genomic expression cassette using Cas9-specific PCR (Figure 6F). In this analysis, T2-4-5 possessed no Cas9 cassette marked by the absence of band and hence was fixed as representative line to avoid incessant mutations through Cas9 machinery.

5.1.2 Mutation led to 5% alteration of all rDNA copies

The fixed line segregated into three phenotypic groups based on severity (discussed further in next section) and these characteristics were used to determine the proportion of rDNA copies carrying mutations. To roughly estimate the mutated copy levels, the intensity of heteroduplex band was used relative to the total intensity of rDNA band, to calculate the proportion of mutations in three groups: +/+ (WT like), +/- (mild) and -/- (severe) plants (Figure 7A). Using targeted loci-flanking PCR (Table 1. Flanking-F/R oligos) with 5 ng of genomic DNA and linearly increasing cycles for quantification, our analysis showed that 2.54% and 5.52% were perturbed relative to the intact overall intensity in mild and severe phenotypic groups (Figure 7B).

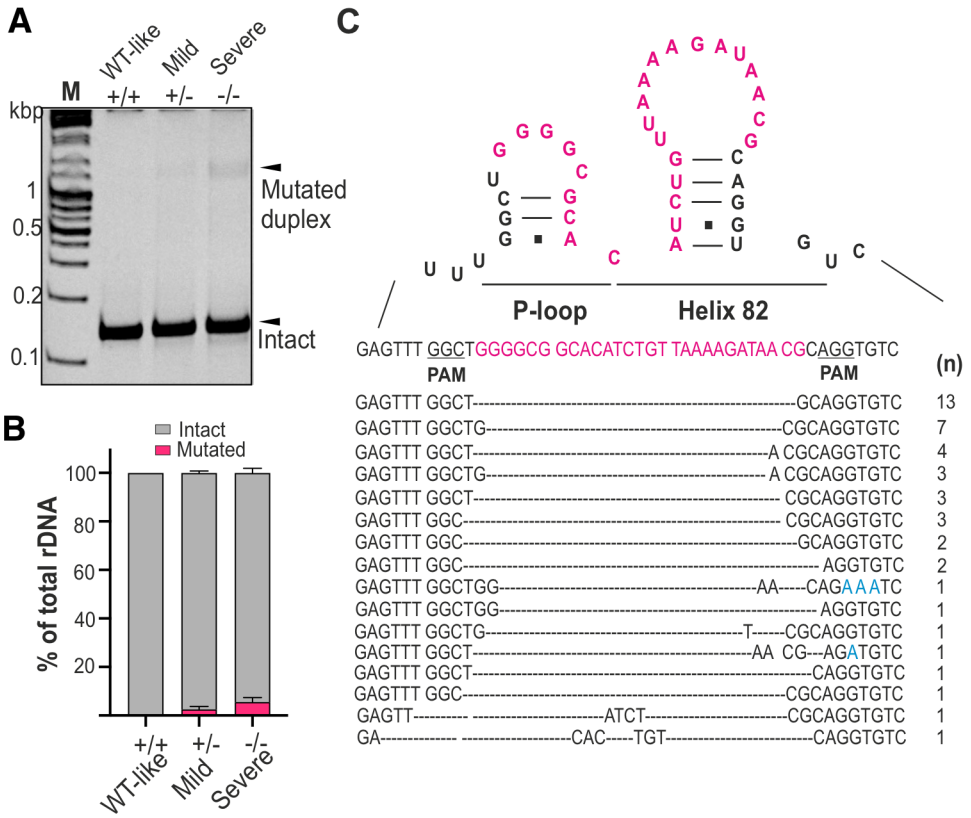

Figure 7. Analysis of proportion of mutated copies

A. Heteroduplex PCR products of three genotypes electrophoresed at 15% Native PAGE conditions. **B.** Quantification of mutated and intact rDNA copies of the PCR products analyzed in panel C (n=6 linearly increasing PCR cycles). **C.** Cloning and sequencing of heteroduplex PCR products at panel C resulting in mosaic mutation pattern on the rDNA.

Next, the patterns of mutations in the Cas9-free segregating plants were finely mapped by cloning and sequencing of heteroduplex bands (Figure 7B). This resulted in Cas9 excisions that are predominantly deletion between the two guide recognition sites (Figure 7C). Due to the inherent multiple target regions on the target genome, the Cas9 and guide RNAs mediated nick and repair mechanism was therefore found to be mosaic in nature. This resulted in frequencies of mutation pattern summarized after sequencing of target mutations (total = 44) with 8 patterns occurring only once. The dominant patterns turned out to be complete excision of the target region with one-nt excess on the guide 2 (13/44), followed by one-nt excess on guide 1 and two-nt excess of guide 2 (7/44), three-nt excess on guide 2 (4/44), one-nt excess on guide 1 and three-nt excess on guide 2 (3/44) and two-nt excess on guide 2 (3/44). In addition, there were also patterns where in PAM site was cleaved precisely on guide 1 (3/44) and guide 2 (2/44). The infrequent patterns usually are those of repair

mechanisms introducing substitution mutations (2/44) and addition mutations (5/44). Overall, the CRISPR-Cas9 targeting of 25S rDNA using dual-guide RNAs resulted in stable inheritance of mosaic mutation patterns on the ribosomal DNA copies.

5.1.3 Mutation caused dosage dependent phenotypic effects

Next, the resulting morphology of the plants induced by the mutations were analyzed. Owing to large number of copies targeted, the mutants displayed dosage-dependent growth developmental defects.

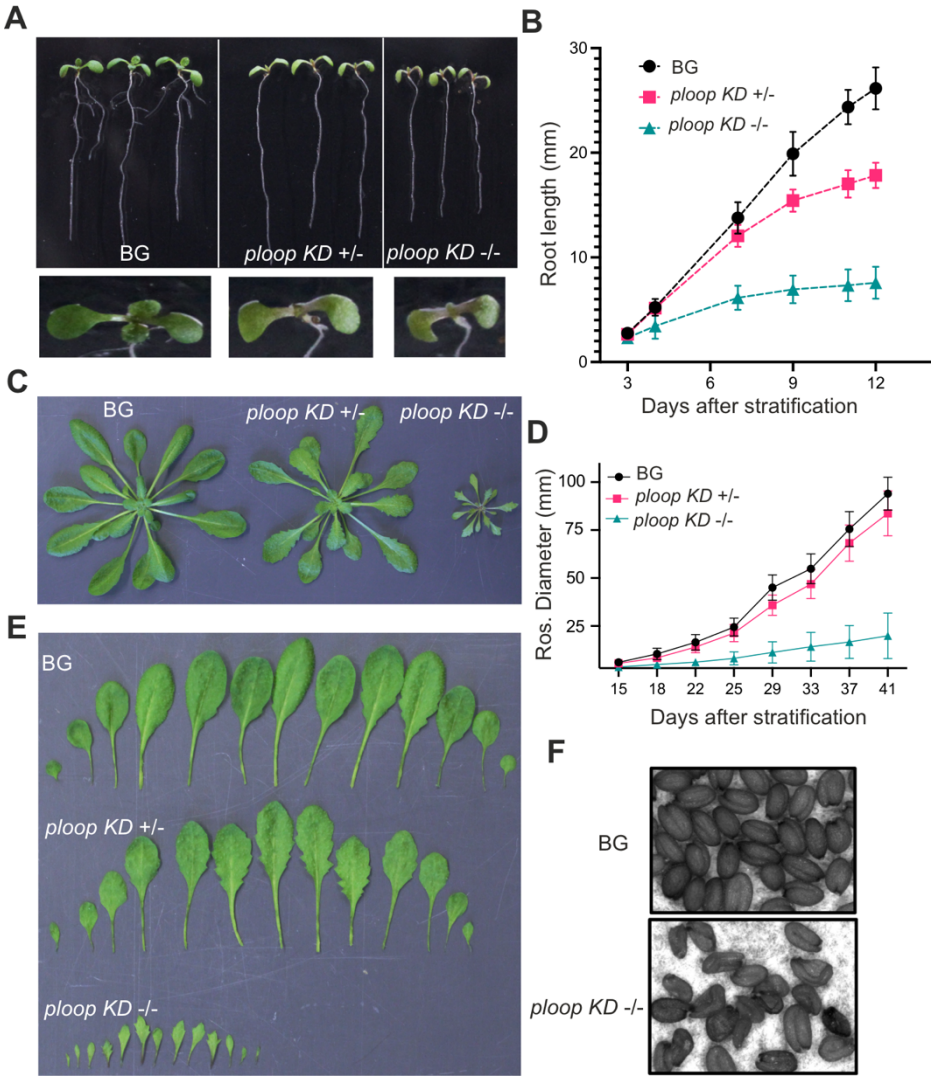

Figure 8. Phenotypical aberrations of resulting 25S rRNA mutation

A. Seedling growth phenotypes of segregating heterozygous plants. **B.** Root length variations analyzed during seedling growth. **C.** Rosette morphology of soil-grown mutant plants. **D.** Rosette diameter of mutants through vegetative phase. **E.** Heteroblasty in leaf form and shape among three genotypes from panel C. **F.** Seed morphology of BG and *KD* -/- mutants.

The heterozygous mutations segregated at 1:2:1 ratio resulting in background WT-like phenotype (BG), heterozygous (*ploop KD* +/-) and homozygous (*ploop KD* +/-) for the mutated ploop allele copies. The segregating seedlings consistently displayed obvious morphological distinctions between three genotypes (Figure 8A). In comparison to BG, the *ploop KD* +/- seedlings lacked lateral root growth and exhibited delayed first-leaf emergence. On the other hand, *ploop KD* -/- seedlings were overall smaller in size in comparison to both WT and *ploop KD* +/- and but showed other morphological similarities to *ploop KD* +/- in terms of absence of lateral root growth and first leaf emergence. The root growth rate (Figure 8B) measured on vertically grown seedlings over 12 days for the three genotypes showed that BG and *ploop KD* +/- showed comparable root lengths up to 7 DAS but *ploop KD* +/- were subsequently reduced up to 8 mm at 12 DAS. Meanwhile, *ploop KD* -/- in comparison to WT, showed markedly reduced root lengths of up to 7 mm at 7 DAS and 18 mm at 12 DAS suggesting significant growth defects.

At later vegetative growth stages, the rosette morphology of *ploop KD* +/- plants reached the same size as that of BG-like plants, while the *ploop KD* -/- remained severely stunted in overall growth with drastically reduced leaf size (Figure 8C). The rosette diameter of the three genotypes showed that the *ploop KD* -/- plants were almost ten times reduced in comparison to BG (Figure 8D). The distribution of detached leaves emerging from the shoot apical meristem of the three genotypes indicated that the leaves of *ploop KD* +/- were slightly more serrated on the sides and possessed slightly pointy tips in comparison to BG-like plants while the *ploop KD* -/- were sharply serrated and pointed at the tip and lacked any similarity to BG-like plants (Figure 8E). Comparing their seed morphology, most *ploop KD* -/- failed to set seeds, occasionally, few independent plants set seeds, but their seeds were shrunken and deformed (Figure 8F).

5.1.4 Severe mutation class exhibited global proteome defects

To gain deeper understanding of resulting mutant morphology, proteome analysis on BG and *ploop KD* -/- seedlings (n=4 biological replicates) was conducted to detect variations in mutant. The principal components 1 and 2 amounting to 62% of total variance resolved the two genotypic groups apart (Figure 9A).

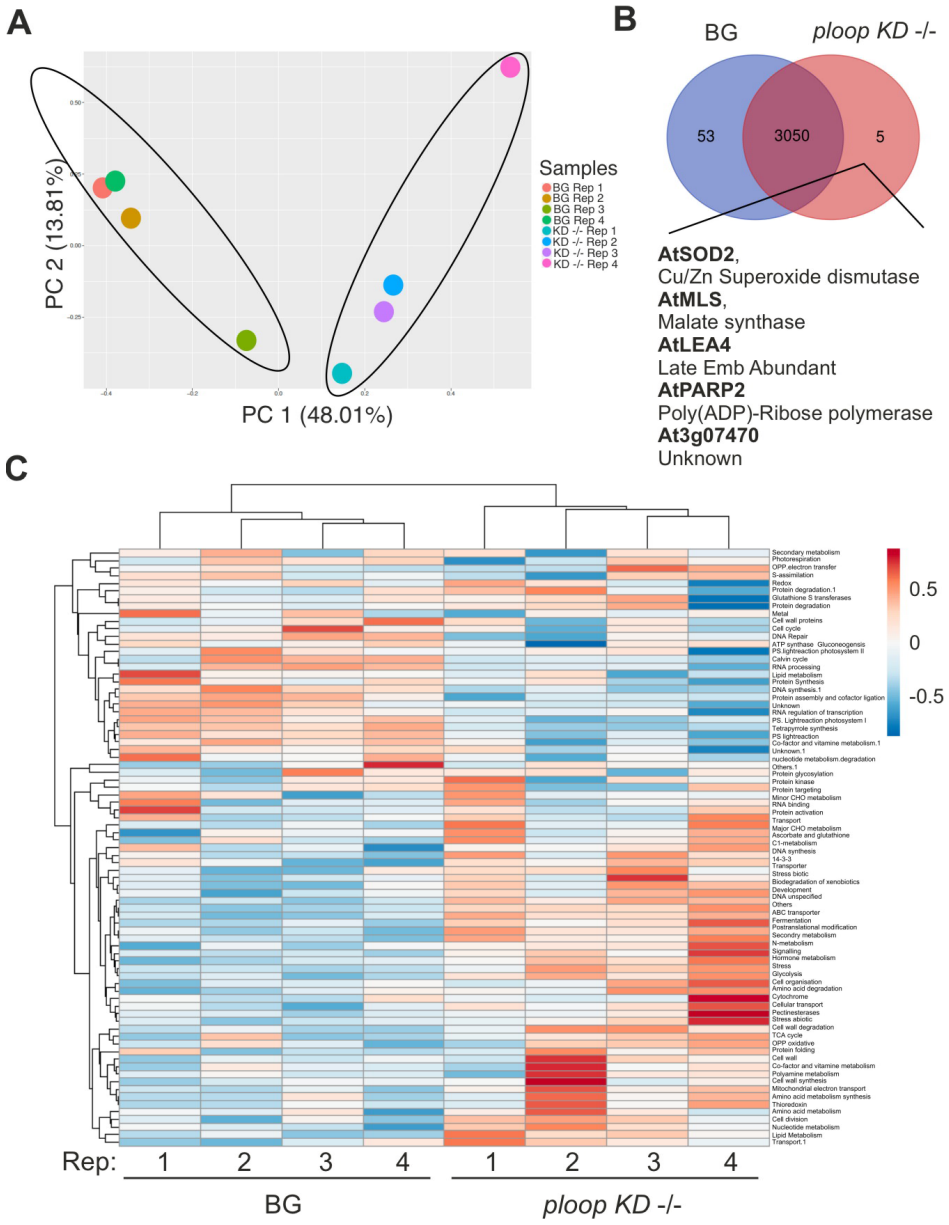

Figure 9. Global proteomic changes in the mutant

A. Principal component analysis of 4 biological replicates (Rep1-4) of BG and *ploop KD* -/- used in proteomic analysis. **B.** Venn analysis of identified proteome from 4 replicates of BG and *ploop KD* -/-. **C.** Biclustering analysis of identified proteins between 4 replicates according to their GO terms with blue and red indicating decrease and increase in abundance levels respectively.

Venn analysis of identified proteins resulted in 3050 proteins commonly present in both genotypes (Figure 9B). In addition, 53 proteins were uniquely detected in BG (Table 7) and five proteins (AtSOD2, AtMLS, AtLEA4, AtPARP2, and At3g07470) only in *ploop KD* -/- seedlings. Biclustering analysis of both BG and *KD* -/- genotypes together with the cumulative functional ontological grouping showed multiple groups

of proteins globally altered in the mutants (Figure 9C). Proteins involved in photosynthesis, protein synthesis and assembly, DNA synthesis, RNA processing were markedly decreased in mutants. In turn, the levels of proteins involved in both biotic and abiotic stress responses, hormone metabolism, signaling, ABC transporters and glycolysis were increased in the *ploop KD* -/- mutants relative to BG.

The averaged abundance values across replicates of proteins related to GO terms, ribosome biogenesis and prokaryotic and eukaryotic origin ribosomal proteins shows that RP and RBF stoichiometry is similar between both genotypes except for few individual cases of variable abundance (Appendix Figure 1). In terms of RBFs, out of 52 identifiable proteins, NOP10 (a H/ACA snoRNA complex protein), AT2G41380 (SAM-dependent methyltransferase), IMP4 (a snoRNP complex protein) were reduced in the mutant while in turn a BRIX domain containing protein, ARPF2 levels was increased in the mutant. In terms of prokaryotic origin ribosomes, the levels of plastid specific 50S ribosomal protein 6 (PSRP6) levels were relatively higher in the mutant. With respect to eukaryotic origin RPs, at least 21 proteins were relatively decreased in the mutant among 124 detected proteins. Taken together, the mutation led to allele's dosage dependent defects in terms of root and rosette developmental morphology and the severe KD -/-phenotype is exemplified by global proteomic changes in KD -/- seedlings.

Table 7. List of proteins distinctly present in BG seedlings

At Locus ID	Protein Description	Name[1]
AT5G17870	plastid-specific 50S ribosomal protein 6	AtPSRP6
AT2G42530	cold regulated 15b	AtCOR15B
AT5G58110	chaperone binding; ATPase activators	-
AT5G20935	Chloroplast NADH dehydrogenase assembly protein	AtCRR42
AT5G66550	Maf-like protein	-
AT3G10620	nudix hydrolase homolog 26	AtNUDX26
AT1G48610	AT hook motif-containing protein	-
AT4G16500	Cystatin/monellin superfamily protein	ATCYS4
AT5G15530	biotin carboxyl carrier protein 2	At BCCP2
AT3G52730	ubiquinol-cytochrome C reductase UQCRX/QCR9-like family protein	-
AT4G36430	Peroxidase superfamily protein	-
AT5G39210	chlororespiratory reduction 7	AtCRR7
AT3G10860	Cytochrome b-c1 complex, subunit 8 protein	-
AT1G77710	Ubiquitin-like, Ufm1	ATCCP2
AT1G01170	ozone-responsive-stress-like protein	-
AT5G20140	SOUL heme-binding family protein	AtHBP5
AT1G13730	Nuclear transport factor 2 (NTF2) family protein with RNA binding (RRM-RBD-RNP motifs) domain	-
AT2G05310	transmembrane protein	-
AT2G30695	bacterial trigger factor	-
AT3G05020	acyl carrier protein 1	AtACP1
AT4G39860	hematological/neurological-like protein	-
AT2G35390	Phosphoribosyltransferase family protein	-
AT5G26210	alfin-like 4	AtAL4
AT3G58990	isopropylmalate isomerase 1	AtIPM1
AT5G22580	Stress responsive A/B Barrel Domain	-
AT2G47580	spliceosomal protein U1A	AtU1A

AT1G32380	phosphoribosyl pyrophosphate (PRPP) synthase 2	ATPRS2
AT2G16850	plasma membrane intrinsic protein 2;8	AtPIP2, AtPIP3B
AT3G09150	phytochromobilin:ferredoxin oxidoreductase, chloroplast / phytochromobilin synthase (HY2)	ATHY2, ATGUN3
AT4G05520	EPS15 homology domain 2	ATEHD2
AT3G51820	UbiA prenyltransferase family protein	AtG4, AtPDE325
AT5G16810	Protein kinase superfamily protein	-
AT5G63140	purple acid phosphatase 29	ATPAP29
AT1G16410	cytochrome p450 79f1	ATBUS1,ATBUSHY1, ATSPS1, ATCYP79F1
AT4G36390	Methylthiotransferase	-
AT2G35795	Chaperone DnaJ-domain superfamily protein	AtPAM18-1
AT4G18970	GDSL-like Lipase/Acylhydrolase superfamily protein	AtGGL22
AT4G31780	monogalactosyl diacylglycerol synthase 1	AtMGD1, EMB2797
AT1G08530	chitinase-like protein	-
AT3G09250	Nuclear transport factor 2 (NTF2) family protein	-
AT3G25680	SLH domain protein	-
AT4G08360	KOW domain-containing protein	-
AT1G04970	lipid-binding serum glycoprotein family protein	AtLBR-1
AT3G51670	SEC14 cytosolic factor family protein / phosphoglyceride transfer family protein	AtPATL6
AT3G18240	Ribosomal protein S24/S35, mitochondrial	AtRPS24/35
AT3G20680	Domain of unknown function (DUF1995)	-
AT1G50140	P-loop containing nucleoside triphosphate hydrolases superfamily protein	-
AT1G06070	Basic-leucine zipper (bZIP) transcription factor family protein	AtBZIP69
AT4G20010	plastid transcriptionally active 9	ATOSB2, ATPTAC9
AT4G34020	Class I glutamine amidotransferase-like superfamily protein	ATDJ1C
AT3G13560	O-Glycosyl hydrolases family 17 protein	-
AT4G27180	kinesin 2	AtK2, ATKATB, ATKINESIN2
AT5G20360	Octicosapeptide/Phox/Bem1p (PB1) domain-containing protein / tetratricopeptide repeat (TPR)-containing protein	AtPHOX3

[1] The At Locus ID refers to the accession numbers, and names given according to the latest information on The Arabidopsis Information Resource (TAIR) in www.arabidopsis.org.

5.1.5 Mutated copies are linked to NOR regions of Chr 4

Next, I set out to determine the chromosomal location of the mutated copies. rDNA copies are majorly distributed in nucleolar organizing regions (NORs) of chromosomes 2 and 4, designated NOR2 and NOR4 with additional copies of rDNA known to be located on the Chromosome 3. Based on length polymorphisms of the 3'ETS region of the 45S rDNA, the A. thaliana Col-0 accession's rDNA copies have been distinguished into for major variants, VAR1 to VAR4 (Figure 10A). These variants are distributed unevenly across two NORs with NOR2 containing VAR1 and VAR3 while NOR4 containing VAR2, VAR3 and VAR4. The Chromosome 3 copies of rDNA are only known to be associated with VAR4. While there are further subtypes for each variant that varies within *A. thaliana* accessions, VAR1 and VAR4 can act as specific markers for corresponding chromosomes. Using mutation specific forward oligo (Mut-F) and a reverse oligo specific to 3'ETS that can distinguish VAR1-4 based on the polymorphism on three genotypes (BG, KD +/-, KD -/-), the PCR products resulted in specific bands unique to KD +/-and KD -/- genotype (Figure 10B). The KD -/- product was further cloned, and independent clones were sequenced to obtain VAR profile

associated with the mutation. The sequencing analysis showed that among n=33 clones (Figure 10C), the mutations were only correlated with VAR2, VAR3 and VAR4, all of which are associated with NOR4 of Chr4. However, this analysis did not detect a single clone corresponding to VAR1 polymorphism, marker for NOR2 of Chr2.

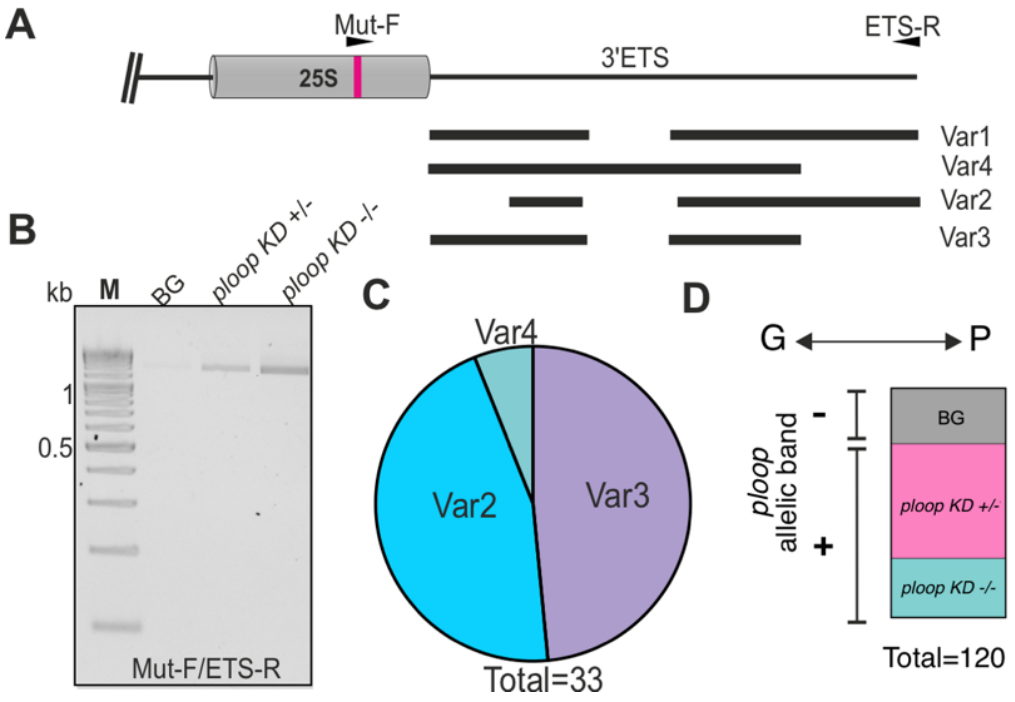

Figure 10. Mapping of mutational locus and its phenotypic correlation

A. Schematical distribution of rDNA' 3'ETS polymorphism and location of oligos for the PCR analysis. **B.** PCR products of three genotypes resolved on 2.5% TTE gel with indicated oligos on panel A. **C.** Sequencing of independent clones of panel C on *ploop KD* -/- and subsequent mapping to their VAR subtypes. **D.** Summary of Genotype-phenotype correlation of randomized 120 seedlings based on the phenotypical segregation (Appendix Figure 2A) as in Figure 8A and subsequent genomic analyses for presence (denoted +) or absence (denoted -) of ploop allelic band on genomic DNA PCR with Mut-F and 25S-R oligos (Appendix Figure 2B)

Furthermore, the mutation-specific PCR analysis was employed on the back-crossed segregating progenies to establish the genotype-phenotype correlation. The randomized 120 seedlings phenotypically segregated as BG-like (29), KD +/- (60), KD -/- (31) plants at 1 2 DAS (Figure 10D, Appendix Figure 2A). The genomic DNA PCR was performed on these individuals using mutation allelic forward (Mut-F) and 25S-R reverse. All the BG-like (29) plants lacked mutation specific band (408 bp) but still

possessed ambiguous PCR run-through band. On the other hand, the respective KD +/- (60) and KD -/- (31) plants were all typified by the presence of specific mutation allelic band (Appendix Figure 2B) below the PCR run-through band. Taken together, these results show that the mutated versions of rDNA copies are located on NOR4 of Chr 4, and that the mutation (genotype) and the phenotype are segregated together.

5.1.6 NOR4 mutation led to compensation from NOR2 copies

Next, the profile of rRNA variants among three genotypes distinguished by their 3' ETS polymorphism were investigated. First, the 3'-ETS specific PCR was performed using the genomic DNA (Figure 11A). The VAR distribution pattern was largely consistent with previous studies and the quantification suggested, that there were no major changes within the genotypes. Overall, across genotypes, VAR1 remained the dominant type followed by VAR2 and VAR3 with VAR4 being barely detectible (Figure 11B). Subsequently, the same analysis was performed using the complimentary DNA, reverse-transcribed from equal amount of RNA of three genotypes (Figure 11C). In this assay, VAR 1 levels were consistently elevated at the KD +/- and KD -/- mutants. On the contrary, the levels of VAR 4 and VAR 2 were significantly reduced in the mutants. However, the levels of VAR 3 remained same across genotypes (Figure 11D). Based on the expression dyna mics of four variants during early seedling growth stages in wild-type, VAR1 is expressed through 1, 3, 6 and 15 DAS, but peaks at 3 DAS, and decline afterwards (Figure 11E). Later during adult developmental stages, in emerging apex tissues of BG and heterozygous tissues where the pointy leaf phenotype is prominent, the VAR 1 was moreover absent in BG, but was still expressed in *ploop KD* +/- plants indicating the consistent VAR1 ectopic expression in the mutant from early to adult stages (Figure 11F). This resulted in overall imbalance of rRNA variants distribution in the mutants in comparison to BG.

The ectopic expression of VAR1 is further ensued by global variations in single nucleotide polymorphisms (SNPs) across the rRNA region. The total RNA-seq analysis of 14 DAS BG and *KD* -/- seedlings revealed variations in the frequencies in comparison to reference rDNA sequence (Figure 11G). The SNP frequencies were up to 60% higher in the *KD* -/- at the 3'-ETS region while 5'ETS related SNP frequencies also varied between BG and *KD* -/- genotypes. More importantly, a SNP island associated with 3' region of 18S and 5S was also revealed in RNA-seq analysis.

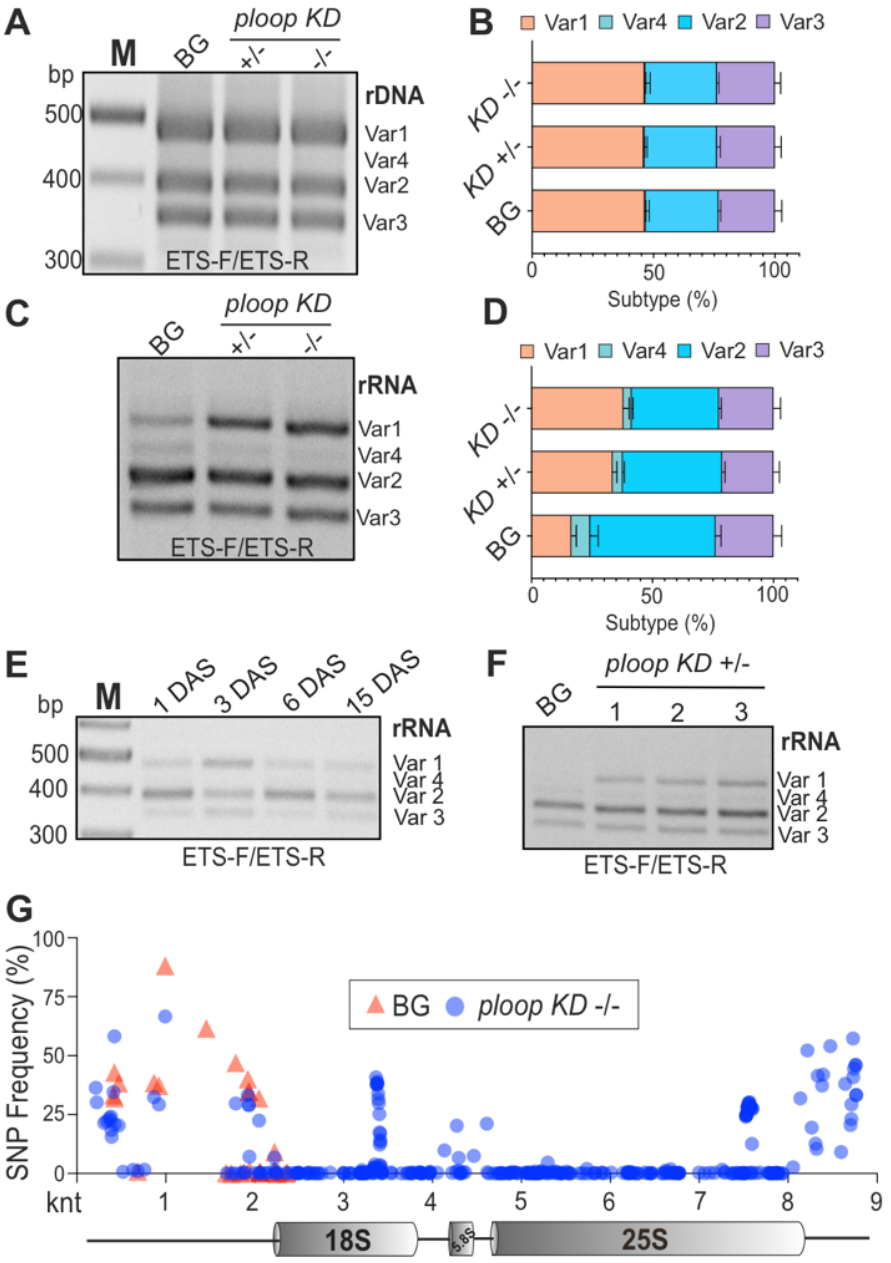

Figure 11. Dosage compensation and its related defects

A. 3' ETS-specific PCR on three genotypes with genomic rDNA template. **B.** Quantification of VARs distribution in panel A of four VAR subtypes in three genotypes. **C.** 3' ETS-specific PCR on three genotypes with cDNA template reverse transcribed from rRNA. **D.** Quantification of VARs distribution in panel C of four VAR subtypes in three genotypes. **E.** rRNA VARs expression levels in WT seedlings. **F.** rRNA VARs expression pattern in 35 days-old apex tissues of BG and *ploop KD* +/- tissues. **G.** The frequency of single nucleotide polymorphism for each position of ribosomal RNA derived from RNA-seq reads between BG (orange triangle) and *ploop KD* -/- (blue circle) mapped relative to rDNA reference sequence of Sims et al., 2021. The rRNA drawn below with knt (kilo nucleotide) indicates the length scale relative to transcription start site.

5.1.7 Mutants displayed pre-rRNA maturation defects

To verify if there are the any downstream effects of observed rRNA variant imbalance, the levels of high and low molecular weight pre-rRNAs were estimated in BG, *ploop KD* +/- and *KD* -/- mutants.

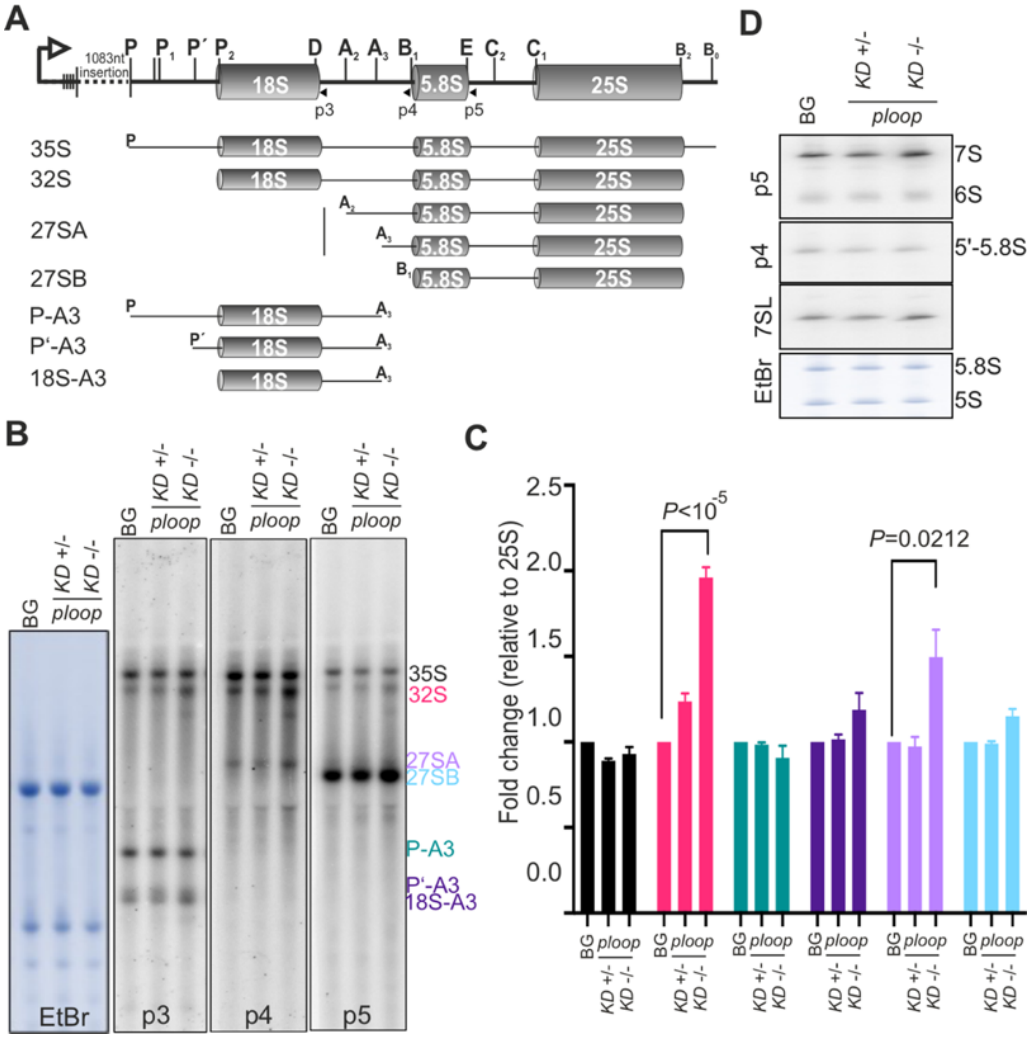

Figure 12. Analysis of pre-rRNA based defects in *ploop KD* mutants

A. Schematics of binding position of oligonucleotide probes (p3, p4, p5) to the pre-rRNA and the list of high molecular weight precursors identified after northern hybridization. **B.** Northern hybridization analysis of the total RNA from three genotypes with the indicated probes (bottom) and the EtBr staining on the left given as loading control. The identified precursors (colored) are given in right **C.** Quantification of each colored pre-rRNA precursors given in panel B relative to the 25S rRNA. (n=4 biological replicates) P-values indicate significance obtained with two-tailed unpaired student t-test **D.** Northern hybridization and probing of low molecular weight pre-rRNA precursor levels in BG, *ploop KD* tissues analyzed on 10% PAGE gel using p4 and p5 probes. 7SL was used as loading control.

The total RNA was hybridized with complementary radioactively labeled oligonucleotides (p3, p4 and p5) binding to the immature regions of ITS1 and ITS2 (Figure 12A) Combined probing revealed steady-state levels of seven high molecular weight pre-rRNAs with 35S and 32S detected by all probes, while other pre-rRNAs are specific to unique probes (Figure 12B). Upon normalization to steady state levels of radio-labeled 25S rRNA, the pre-rRNA levels were estimated in BG and *ploop KD* mutants (Figure 12C). The major primary transcript 35S was moreover similar across genotypes. Between the diagnostic precursors of major (P-A3) and minor pathway (32S), the levels of 32S in the KD -/- mutant was one-fold higher ($P < 10^{-5}$) than that of BG, while the P-A3 levels remain largely unchanged. The levels of theoretical downstream precursors of 32S, i.e., 18S-A3, 27SA ($P = 0.0212$) and 27SB followed similar trends to 32S, but not at similar level to 32S. With respect to low molecular weight pre-rRNAs (Figure 12D), probing with p4 and p5 did not reveal any obvious change in levels of corresponding 5'-5.8S, 6S and 7S precursors.

5.1.8 Mutated copies are not incorporated in polysomes

To deduce the distribution of mutated rRNA copies on the corresponding ribosomal pre-subunits, their distribution was analyzed on the maturing pre-ribosome and polysome population after density-gradient fractionation of BG and *ploop KD* +/- floral tissues. The absorbance profile of lysates after density-gradient separation were measured from top to bottom, beginning with lower towards higher density (Figure 13A). The profile revealed proper separation of peaks consisting of free pool, 40S, 50S, 60S, 80S monosomes and polysomes on both BG and *ploop KD* +/- samples. RNA and protein were purified separately from the density fractions. From the purified RNA, RT was performed with 25S specific oligo but PCR with mutation specific forward primer to detect the distribution of mutated rRNA copies (Figure 13B).

The PCR revealed BG tissues still contained a PCR run-through product, predominantly through 60S to all polysome fractions, revealing the forward oligo's poor fidelity in the absence of specific product. In case of *ploop KD* +/- tissues however, there was a clear band appearing below the run-through band corresponding to the deletion of 20 bp indicating the specific-mutated-allelic product. The distribution of this mutated product shows that they were majorly associated with the free pool fractions and 50S. Beyond 50S, while a weaker band could still be detected in other fractions

of 60S to lower order polysomes, the analysis revealed higher order polysomes did not contain the mutated product, suggesting their non-association with these fractions.

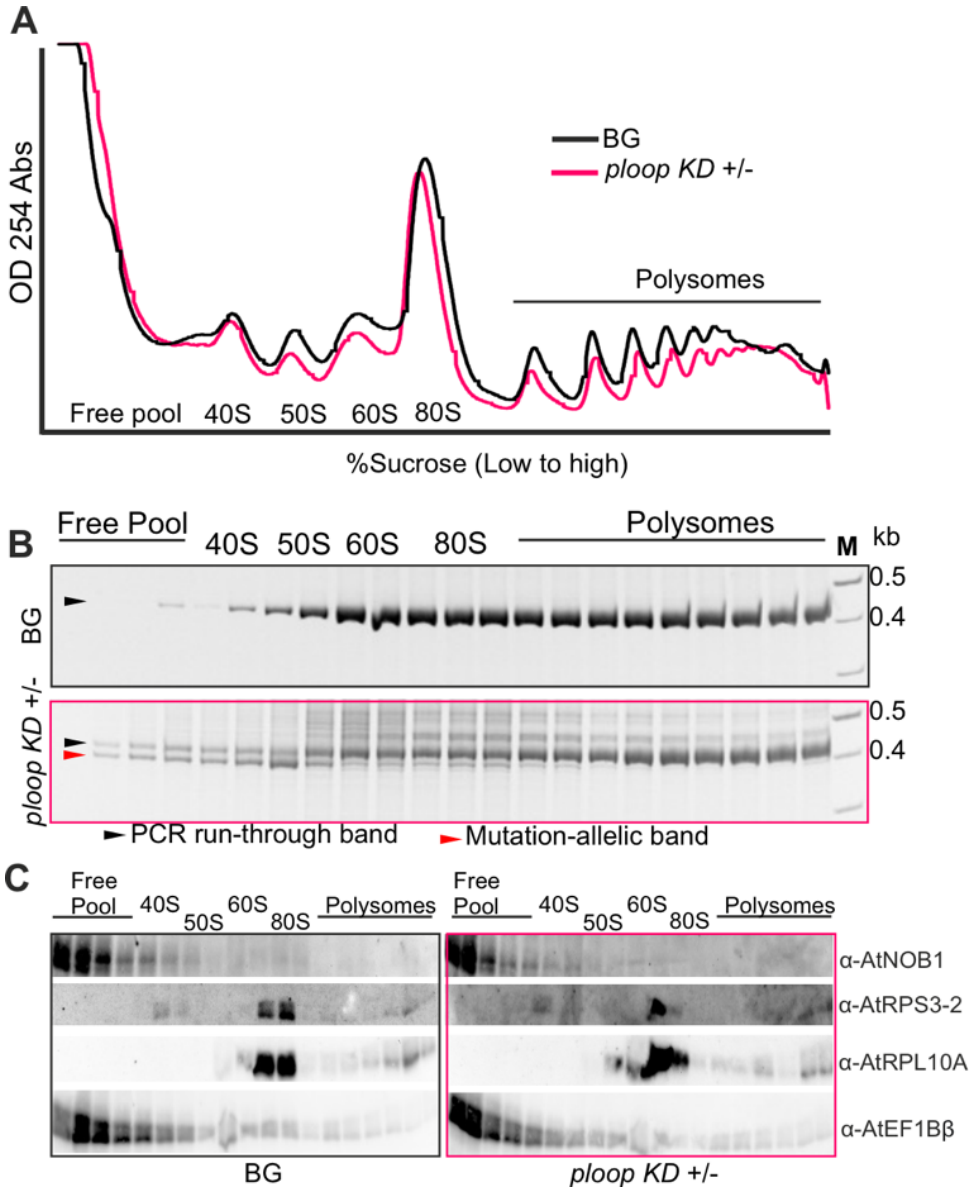

Figure 13. Analysis of mutational copies distribution in ribosomal complexes

A. Absorbance profile at 254 nm of floral tissues from BG and *ploop KD* +/- plotted with time of detection from top to bottom subsequent to sucrose-density gradient centrifugation. **B.** The RNA from the according fractions at panel A of both genotypes purified, reverse transcribed with 25S rRNA-specific oligo and the PCR products with mutation specific forward oligo and 25S-specific reverse oligo resolved in 12% Native PAGE gel. The black arrow denotes PCR-run through product and the red arrow indicates mutated rRNA product. **C.** The protein from the fractions at panel A of both genotypes were resolved on 10% SDS-PAGE and blotted with indicated antibodies.

In addition, I analyzed the fractions to determine the subunit identity by performing immunoblotting against specific antibodies of a ribosome biogenesis factor (NOB1), small subunit ribosomal protein (RPS3-2), large subunit ribosomal protein (RPL10A) and a translation elongation factor (EF1Bβ) (Figure 13C). Probing with α-NOB1 and α-EF1Bβ showed that they are mostly concentrated at the free pool fractions on both genotypes, while polysome fractions contained additionally EF1Bβ signals. In case of RPs, the probing with α-RPS3-2 resulted in unique signal at 40S fractions in addition to 80S, while probing with RPL10A resulted in predominant signal at 80S and weaker signals at polysomes and 60S fractions. Overall, the signals corresponded to the expected distribution of each of the tested proteins except for the observed weaker signals of RPS3-2 in the polysome fractions. In addition, the ribosomal subunit profiling of BG and *ploop KD* +/- with silique tissues, and subsequent RT-PCR and immunoblotting analysis (Appendix Figure 3) was performed. Overall results indicated similar pattern of absence of mutated rRNA segments on the polysome fractions while accumulating on free pool and maturing subunit fractions.

5.1.9 Autophagic flux is elevated in the severe mutant class

Given that major copies of mutated rRNAs are absent in polysomes, I postulated that the autophagic turnover rate may be elevated in the *ploop KD* -/- genotype due to defective immature or matured-but-nonfunctional ribosomes produced as a result of mutation itself. The autophagic levels in the mutant was analyzed by expressing a fluorescent reporter transgene, GFP-ATG8e. Autophagy related protein, ATG8e forms the structural component of autophagosomes, and it is routinely used for marking the autophagosomes. While the full-length protein is localized to cytoplasm under control conditions, the elevated levels of autophagy can mobilize the fusion protein to the vacuoles. Consequentially, the free N-term GFP residue upon internalization by the vacuoles remains resistant to vacuolar hydrolases and proteases and hence free GFP formation is the indication of turnover of these proteins to the autophagosomes (Figure 14A).

In the BG plants, the GFP signal was mainly localized to the cytoplasm with fuzzy pattern observed through out the root tip region. On the other hand, in *ploop KD* -/- genotype, the GFP signal was closely packed forming dense structures reminiscent of smaller vacuolar like structures throughout most cells (Figure 14B). Another

indication of measuring the autophagic turnover with the GFP signals is through immunoblotting the ratio of full length GFP-ATG8e and the free GFP (Figure 14C). In the BG genotype, the full length GFP-ATG8e signal was the dominant form accompanied by the slight intensity of free GFP signal. In contrast, the full length GFP-ATG8e form was barely detectable in the *ploop KD* -/- seedlings with free GFP signal predominating the overall distribution pattern. The quantification of the observed signals (Figure 14D) after normalizing with HSC70 indicated that in comparison to BG genotype, the ratio of free GFP was at least three-fold higher while the fused GFP-ATG8e ratio was at-least seven-fold lower in the *ploop KD* -/- seedlings.

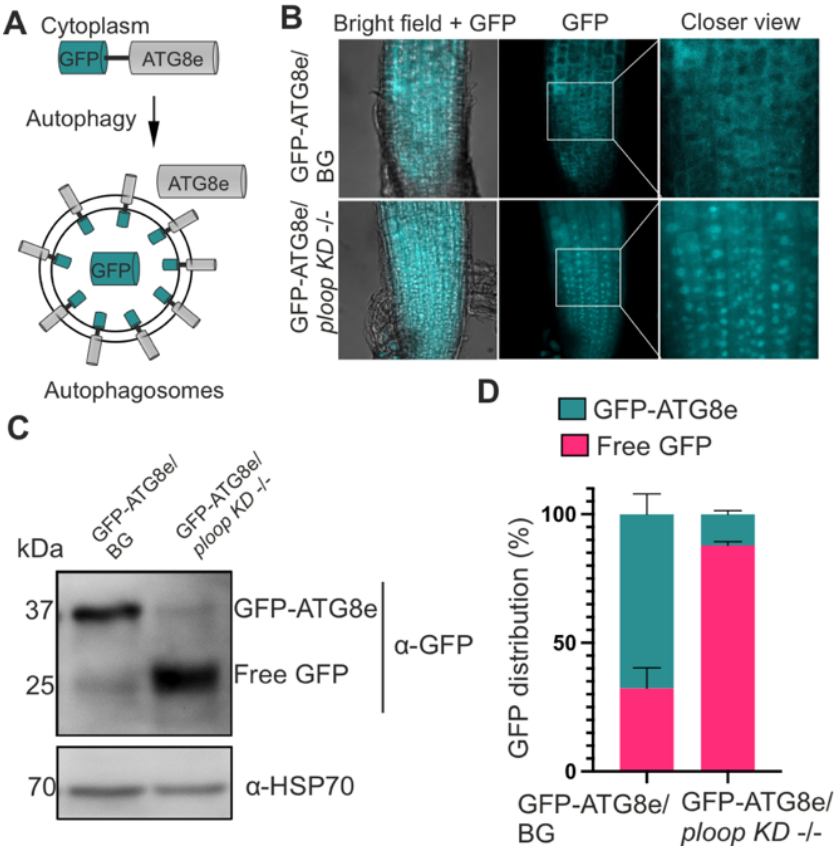

Figure 14. Status of autophagic flux in *ploop KD* mutants

A. Schematics of GFP-ATG8e fusion protein localization under routine growth and autophagic conditions. **B.** Localization of GFP signals from GFP-ATG8e fusion proteins in BG and *ploop KD* -/- seedlings. **C.** Immunoblotting analysis with Anti-GFP antibodies of GFP-ATG8e levels in BG and *ploop KD* -/- seedlings. Anti-HSC70 blotting served as loading control. **D.** Quantification of full length GFP-ATG8e and free GFP signals from panel C represented to the total levels after normalization to HSC70 loading control (n=3 biological replicates)

5.1.10 Small RNAs associated with P-loop region are unaffected

Around the Cas9 targeting region of 25S rDNA, up on re-analysis of previous suspension culture small RNA-seq study (Streit et al., 2020), a novel 139 nt small nuclear RNA encoded within the Crick-strand of rDNA named herein, SnRn5 (Figure 15A, B) was identified.

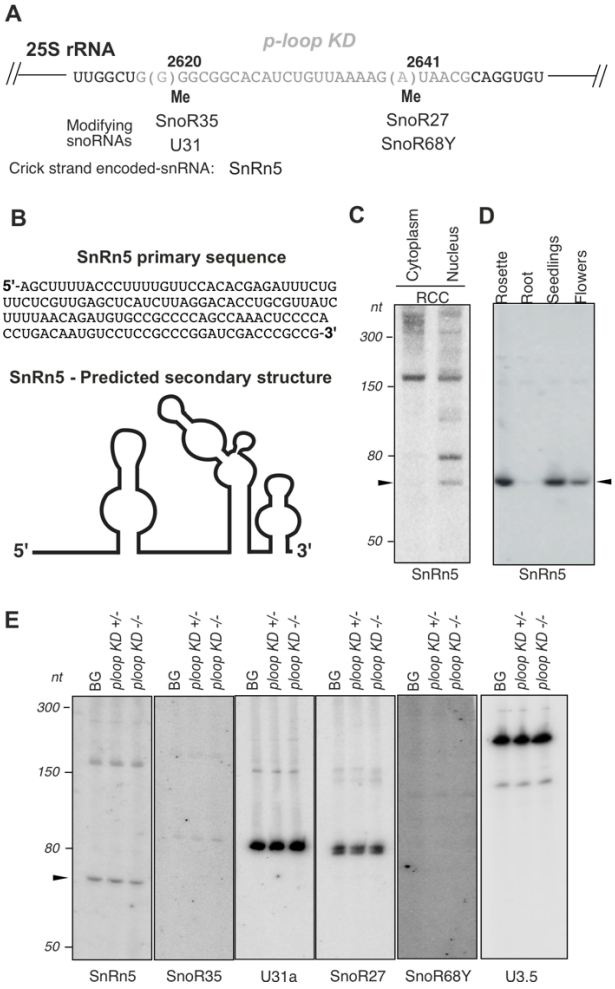

Figure 15. Trans and cis-derived snoRNAs on the P-loop region

A. Small RNAs that are cis-derived and trans-acting in the mutated P-loop region of 25s rDNA/rRNA with grey sequence indicating mutated region and numbers indicating position relative to 25S. Me denotes methylation of residues achieved by transacting snoRNAs indicated below. **B.** Primary sequence and secondary structure of the snRn5 as predicted by RNAstructure (https://rna.urmc.rochester.edu) **C.** SnRn5 expression in fractionated cytoplasmic and nuclear extract of root cell cultures (RCC). **D.** SnRn5 expression in plant tissues; rosette, root, seedlings, and flowers. **E.** Expression levels of snRn5 and snoRNAs targeting the mutagenized region in BG and *ploop KD* mutants.

First, the existence of SnRn5 transcript was corroborated in suspension culture with cytoplasmic and nuclear fraction using northern hybridization and led to detection of a >150 nt transcript on both fractions, along with 2 distinct transcript around 80 nt RNA marker on nuclear fraction (Figure 15C). Probing with total RNA derived from four tissue types, rosette, root, seedlings, and flowers further confirmed the expression of SnRn5 even in plant tissues and the size corresponded to the nuclear fraction specific -80 nt transcript (Figure 15D). In addition, the mutated region contained two residues, G2620 and A2641 that are methylated by at least four known C/D box snoRNAs, SnoR35, U31, SnoR27 and SnoR68Y (Figure 15A). I postulated whether the cis-mutation of rDNA regions has caused inadvertent effects on the trans-regulatory snoRNAs. Accordingly, I tested the expression levels of SnoR35 and U31 targeting G2620 methylation; SnoR27 and SnoR68Y targeting A2641 methylation in 15 DAS BG and the *ploop KD* plants (Figure 15E). While the U31a and SnoR27 are strongly expressed relative to weakly expressed SnoR35 and SnoR68Y, there were no obvious differences at the transcript levels of the targeting snoRNAs associated with the mutated rRNA segment.

5.2 Redefining of pre-rRNA maturation schematics in plants

Plant pre-rRNA maturation schemes have been revised to include both pathways that are dominant in yeast, 5'ETS-first cleavage and humans, ITS1-first cleavage for their biogenesis. In order to investigate the further diversified maturation schemes if any that are specific to plants, precursor-based screening was performed on RCC and growth conditions that favor the formation of such novel precursors.

5.2.1 RCC contains ITS2-derived precursor in control conditions

Upon revisiting the results of total RNA blots from highly dividing RCC and flower tissues (Weis, 2015) probed with extensive number of complementary probes against 5'ETS region (p23, p22, p2); ITS1 region (p3, p42, p4), ITS2 region (p5), a specific band resembling of yeast 24S migrated below the mature 25S rRNA and above P-A3 precursor, and yet its origin and cleavage sites remained unknown. A similar precursor in addition also appeared upon auxin treatment in a mutant lacking a factor, Involved in rRNA processing (IRP) 7 (Palm et al., 2019). To deduce the precise terminus of this precursor, a circular RT-PCR approach was taken with three fractionated total RNAs from cytoplasm, nucleus, and nucleolus of RCC. RT was conducted using cRT specific to 18S region, and PCR oligos were positioned to exclude the dominant P-A3 precursor (Figure 16A). PCR with cRT-R and cRT-F binding downstream of A3 site thus allowing the amplification of pre-rRNAs resulted in a predominant band above 400 bp specifically in nucleus and nucleolus fraction (Figure 16B). Upon cloning and sequencing (n=20) of this PCR product and further mapping to the pre-rRNA, this precursor is shown to contain a common 5' precursor ending with P-site of 5'ETS. On the 3' side of the precursor, the ends were mapped to multiple positions of the ITS2 region. At least 1 clone possessed precise C2 site, and multiple derivatives relative to C2 site: C2-9 nt, C2-15 nt, C2-17 nt (2X), C2-19 nt(4X), C2-20 nt, C2-22 nt (2X), C2-23 nt (2X), C2-32 nt, C2-56 nt, C2-66 nt (2X), C2-88 nt and C2-107 nt (Figure 16C).

Moreover, roughly half of these precursors (8/20) were found to be terminally mono or polyadenylated in orders A_1 to A_{15} marked by asterisks. Resulting from the C2 derived precursor identification in RCC tissue, the maturation schemes were revised accordingly wherein the primary 35S transcript can undergo three means of first cleavage steps resulting in three unique intermediate wherein, 32S result from

5'ETS-first; P-A3 result from ITS1-first and P-C2 result from ITS2-first cleavage (Figure 16D).

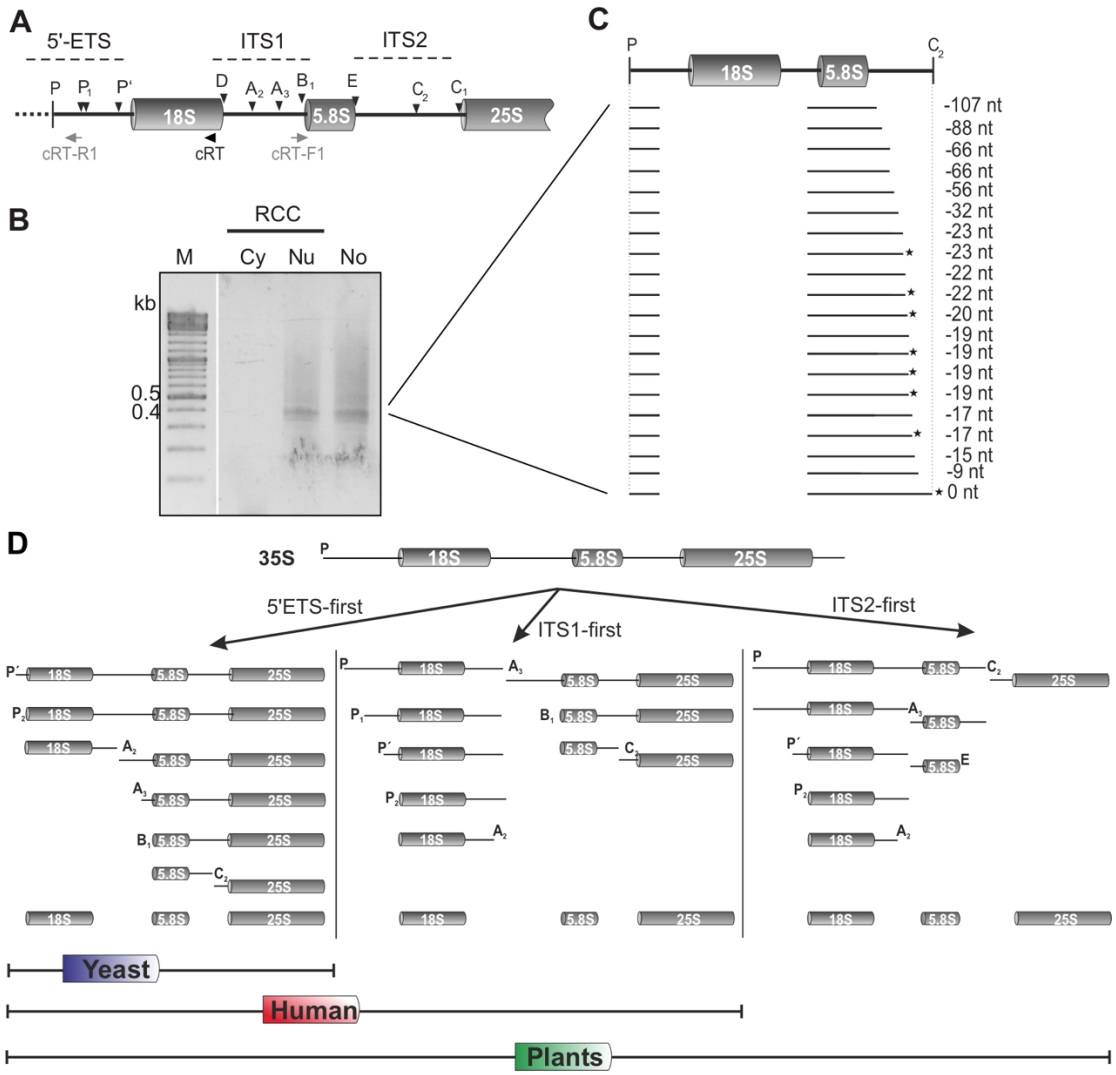

Figure 16. Identification and fine mapping of ITS2-first cleavage precursors

A. Location of binding positions of cRT and PCR oligos to fine map precursors detected below mature 25S rRNA in Benny Thesis **B.** The PCR products obtained after cRT-PCR from three compartments (denoted as Cy, cytoplasm; Nu, nucleus; No, nucleolus) of fractionated RCC electrophoresed on 2.5% TTE gel. The marker lane on the left is separated to indicate the in between lanes not shown **C.** Cloning and sequencing (n=20) of Nu and No specific band and further mapping of the jointed ends relative to 5' P-site and 3' C2 site. The numbers indicate heterogeneous ends relative to C2 site and stars indicate presence of non-templated adenylations. **D.** The redrawn schematics of pre-rRNA maturation in Arabidopsis thaliana based on the identification of ITS2-first cleavage derived precursors in RCC in control conditions marked by unique precursor for each maturation but overlapping paths compared with Yeast and Human models. Adapted from Palm et al., 2019.

5.2.2 Viable RRP5 mutant display ITS2-derived pre-RNA defects

The ITS2-first cleavage path has been reported in Yeast and Human with a similar derivative precursor semblance with their denominative 24S and 30SL3' respectively. In both cases, a mutant deficient in ribosome biogenesis factor RRP5 resulted in accumulation of these precursors. In plants, *rrp5* mutation resulted in embryo lethality. To deduce the commonality of this precursor formation in plants, a mutant lacking 30 bp (hence 10 amino acids at the 3' terminus of RRP5, named *rrp5Δ10*), as a result of failed T-DNA insertion event (unpublished) was obtained from Dr. Christian Wenzl (Universität Heidelberg). The mutant possessed WT-like phenotype under control growth conditions.

The total RNA from the mutant and wild type floral tissues were used to probe for the pre-rRNA maturation defects. Upon probing with complementary probes (p3, p42, p4 and p5) to detect major HMW precursors (Figure 17A), the 35S primary transcript was found to be overly accumulated in the mutant. More importantly, a similar precursor to ITS2-derived, P-C2 appeared as a high-density band in the mutant but at slightly lowered position (<P-C2) than usual P-C2 migration pattern with probes p3, p42 and p4. Nevertheless, this band signal was not detected with p5 probe, unlike P-C2. Additionally, p3 probing resulted in detection of 20S in the mutant while it is undetectable in WT plants. Quantification of pre-rRNA levels relative to 25S rRNA radioactive probing was used to estimate the order of accumulation patterns between *rrp5Δ10* and WT (Figure 17B). Accordingly, 35S accumulation was found to be 4-fold and 20S was found to be 8-fold accumulative in the mutant. Most of all, the novel <P-C2 precursor was found to be accumulating at 80-fold levels in the mutant. Besides the accumulative pattern, the 27SA precursor was undetectable in the mutant alongside the cumulative lowered levels of P'-A3/18S-A3 precursors. In addition, the levels of LMW precursors were probed using p23, p4 and p5 (Figure 17C). Probing with p23 resulted in identification of 3 distinct P-P' fragments while in mutant these fragments were at lowered levels. The other complementary probes did not result in major changes at the low molecular weight precursors of 5'-5.8S, 6S and 7S.

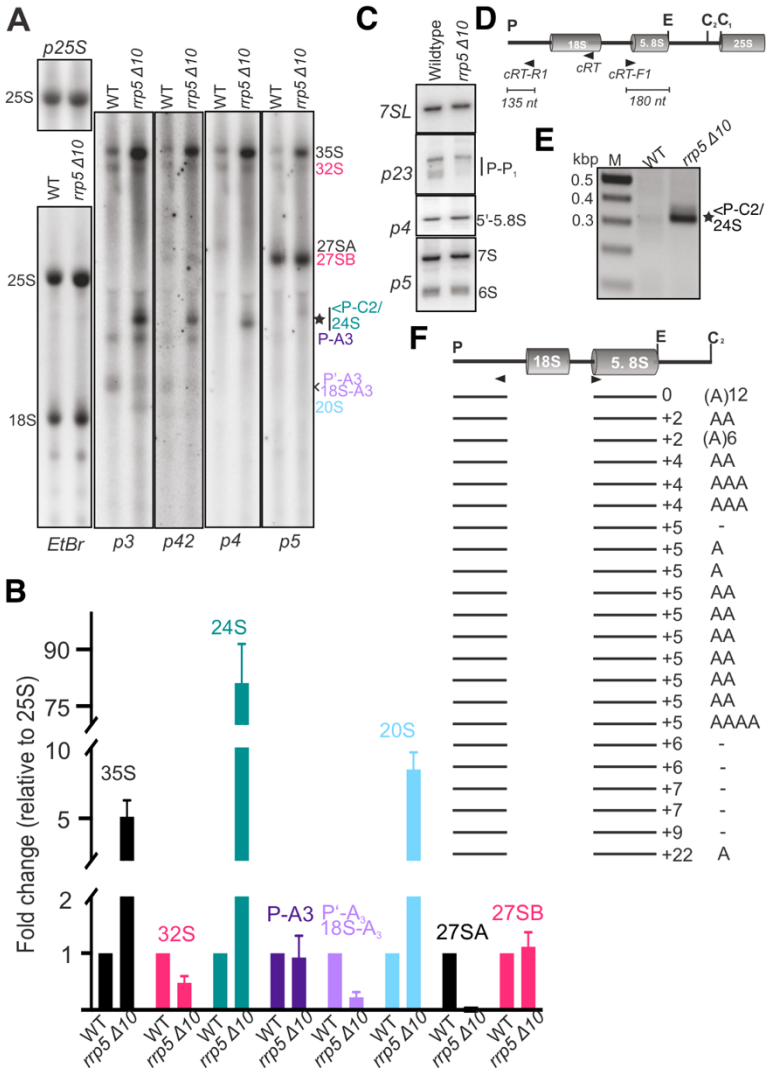

Figure 17. Characterization of a factor controlling ITS2-first maturation path

A. Northern hybridization analysis of the total RNA from WT and *rrp5Δ10* mutant with the indicated probes (bottom) and EtBr staining on the left in addition to probing with p25S for 25S rRNA. served as loading control. The identified precursors (colored) are given in right **B.** Northern hybridization and probing of low molecular weight pre-rRNA precursor levels in WT and *rrp5Δ10* mutant analyzed on 10% PAGE gel using p23, p4 and p5 probes. 7SL was used as loading control. **C.** Quantification of each colored pre-rRNA precursors given in panel A relative to the 25S rRNA (n=3 biological replicates) **D.** Binding positions of oligos for cRT-PCR on pre-rRNA regions. **E.** The PCR products obtained after cRT-PCR from WT and *rrp5Δ10* mutant electrophoresed on 2.5% TTE gel. **F.** Cloning and sequencing (n=22) of mutant-specific band and further mapping of the jointed ends relative to 5' P-site and 3' E site. The numbers indicate additional nucleotides relative to E site alongside non-templated adenylations.

To deduce the variations in nature of P-C2 derived precursors due to its smaller size in agarose gel mobility, between RCC and the *rrp5Δ10* mutant, cRT-PCR was employed to deduce the nature of this specific precursor (Figure 17D). Amplification of circularized RNA-derived complimentary cDNA using the same RT and PCR oligos (Cite previous figure and results) resulted in a unique band (-315 nt) formation abundantly with total RNA samples of *rrp5Δ10* mutant (Figure 17E). The cloning and sequencing of these bands in independent clones (n=22) resulted in precursors mapped with a precise 5' deterministic P site, and multitude of 3' sites conserved around E site of 5.8S itself. The heterogeneity at the 3' sites amounted to 5.8S (E-site) (1X), 5.8S+2 nt (2X), 5.8S+4 nt (3X), 5.8S+5 nt (10X), 5.8S+6 nt (2X), 5.8S+7 nt (2X), 5.8S+9 nt (1X) and 5.8S+22 nt (1X) with A-tailing lengths of A_1 to A_{12} thus explaining the reduced size of P-5.8S (yeast 24S) in the mutant as opposed to P-C2-like precursors in RCC (Figure 17F).

5.3 Dynamics and thermal susceptibility of rRNA maturation in plants

Having determined a novel processing path at the control growth conditions, albeit in RCC, the conditions in which this multi-maturation becomes pre-dominant was investigated further. Moreover, this maturation path's role remained unknown in Arabidopsis plants until exposure to high growth temperature resulted in formation of similar ITS2-like precursors (Schroll, 2019). With three unique diagnostic precursors resulting from 35S pre-rRNA splitting paths, the overall processing kinetics of these pathways and the influence of high temperature growth conditions on these processing paths were investigated.

5.3.1 Pulse labeling reveals rate limiting steps in rRNA production

Between wild-type and mutants of biogenesis factors involved in pre-rRNA maturation, multiple pre-rRNA intermediates that have been identified so far are summarized (Appendix Figure 4). Pulse-labeling of pre-rRNA synthesis was performed between 15 - 120 min in increasing time points to deduce the dominant pre-rRNA intermediates in root cell culture (RCC) and 4d old seedlings using radioactive tracer, ^{32}P-orthophosphate ($^{32}PO_4$) (Figure 18A). The electrophoresed total RNA on a high-resolution agarose gel resulted in separation of high molecular weight precursors, with primary transcript 35S identified even after 15 min in RCC. The same pulse-labeling assay performed with *xrn2* mutant seedlings defective in 5' ladder sequence maturation led to accumulation of precursors larger than 35S thus confirming the primary transcript identity. Below 35S, the minor pathway diagnostic precursor, 32S was readily detectable at 30 min in RCC while the same transcript was identified at 45 min in WT seedlings. Besides the 32S, the major pathway diagnostic precursor, P-A3 was detectible at the same time point as 32S in RCC while in WT seedlings, the P-A3 was only faintly present during later time points. Consequently, the common large subunit precursor between both pathways, 27SB appeared to be dominant as 35S after 60 min in RCC. In seedlings, this precursor was found to be more abundant than even 35S precursor at 60 min marking its dominance at the pre-rRNA level. Concerning the mature rRNAs, the maturation product of 27SB, the 25S was reliably detected at 90 min in RCC and 60 min in WT seedlings. The 18S rRNA was apparent in RCC and seedlings at same 45 min of pulse analysis. Taken together, the RCC

and seedlings exhibited similar pattern of precursor formation with seedlings displaying lower uptake efficiency.

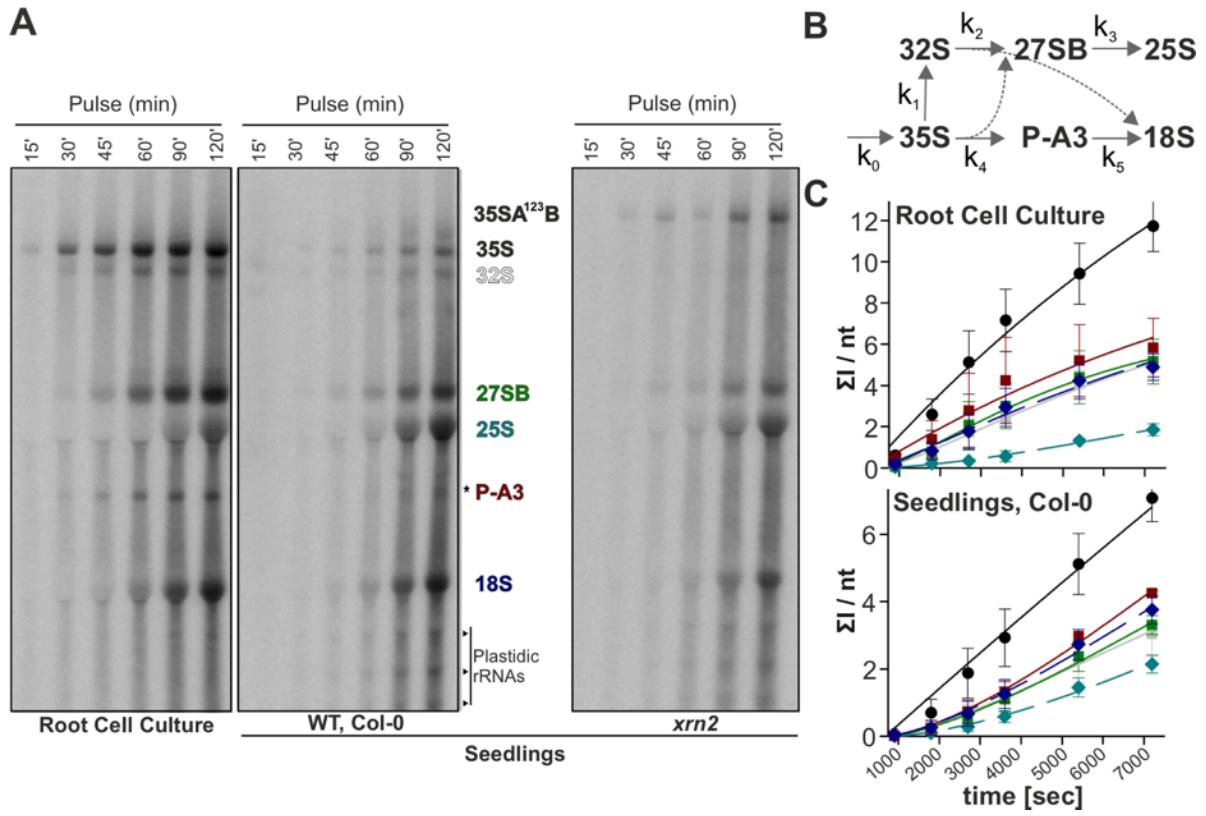

Figure 18. Pulse-labeling analysis of pre-rRNA synthesis in RCC and seedlings

A. Autoradiograph of electrophoresed high molecular weight RNAs after pulse-labeling of ribosomal RNA synthesis for the indicated times in root suspension cell culture (RCC) and 4d old WT and *xrn2* seedlings is shown. **B.** Reaction regime inferred based on the dominant intermediates and the rate constants presented in Table 8. **C.** Radiation signal quantification of panel A for calculation of total radioactivity of a species of pre or mature rRNA based on the number of nucleotides according to color coding on panel A. Error bars are standard deviation of three experimental values and the lines are derived throgh least square fit analysis based on equation 1 and 2 (methods). *xrn2* blots were not included for this analysis. Adapted from Shanmugam et al., 2021.

Based on the identifiable precursors upon pulse-labeling and to accurately quantify the variations within the tissue types, a regime for maturation schemes (Figure 18B) was developed to analyze the processing rates of each precursor according to least square fit method using equations 1 and 2 described in Methods (Figure 18C, Table 8). Based on the radiotracer incorporation rate, the synthesis was at least two-

fold higher in RCC than in seedlings. The 35S processivity rate to major P-A3 and minor 32S precursors (k_1 vs k_4) are vastly comparable in RCC, while in seedlings, the rate of 32S dependent minor pathway was five-fold higher than the major diagnostic precursor. On the comparison of synthesis and processing rates of SSU diagnostic precursor, the P-A3 (k_4 vs k_5), the processing rates were two-fold slower in both RCC and seedlings. However, the rate constant of P-A3 synthesis was approximately ten-fold higher in RCC than seedlings. In terms of LSU mature 25S rRNA synthesis (k_3), both tissues exhibited similar rates while the synthesis of 18S rRNA was at least ten-fold slower in seedlings than RCC (k_5).

Table 8. Rate constants of control and heat stressed pre-rRNA synthesis.

Con	Tissue	k_0 [sec^{-1}]	k_1 [sec^{-1}]	k_2 [sec^{-1}]	k_3 [sec^{-1}]	k_4 [sec^{-1}]	k_5 [sec^{-1}]	Figure
P	RCC	$(0.9 \pm 0.2)*10^{-4}$	$(9.1 \pm 0.9)*10^{-4}$	$(3.0 \pm 0.8)*10^{-4}$	$(1.2 \pm 0.9)*10^{-4}$	$(11 \pm 3)*10^{-4}$	$(6 \pm 1)*10^{-4}$	Figure 18
C	RCC	-	$(3 \pm 1)*10^{-4}$	$(1.5 \pm 0.5)*10^{-4}$	$(1.2 \pm 0.4)*10^{-4}$	$(4 \pm 1)*10^{-4}$	$(2 \pm 1)*10^{-4}$	Figure 23
C/H	RCC	-	$(1.6 \pm 0.6)*10^{-5}$	$(1.9 \pm 0.7)*10^{-4}$	$(2.4 \pm 0.9)*10^{-5}$	$(3.4 \pm 0.2)*10^{-4}$	$(1.6 \pm 0.4)*10^{-4}$	Figure 23
P	PL 4d	$(0.3 \pm 0.1)*10^{-4}$	$(5.4 \pm 0.9)*10^{-4}$	$(2.5 \pm 0.6)*10^{-4}$	$(1.0 \pm 0.1)*10^{-4}$	$(9 \pm 3)*10^{-5}$	$(3.9 \pm 0.7)*10^{-5}$	Figure 18
H	PL 14d	-	$(2.2 \pm 0.3)*10^{-5}$	$(3.8 \pm 0.9)*10^{-4}$	$(2.8 \pm 0.9)*10^{-4}$	$(2.4 \pm 0.4)*10^{-5}$	$(2.2 \pm 0.7)*10^{-5}$	Figure 22

Rate constants (k_0 to k_5) of precursors observed in the maturation scheme (Figure 18B) was calculated based on standard deviation values of three biological replicates. 'Con' denotes the experimental condition of analysis in which P, Pulse labeling; C, Chase; C/H, Chase at 38°C and H, heat stressed at 38°C. RCC and PL indicates root cell culture and plant seedlings with age in d. The corresponding experimental figures which they arise from, are indicated on the right. Adapted from Shanmugam et al., 2021.

Worth mentioning, compared to steady state level intermediates detected by northern blotting and hybridization, the other 27SA2/A3 and P'-A3/18S-A3 were not detectible in the pulse labeling assays. From the combined stock of all precursors, only four appears to be rate-limited attributed due to their sheer abundance in both pulse and overall steady state levels. More importantly, even in RCC, the supposed ITS2-derived precursor, P-C2 was not detectible in pulse chase analysis signifying its underwhelming role in given growth conditions.

5.3.2 High growth temperature alters pre-rRNA levels

To analyze the effect of high growth temperature on pre-rRNA maturation schemes, Arabidopsis rosette containing plants were exposed to series of growth temperatures ranging between optimum (NC, 22°C) and bandwidths of sub-optimal growth temperatures (30°C, 33°C, 36°C, 39°C, 42°C) for defined duration of 1h.

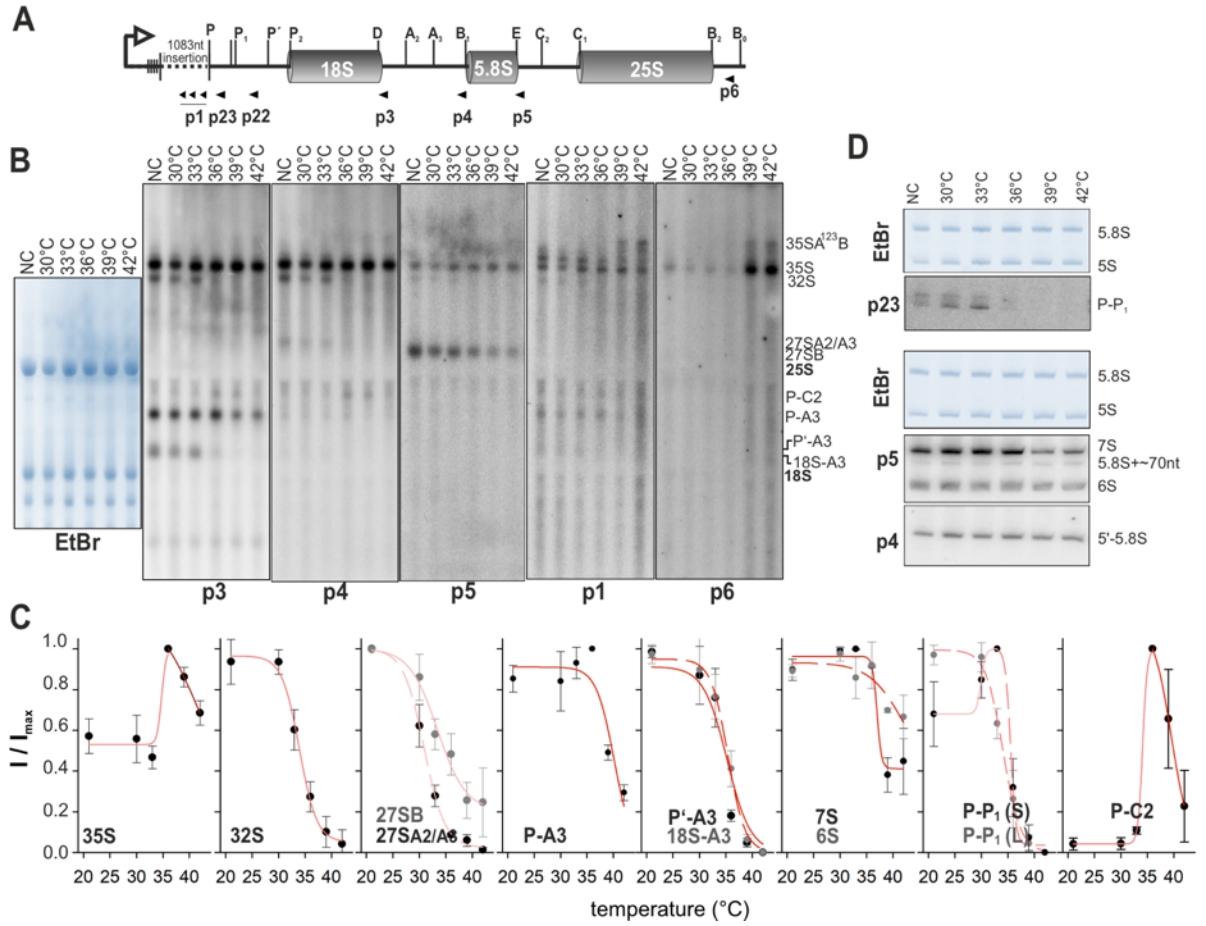

Figure 19. Role of growth temperatures in Arabidopsis pre-rRNA maturation

A. Schematic of probe binding location indicated on the primary pre-rRNA of *A. thaliana* **B.** Plants that were 14d-old were subjected to the temperatures indicated for 1h. Northern hybridization analysis of HMW RNA from plants subjected to indicated temperatures with indicated probes at the bottom. EtBr staining on the left served as loading control. (NC, non-treated control). **C.** Northern hybridization and probing of low LMW pre-rRNA precursor levels using indicated probes of same samples as in panel B. **D.** Quantification of precursor levels in B and C relative to the maximal intensity of each precursor. Error bars indicate standard deviation of three replicate values. The curves were plotted using least square fit analysis according to equation 5 (methods). Adapted from Shanmugam et al., 2021.

The total RNA of the NC and treated plants were probed with complementary oligos (p1, p3, p4, p5, p6 for HMW blots; p23, p4 and p5 for LMW blots) to estimate the corresponding pre-rRNA levels (Figure 19A, B). The precursors observable up on specific probing with these oligos are plentiful (Appendix Figure 4). Quantification of precursors relative to the maximum intensities and further analysis using dose

response equation (Methods) revealed the temperature at which the induction (IC_{50}) or inhibition (EC_{50}) occurred for each precursor (Table 9) (Figure 19C).

In HMW blots, the primary transcript 35S were detected by p3, p4 and p5 oligos resulting in increased levels with IC_{50} value of 35°C and later reduced at EC_{50} of 41°C. Probing with p6 revealed the 35S precursors containing intact 3'ETS were accumulating at high temperature regimes (39°C - 42°C) and more prominently at 42°C. At this same regime, the longest precursor, $35SA^{123}B$ accumulation became apparent. The minor pathway diagnostic precursor 32S levels, probed by p3-5 blots, showed they were absent through 36°C to 42°C with an EC_{50} value of 34°C indicating their correlation with the primary 35S transcript accumulation. The level of 27SA and 27SB probed upon p4 and p5 revealed that 27SA followed similar pattern to 32S in disappearance of precursor levels with a slightly lowered EC_{50} value of 31°C while 27SB was reduced with EC_{50} value of 33°C. While 27SA was undetectable post 33°C, the 27SB levels remained detectable even at 42°C. Concerning the diagnostic major pathway intermediate, p3 probing revealed the levels of small subunit containing precursors, P-A3 as well as their maturation products of P'-A3 and 18S-A3. The P-A3 precursor remained detectable at all regimes but reduced with EC_{50} value of 40°C. On the other hand, the downstream P'-A3 and 18S-A3 were not detectable similar to 32S regime of 36°C to 42°C marked by their similar EC_{50} values of 34°C and 35°C, respectively. Besides the general reduction patterns of minor and major pathway intermediates at elevated temperature, the aberrant ITS2-derived transcript, P-C2 appeared through 36°C and 39°C just below the position of matured 25S. The P-C2 exhibited an IC_{50} value of 34°C but nevertheless the precursor declined with EC_{50} value of 40°C marking its short temperature regime window.

In terms of LMW RNAs (Figure 19D), probing with p23 revealed that P-P_1 fragments, a larger fragment (L) and a smaller fragment (S) completely disappeared through 36°C - 42°C coinciding with the disappearance of upstream P'-A3 precursors, with EC_{50} values were 34°C and 35°C, respectively. Nevertheless, the smaller fragment specifically exhibited a slight increase with an IC_{50} of 30°C. Probing with p5 and p4 resulted in slightly reduced 6S and 7S levels at 39°C and 42°C, while the plant specific precursor 5'-5.8S levels were unchanged upon exposure to high growth temperature.

Table 9. IC_{50} and EC_{50} values of pre-rRNAs during high growth temperature.

Stages	Pre-rRNA	IC_{50} (°C)	EC_{50} (°C)
Reduced Transcription	35S		41.2 ± 0.8
	P-A3		40.2 ± 0.9
	6S		42.1 ± 0.8
	P-C2		39.6 ± 0.7
Reduced Processing	35S	34.7 ± 0.6	
	P-C2	34.1 ± 0.3	
	32S		33.9 ± 0.4
	27SB		33.1 ± 0.9
	P'-A3		34.4 ± 0.3
	18S-A3		35.1 ± 0.5
	S7		37 ± 1
	P-P_1(L)		34.4 ± 0.8
	P-P_1(S)		35 ± 1
Sensitivity during processing	P-P_1(S)	29.9 ± 0.5	
	27SA2/A3		30.9 ± 0.7

The IC_{50} and EC_{50} values represent mid-temperature (°C) at which the given precursor exhibit accumulation or inhibition, respectively. The values were calculated based on Figure 19D. Adapted from Shanmugam et al., 2021.

To gain insight into the nature of heat-induced P-C2 precursors, the similar cRT-PCR and sequencing approach was employed to deduce the heterogeneity and nature of non-templated terminal nucleotidyl additions if any under these conditions (Figure 20A). Accordingly, with total and poly(A) RNA from plants of non-treated control (NC) and 38C treated for 1h, the PCR analysis using indicated oligos lead to formation of four dominant bands (denoted a, b, c, and d) and two bands (denoted e, and f) arising from total and poly(A) RNA samples of heat stressed plants, respectively (Figure 20B).

The representative bands were cloned and sequenced in numbers indicated to reveal their identity. The bands a-d arising from total RNA corresponded to precursors possessing P site of 5'ETS at the 5' end and following four cleavage points derived from ITS2 at 3' end; in and around C2 site (band a), heterogeneous cleavages between C2 and E site (band b), E site itself (band c), 5.8S lacking 3' sequences (band d) which are indicated as heterogeneous precursors lacking or possessing additional number of nucleotides with reference to C2 site of ITS2. The bands e and f arising from poly (A) specific RNA revealed that these precursors were heavily polyadenylated ranging in A_{12-33} or A_{11-46}, respectively (Figure 20C). The precise 3' ends mapped with respective number of clones is summarized (Appendix Figure 5A).

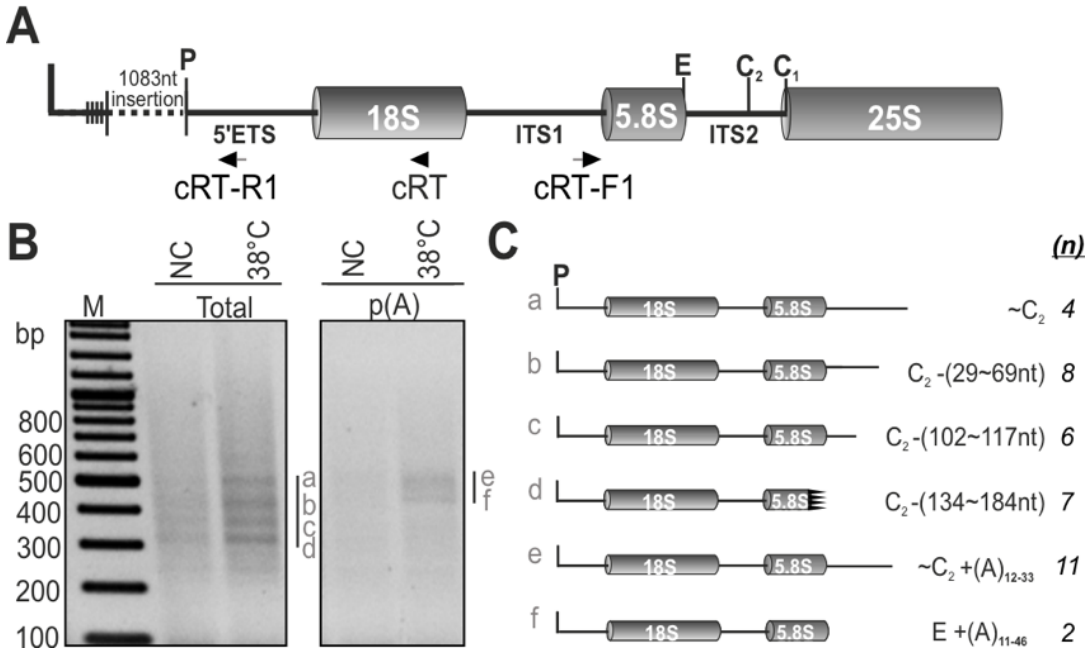

Figure 20. Identities of heat-induced pre-rRNA precursor's identities

A. Binding positions of oligos for cRT-PCR on pre-rRNA regions. **B.** The PCR products obtained after cRT-PCR from non-treated control (NC) and 38°C for 1h total RNA and poly(A) enriched samples were electrophoresed on 2.5% TTE gel. **C.** Cloning and sequencing of HS-induced representative bands (a-f) and further mapping of the jointed ends to 5' P-site and 3' heterogeneous ends relative to C2 or E site are summarized with representative number of clones (n). Adapted from Shanmugam et al., 2021.

5.3.3 Heat-induced maturation schemes are conserved in tomato and rice

To generalize the findings from Arabidopsis and to test if similar heat stress regimes can induce P-C2 derived differential processing pathways in a model dicot (Tomato) and a monocot (Rice) species, these plantlets were subjected to similar heat stress regimes between 30C to 45C. The tomato pre-rRNAs levels were monitored by probing with Sl_p3 (Figure 21A). While the level of 35S is moreover stable, regimes of 36°C-45°C led to detection of a larger precursor above the 35S (termed 35SA^{123}B in Arabidopsis). During the same temperature regime, the 32S levels completely receded. Noticeably at 36°C, both 32S and 35SA^{123}B could be simultaneously detected suggesting that tomato heat-induced pre-rRNA accumulation can occur at both 35S and 35SA^{123}B. More importantly, the precursor corresponding to ITS2-first cleavage, P-C2, appeared through 36°C -45°C, although more dominantly in between

39°C -45°C. During 39°C -45°C regimes, the occurrence of P'-A3 and 18S-A3 were comparatively reduced to control conditions.

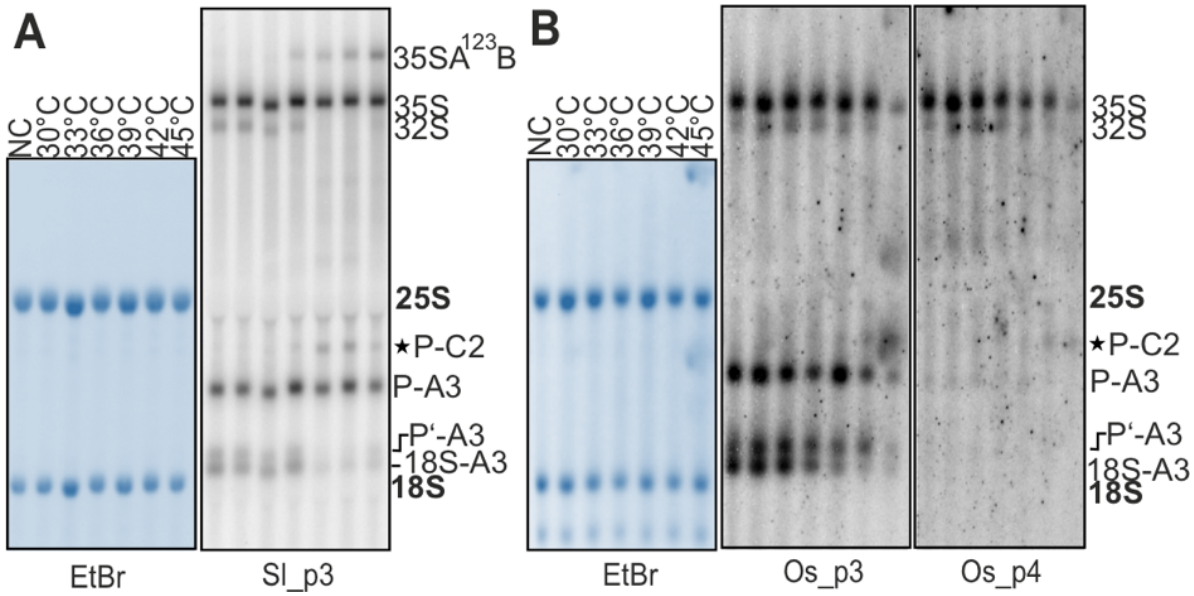

Figure 21. Pattern conservation of HS induced effects in Tomato and Rice

A. Northern hybridization analysis of HMW RNA from tomato plants subjected to indicated temperatures with Sl_p3 probe. EtBr staining on the left served as loading control. (NC, non-treated control). **B.** Northern hybridization analysis of HMW RNA from Rice plants subjected to indicated temperatures with Os_p3 and Os_p4 probes. EtBr staining on the left served as loading control. (NC, non-treated control). Adapted from Shanmugam et al., 2021.

Furthermore, the same stress regimes were imposed on Rice to evaluate the pre-rRNA maturation schemes upon high growth temperature. 18 days old plantlets grown on MS-media were subjected between 30°C-45°C with 3°C increase for 1h and the RNAs were hybridized with Os_p3(S7) and Os_p4) as described earlier (Hang *et al.*, 2018) (Figure 21B). Probing with both the probes revealed that acute 45°C treatment resulted in very low levels of major precursor 35S while the regimes 30°C-42°C treatment did not result in alterations of the major P-A3 precursor levels. In contrast, the minor pathway intermediate 32S was slightly higher under 30°C-42°C conditions in comparison with the control condition as opposed to Arabidopsis and Tomato. Albeit at very minor detection levels, the regimes of 42°C-45°C resulted in a weak band when probed with p4 between the sizes of 25S and P-A3 precursor corresponding to Rice P-C2 precursors similar to Arabidopsis and Tomato. Despite

the observed P-A3 steady state levels, their downstream precursors P'-A3 and 18S-A3 were considerably reduced between 36°C - 42°C and absent at acute 45°C.

In addition to evaluating the temperature sensitivity of pre-rRNA maturation in rice and tomato, the phenomenon was also evaluated in human HeLa cell line. Courtesy of Frank McNicoll (GU-Frankfurt), the non-treated control (NC, 37C) cells were exposed to two regimes of 39°C and 41°C heat stress regime for 2h. Upon probing of total RNA blots with human specific 3'ITS1 and 5'ITS2 probes (Appendix Figure 6), four dominant precursors were identified. Among these, including the primary transcript 45S and its offshoot precursors, 30SL3' and 41S, high temperature treatment did not elicit any variable effect on their abundance.

5.3.4 High growth temperature induced response in quick and reversible

In dose response studies of temperature control, two diagnostic intermediate transcripts, P-A3 and P-C2, possessed EC_{50} value of about 38°C. Therefore, the kinetics of rRNA maturation schemes were examined further at 38°C for 15-90 min using p23, p2, p3, p4 and p5 probes (Figure 22A). Among the blots, p23 and p2 probing was mostly used to ascertain the P-C2 identity aside the routine p3, p4 and p5 (Figure 19B). The p2 probe was employed for the sole purpose of distinguishing 32S from the similarly sized 33S(P') precursor.

Probing and further quantification as described in methods to evaluate the processing rates (Figure 22B), revealed that 35S possessed a decay rate of $2 * 10^{-5}$ sec^{-1} which is approximately 20-fold lower than the non-treated control plants. In the case of 27SB probed with p5, the rate of decline was in the order of $3 * 10^{-4}$ sec^{-1}, similar to non-stressed seedlings (Table 8). The 32S, 27SA2/A3 and 18S-A3 precursors receded to background levels at 38C with respective rate constants of $4 * 10^{-4}$ sec^{-1}, $9 * 10^{-4}$ sec^{-1} and $6 * 10^{-4}$ sec^{-1}, indicating that decay of 27SA2/A3 is slightly higher than 32S signifying its non-rate-limiting nature even under stress conditions. The rate of 18S-A3 decay in these blots were higher than the decay of its upstream precursor P-A3 again denoting its non-rate-limitedness. Upon probing with p3, p4 and p5, the P-C2 precursor could be detected even after as low as 15 min and it lasted up to 90 min of exposure. Overall, P-C2 accumulation demonstrated a near linear relationship between its intensity and the duration of exposure to 38°C. The production

and processing rates analysis of P-C2 precursor revealed significantly lower production rate of 7 * 10^{-6} sec^{-1} and lack of processing rate (<10^{-14} sec^{-1}).

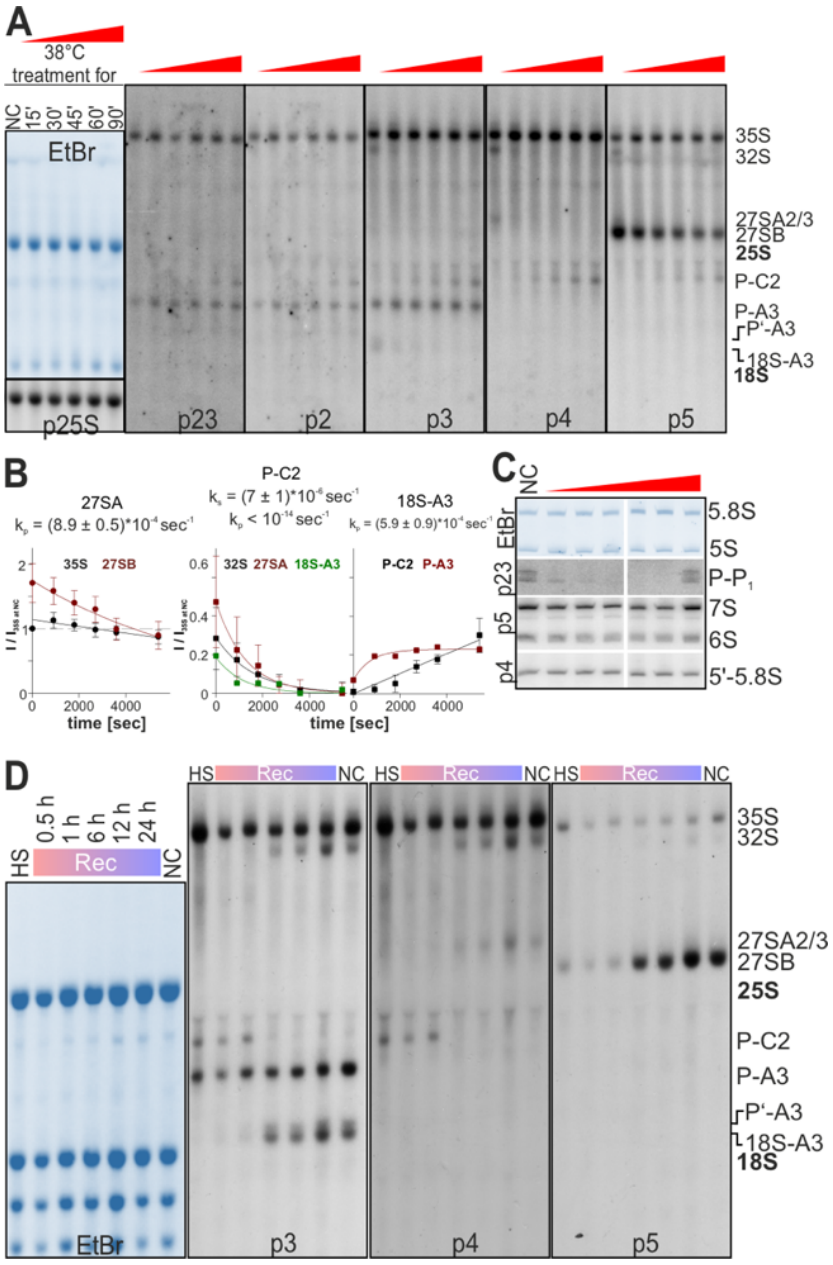

Figure 22. The alteration of maturation scheme is quick and reversible

A. Plants that were 14d-old were subjected to constant 38°C temperature with increasing duration of exposure. Northern hybridization analysis of HMW RNA from plants subjected to indicated temperatures with indicated probes at the bottom. EtBr staining and p25S probing on the left served as loading control. NC, non-treated control. **B.** The signals were quantified for three experiments and the intensity relative to maximal intensity at non-treated control plotted according to equation 1 and 2 (Methods) along with their rate constants. Error bars

indicate standard deviation of three replicates. **C.** Plants that were 14d-old were subjected to constant 38°C temperature for 1h but were subsequently recovered for 0.5 to 24h. Northern hybridization analysis of HMW RNA of the indicated samples using p3, p4 and p5 probes. EtBr staining on the left served as loading control. Adapted from Shanmugam et al., 2021.

While P-A3 levels increased after 15 min compared to control conditions, the levels in other time periods were comparable to non-treated control. This trend agrees with the preliminary decay rate of 35S with overall P-A3 production rate of $2.4 * 10^{-5}$ sec^{-1} (Table 8). Alternatively, the observed steady state levels of P-A3 could be due to their net rates of production and decay.

Probing of low molecular weight RNAs (Figure 22C) with p23 from similar conditions revealed that even after 15 mins, the higher sized P-P_1 fragments started to vanish at moderate heat stress except the lower sized fragment that persisted till 30 mins. The levels of pre-5.8S precursors, 7S, 6S and 5'-5.8S) were largely unchanged upon p4 and p5 probing.

Next, I set out to determine if the heat induced ITS2-first cleavage processing is reset up on return to favorable growth temperature and if yes, the time required for the restoration of processing schemes. I compared the profiles of pre-rRNA precursors between control (22°C), heat stress (38°C for 1h), the plants that are subjected to heat stress (38°C for 1h) and subsequently returned to 22°C growth temperature for 0.5, 1, 6, 12 and 24h using the probes p3, p4 and p5 (Figure 22D). At 0.5 and 1h after return, the P-C2 precursors were still present at nominal levels comparable to the stressed samples while between 6-24h, the P-C2 precursor level receded to control conditions. As such, the processing of this intermediate does not occur immediately upon return to favorable temperatures. On the other hand, the major P-A3 and minor 32S levels also resumed to control conditions after 12h but exceeded the levels of control condition at 24h of return. The 32S minor pathway intermediate levels resumed to control condition levels during 6-12h while was absent after 0.5-1h after recovery. The major and minor pathway's overall changes after 1h of return to normal growth conditions lead to stabilized levels of P'-A3 and 18S-A3. In conjunction with initial decline of 35S and P-A3 intermediates, this signifies that resumption of pre-rRNA processing rely more on pre-rRNA synthesis than recycling of pre-existing precursors.

5.3.5 High growth temperature alters the pre-rRNA intermediate composition

To gain deeper understanding into dynamic changes of precursors under heat stress, I subjected three independent petri dishes of suspension culture that were pulse labeled at 25°C for 45 min at control growth conditions but chased at following three temperature conditions for 5h: control 25°C (Figure 23A), elevated temperature of 38°C (Figure 23B), elevated temp of 38°C for 60min followed by control growth temperature (Figure 23C). The precursor levels were used to estimate the rate constants as described in Methods. Control growth temperature conditions (Figure 23D) were used to compare the effect of elevated temperature (Figure 23E, F).

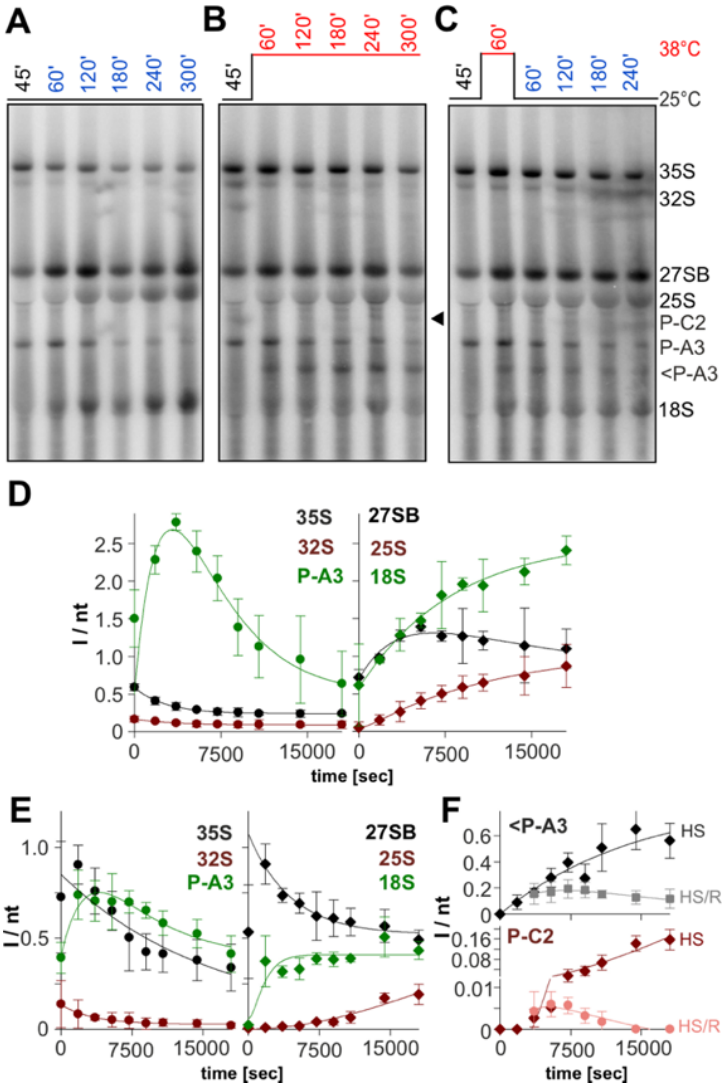

Figure 23. Pulse-chase pre-rRNA analysis under increased growth temperature

A. Autoradiograph of purified total RNA from pulse labeled RCC samples for 45 min at 25°C and subsequently chased at 25°C for 60 to 300 min. **B.** Autoradiograph of samples using same

condition as in panel A except chasing performed at 38°C (marked red). **C.** Autoradiograph of samples using same condition as in panel A except chasing performed at 38°C (marked red) for 60 min and subsequently returned to chase temperature of 25°C for 60 to 240 min. **D-F.** Quantification and plotting of precursors intensities normalized to size of each rRNA of panel A (D), panel B (E) and panel C(F) intensity lines plotted according to least square fit analysis. Error bars represent standard deviation. HS/R denotes recovery after HS. Adapted from Shanmugam et al., 2021.

Between pulse and pulse-chase analysis, the rates were moreover similar except in cases of three-fold reduction in k1, k4 and k5 (Table 8). Similar to plants (Figure 22A, B), subjection of RCC to high temperature 38°C led to stabilization of 35S and 27SB pre-rRNA. Among the rate differences, 35S processing was 20-fold reduced under heat stress while the 25S production rate was six-fold slower under heat stress regime.

At 38°C through 60 to 300 min, a band corresponding to P-C2 appeared after 1h but consisting of an additional band between matured 25S and P-C2. The P-C2 precursor were produced at the rate of 2.3 ± 0.4 * 10^{-4} sec^{-1} while not possessing processivity rate at high temperature (< 10^{-8} sec^{-1}). The intensity of P-C2 corresponded to levels of minor 32S precursor in these conditions. The level of P-A3 precursor levels were stabilized and did not recede significantly even at high temperature. The minor pathway intermediate 32S level though altered between control and high temperature regimes did not flatten as in steady state levels under similar conditions except the data was acquired in seedlings. Notably, the level of P-A3 in control and recovery blots indicate the reducing pattern as time progress correlating with the 18S production. Strikingly, in addition to P-C2 precursor, a novel precursor appeared specifically between major P-A3 and matured 18S, at elevated temperature in all time points as well as under recovery conditions (Figure 23B, C). This designated precursor, <P-A3 was synthesized at (2.0 ± 0.2) * 10^{-5} sec^{-1} which did not possess any processing rate at this elevated temperature (<10^{-15} sec^{-1}). Recovery phase blots showed that this precursor processing can be re-initiated at (5.7 ± 0.7) * 10^{-4} sec^{-1} in RCC.

For determining the precise extremities of <P-A3 precursors, circular RT-PCR was conducted with non-treated control and heat stressed RCC. In order to account for absence of such precursors on Arabidopsis plants, total RNA from NC and 38°C stressed plants were used alongside for circularization, RT and PCR as indicated

(Figure 24A). The PCR analysis led to amplification of a common band (band a) appearing in all lanes and a differential band (band b) appearing specifically at 38°C stressed samples of RCC (Figure 24B).

Cloning and sequencing of independent clones (n=8 for a; n=25 for b) revealed a common P site at the 5' terminus. The abundant band corresponded to P-A3 precursor while the 3' site of band b revealed that it is closer to being A2 site with additional nucleotide extensions at the 3' side between 12 to 59 nt (Figure 24C, Appendix Figure 5B). These precursors were occasionally polyadenylated (11/25) with lengths of A_1-A_{16}.

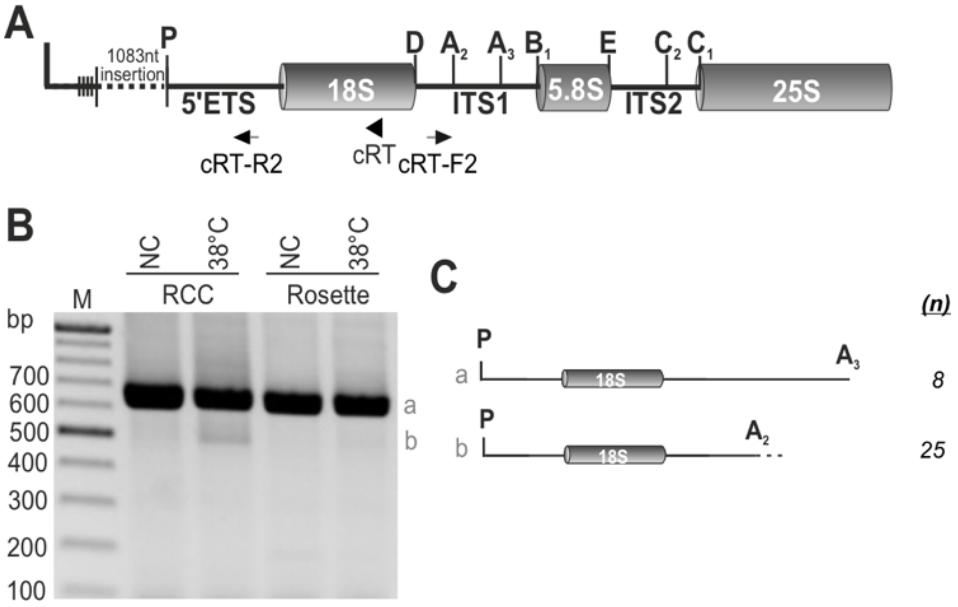

Figure 24. Characterization of novel heat-induced precursor in RCC

A. Binding positions of oligos for cRT-PCR on pre-rRNA regions **B.** The PCR products obtained after cRT-PCR from non-treated control (NC) and 38°C for 1h total RNA from RCC and rosette plants were electrophoresed on 2.5% TTE gel. **C.** Cloning and sequencing of HS-induced representative bands (a, b) and further mapping of the jointed ends to 5' P-site and 3' deterministic sites to A3 (n=8) and heterogeneous ends relative to A2 site (n=25), with n being independent clones. Adapted from Shanmugam et al., 2021.

5.3.6 Acute heat stress affects the assembly and overall precursor levels

By utilizing density gradient centrifugation and northern hybridization, I set out to determine the pre-rRNA composition of ribosomal subunits under enhanced conditions of 42°C for one hour (HS) in fractionated RCC. After centrifugation, the

measured absorption profile at 254nm was compared between non-treated control (NC) and HS (Figure 25A). The free pool fraction between samples indicated the loading was moreover equal. It should be noted that acute temperature (HS) resulted in polysome run-off, illustrated by a flat line after the monosome fraction. Consequently, both the peak absorbance for 40S as well as 60S/80S ratio was increased by the aforementioned polysome dissociation under HS conditions. The assay indicated a merged peak for the 60S and 80S in the control samples, likely due to the reduced resolution of the sucrose, and this trend was more pronounced with the HS samples marked by its merged peak.

RNA was purified from the NC and HS fractions and further electrophoresed to assess the difference between the subunits (Figure 25B). As seen from the mature RNA composition of 40S subunits, the archetypal mature 18S rRNA is reasonably distributed in both the first and second fractions. In agreement with the merged peak observation of 60S and 80S, the ratio of their constituent 25S rRNA to the 18S rRNA was higher in the first fraction than the subsequent two fractions. The NC fractions contained more mature rRNAs than the HS fractions, indicating overall reduced levels of polysomal RNA, as earmarked by the polysome dissociation.

To determine the relative levels of precursor rRNA between the NC and HS conditions, northern hybridization was conducted concurrently using probes p1, p23, p3, p4 and p5 (Figure 25B). Foremost, the fractions of HS conditions resulted in undetectable levels of any pre-rRNA, including P-A2, that conditionally accumulated under HS (Figure 24B). In the NC sample, the first fraction of 40S encompassed P'-A3/18S-A3, whereas the second fraction of 40S possessed both the diagnostic P-A3 and the P'-A3/18S-A3. These results suggest there are at least two types of pre-40S subunits present in the 40S peaks. The probing revealed other fractions of merged 60S/80S and polysomes were mostly dominated by the rate limiting precursors of P-A3 and 27SB.

In addition to probing of pre-rRNAs, western blot analysis of the same fractions was performed to reliably deduce the subunit identity and any differential distributions using corresponding antibodies against RPs (RPS3, RPL5, RPL10) and RBFs (ENP1, NOB1) (Figure 25C). The analysis showed that 40S marker protein, RPS3-2 were detectible across all NC fractions but were reduced under polysome fractions despite being abundant in 40S and 60S/80S fractions. Analysis of large subunit proteins, RPL5

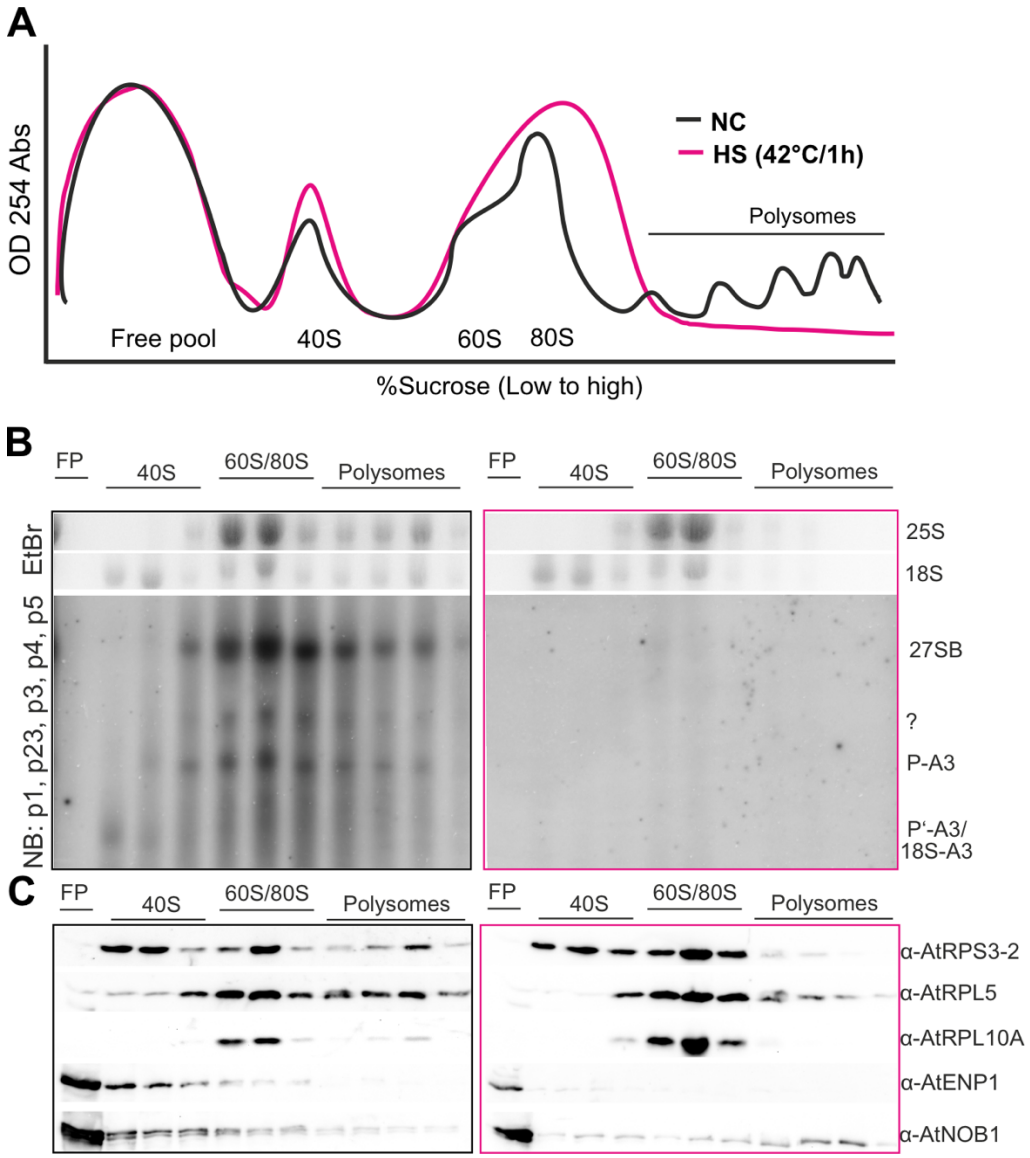

Figure 25. Polysomal reduction and subunit pre-rRNA distribution under HS

A. Absorbance values at 254 nm plotted for ultracentrifuged lysates of RCC samples that were treated at 42°C for 1 h (HS, Cyan coded) alongside non-treated control (NC, black). **B.** Northern hybridization analysis of total RNA from the indicated fractions at the top from both sample types using probes (p1, p23, p3, p4 and p5). EtBr staining of 25S and 18S served as markers for corresponding fractions. Color coding as in panel A. **C.** Western blotting analysis of denatured proteins purified from indicated fractions on top using antibodies marked on the right. Color coding as in panel A. Adapted from Shanmugam et al., 2021.

and RPL10 indicated these proteins were dominantly present in 60S/80S fractions while still detectable in other fractions as well. The subunit RP levels were overall reduced in the polysome fractions of HS compared to NC. With respect to RBFs, the

signals were dominant in the free pool fractions relative to subunit fractions. However, HS fractions contained almost no ENP1 signal under the 40S peaks while the NOB1 levels were slightly increased in polysome fractions under HS.

5.3.7 Heat Stress affects pre-rRNA maturation in *hot* mutants

Having established a role of ITS2 maturation paths in wild type plants, I investigated whether classical *hot* mutants (*hot1-3*, *hot3-1* and *hot3-2*) named after their inability to cope with 'hot' temperature stress treatment are impaired in ITS2-dependent adaptive response.

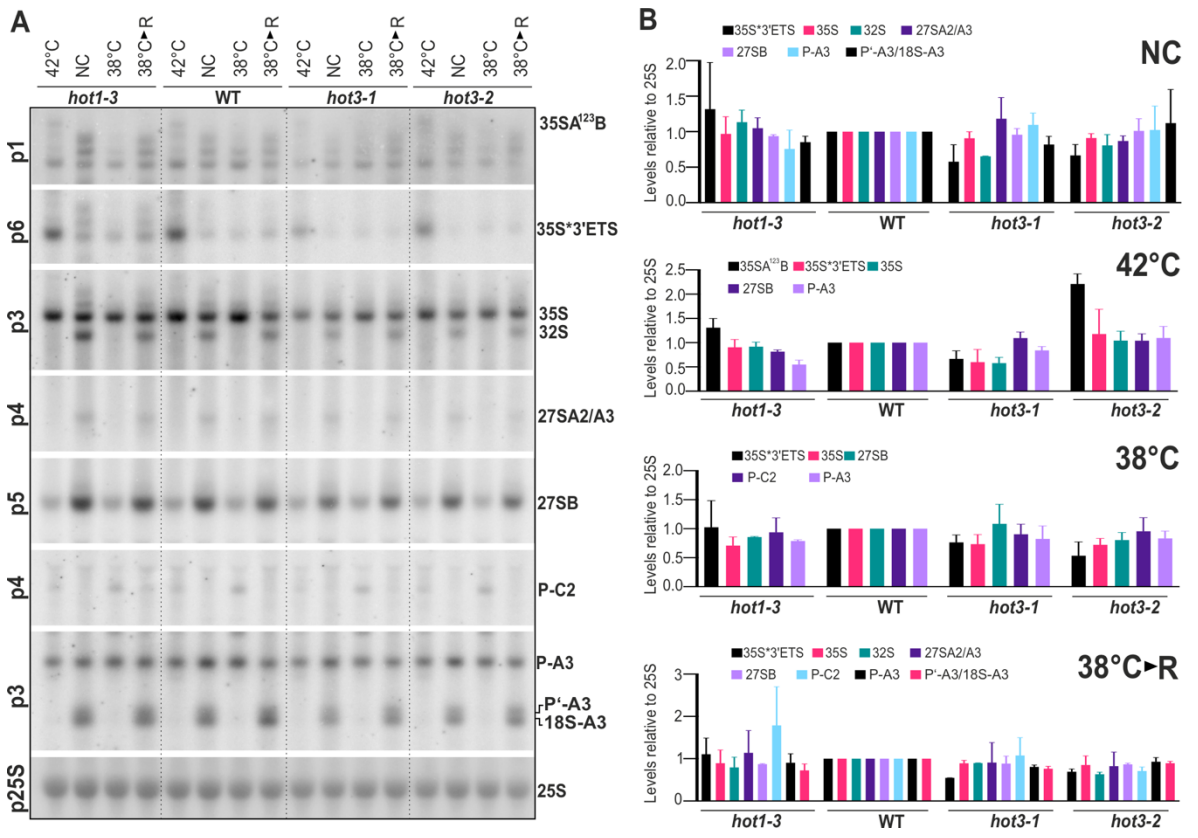

Figure 26. Pre-rRNA non-perturbations in heat sensitive mutants

A. Northern hybridization analysis of WT and *hot* mutants (*hot1-3*, *hot3-1,* and *hot3-2*) treated to extreme heat stress (denoted 42°C), moderate heat stress (denoted 38°C), same treatment but recovered for 2h (denoted 38°C➤R) alongside non-treated control (NC) with indicated probes on the left and the identified precursor on the right. p25S probing served as loading control. **B.** Quantification of precursor levels on panel A relative to mature 25S rRNA. Error bars indicate standard deviation of two biological replicates for four regimes indicated on top right corner of each panel.

hot1-3 is deficient in Heat Shock Protein 101 (HSP101) (Hong and Vierling, 2001) while *hot3-1* and *hot3-2 a*re disrupted in eukaryotic translation initiation factor (eIF5B), with *hot3-2* being reported as a more severe allele (Zhang et al., 2017). The pre-rRNAs of 16d old heat treated (38°C and 42°C for 2h) and recovered (38°C pretreated) plants for 2 h (Figure 26A), were probed using complimentary oligos (p1, p3, p4, p5, and p6; Appendix Figure 4) and their quantified levels were compared (Figure 26B). At control conditions (NC) and even at 38C treatment conditions, the multiple probing and quantification of precursors in mutants showed that all precursor levels remained moreover at the wild type level. The p1 probing revealed higher order 35S molecules containing unprocessed 5'ETS regions, $35SA^{123}B$, which is noticeably higher up on 42°C treatment. Quantification revealed the severe allele of eIF5B, *hot3-2* accumulated at least one-fold of this precursor at this elevated temperature relative to wild type. On the other hand, the less severe allele, *hot3-1* possessed 0.5-fold reduced level of the same precursors up on 42°C treatment. The major diagnostic precursor was moreover comparable between wildtype and the hot mutants in all conditions except *hot1-3* contained slightly reduced levels of P-A3 after 38°C. The other diagnostic precursor while unchanged at control conditions and completely absent after heat treatment, their levels in recovering tissues were largely comparable between wildtype and mutants. More importantly, the heat induced precursor, P-C2 levels were moreover comparable in the mutant after 38°C treatment but *hot1-3* mutant contained persisted levels of P-C2 precursors even after return to recovering conditions. Taken together, the pre-rRNA maturation schemes were unaffected at control conditions but showed signs of heat induced impairment of pre-rRNA processing in tested *hot* mutants.

6 DISCUSSION

6.1 Cas9 editing of ribosomal DNA copies

Cas9 and its multiple spin-offs have been successfully utilized to edit the coding and non-coding regions of eukaryotic genomes. However, reports on repetitive regions of genome editing are insufficient. Among them, in bacteria, a synthetic genome derivative of *M. mycoides* without any viable ribosomal small subunit 16S rRNA (*rrs*) copies have been further engineered with phylogenetically distant and closest copies of synthetic rrs to evaluate the minimal *rrs* required to sustain the genome (Kannan et al., 2016). Concerning Yeast, the replication origin Cas9 editing of rDNA copies has been successfully employed to determine that minimum 10 out of 150 repeats are required to sustain the defective slow growth phenotype beyond which suppression mechanisms takes over (Sanchez et al., 2019). In Arabidopsis, using non-Cas9 approach, an identification of tandem duplication mutational events leading to loss of up to 20% of rDNA copies resulted in genome wide expression changes coupled by increased pathogen resistance (Picart-Picolo et al., 2020). In another independent study in Arabidopsis, a single guide RNA approach to induce egg-cell specific double strand breaks in 18S rDNA regions induced nicks leading to large scale deletions (up to 20%) and insertions (up to 160%) of the original rDNA copy numbers (Lopez et al., 2021).

6.1.1 A case for selective role of ribosomal DNA copies

Our analysis on the other hand use two-guide RNA based-approach leading to excision of roughly 20 bp at the 25S rRNA regions (Figure 6A, B) and only resulted in disruption of less than 5% of total copies (Figure 7B). Moreover, given that VAR1 is associated with 50% of rDNA copies, and the mutated copies were not associated with VAR 1 in our sequencing analysis, the Cas9 disruption of NOR2 copies can be faithfully ruled out (Figure 10C). The activity of Cas9 on specific NOR could in part be ascribed to their higher order nucleolus-associated chromatin domain (NAD) configurations of specific NOR during plant development (Pontvianne et al., 2016). From our mosaic pattern of analyzed mutational events (Figure 7C), the repair mechanism suggests predominant scarless excision as major event in comparison to scars in the form of mutations or insertions. The precedence to such phenomenon may lie in the characteristics of the NOR relative to non-repetitive regions of the

genome. Ribosomal DNA has been shown to use two modes of double strand nick (DSB) repair mechanisms. While error prone non-homologous end joining might suffice for moderate breaks, highly ordered nuclear cap structures consisting of various repair factors are known to control severe repetitive double strand breaks in higher eukaryotes leading to homology-directed repair (HDR) mechanism (van Sluis and McStay, 2019). In this study, two lines of evidence supports for unlikelihood of major loss of rDNA copies. First, the heteroduplex PCR analysis of WT and *ploop KD* mutant shows that the mutated copies are significantly lower relative to intact copies supporting lesser likelihood of major loss of rDNA copies during the repair (Figure 7). Second, validation of VAR polymorphism PCR also shows that there are no significant changes at the rDNA VAR levels between the genotypes (Figure 11A, B).

6.1.2 Growth manifestation due to mutation

The defective phenotype of *ploop KD* +/- and *ploop KD* -/- plants showed similarities to that of characterized phenotypes of RPs and RBFs gene mutants, typified by overall reduced size and markedly pronounced serrated and pointed leaves in comparison to rounded leaves of wild-type (Figure 8). Among mutants lacking large and small subunit RPs, from the first described *pointed first leaf, pfl1* coding for RPS18A (Lijsebettens et al., 1994) and subsequently characterized *pfl2/rps13* (Ito et al., 2000); *rpl4a* (Rosado et al., 2010); *rpl5a* (Rosado et al., 2012); *rpl7b*, *rpl10ab*, *rpl17b*, *rpl18c*, *rpl38b*, *rpl39c*, *rps6a*, *rps24b* (Horiguchi et al., 2011); *rpl36a* (Casanova-Sáez et al., 2014); *rpl27a* (Zsögön et al., 2014); *rpl9* (Devis et al., 2015); *rps21b* (Wang et al., 2018), the mutants display relatively smaller size and sharp first leaf apex leading to derivations of pointy leaves at tested growth conditions as in the case of *ploop KD* (+/- and -/-) plants. Among RBFs, the phenotypic similarity of pointy first leaf extends to mutants lacking in *prmt3* (Hang et al., 2014), *midasin1* (Li et al., 2021), *apum24* (Maekawa et al., 2018), *brx1-2* (Weis, Palm, et al., 2015), *rh7* (Huang et al., 2016) and *irp2* (Palm et al., 2019).

The common phenotypic pattern between mutants lacking RPs, RBFs, and selective copies of rRNA (Figure 8C) in this study signifies the global reduction of either unspecialized or specialized ribosome population resulting in decreased translation potential. Such mutation in principle can lead to non-translation of selective target mRNAs leading to observed imbalance in proteome homeostasis (Figure 9B, C). Whether such selective mRNA non-translation led to direct perturbation at the

proteome level and thus leading to observed growth pleiotropy remains to be established. The leaf patterning defects leading to pointy leaves up on RPs and RBFs mutation have been attributed to impaired auxin signaling in several mutants (Rosado et al., 2010; Abbasi et al., 2010; Rosado et al., 2012; Li et al., 2021). It is likely that similar mechanisms influence the common phenotypic outcomes. Between *ploop KD* +/- and -/- genotypes, the phenotypic similarity in terms of lack of lateral roots and slower emergence of first leaf, but the same defect more severely pronounced in *ploop KD* -/- plants is noteworthy (Figure 8A, B), since the mutated alleles were double that of *ploop KD* +/- (Figure 7A, B) thus resulting in proportional lack of functional ribosomal population during critical cellular processes.

Moreover, the absence of lateral roots on *ploop KD* +/- and -/- mutants could in part be due to ectopically present AtPARP2 in the mutant (Figure 9B), which is a proven negative regulator of lateral roots emergence in that the mutants of *parp2* possess excessive lateral root numbers (Liu et al., 2017). Furthermore, a defect in specific 32S-dependent minor-pathway processing (Figure 12B, C), similar to *prmt3* perturbation (Hang et al., 2014), can also be attributed to the growth disorders in *ploop KD* -/- plants.

6.1.3 Ectopic rRNA expression and dosage compensation

Disruption of NOR4 dependent rDNA copies in the mutant led to ectopic expression of NOR2-derived VAR1 rRNA subtype arising from the chromosome 2 (Figure 11C, D). This dosage compensation mechanism is consistent with two previous reports. Mutants lacking histone deacetylase 6, HDA6 that reverses acetylation of lysine residues at three known substrates H3K14, H4K5 and H4K12 exhibited such ectopic expression of VAR1 subtype at both seedling and adult stages (Earley et al., 2006; Chandrasekhara et al., 2016; Chen et al., 2018). Similar phenomenon of VAR 1 dosage compensation has also been the feature of mutants possessing reduced copy numbers of ribosomal DNA in Arabidopsis (Lopez et al., 2021). It is likely that surveillance pathways exist in cells to monitor the transcriptional outcomes of rDNA repeats at both chromosomes to compensate for the production of defective ribosomes. Alternatively, the factors regulating the rDNA loci repression at Chromosome 2 if dysfunctional can also lead to derepressed state in the *ploop KD* mutants. It remains to be investigated if this phenomenon is widespread and whether

it also holds true for previously described RBF and RP mutants. The VAR1 ectopic expression also led to its associated increase in the frequency of single nucleotide polymorphisms at the whole ribosomal RNA sequence (Figure 11E). The coordinated expression of specific rDNA repeats in the genome and its associated variable SNP frequencies has been documented as a source of specialized ribosomes (Sims et al., 2021). In terms of processing of the transcribed pre-rRNAs, the specific accumulation of 32S pre-rRNA in the *ploop KD* -/- mutant is significant (Figure 12C). While any of the factors controlling minor pathway maturation may be defective in *ploop KD* -/- mutant, the ectopically expressed VAR1 pre-rRNA may also contribute to such pathway-specific breakdown. It is well known that RBFs exhibit tissue specific expression (Kovacevic et al., 2019) and given that pre-rRNAs types are unique depending on developmental stages and tissues, it is plausible that pleiotropic expression of VAR1 could simply lead to a scenario without its cognate tissue-specific or sequence-specific RBFs, thus, leading to a specific defect in minor maturation path.

6.1.4 Overarching consequence of ribosomal DNA mutations

The maturation of ribosomal RNA along with the ribosomal proteins and biogenesis factors begins in the nucleolus. The span of maturation steps encompasses initial large pre-90S, pre-40S and pre-60S subunits before they maturate to 40S and 60S. Our data shows that between these pre-complexes, the mutated ribosomal RNA copies were mostly confined to maturing subunit fractions of pre-40S to 60S. Additionally, they were also detectable in and around the 80S monosomes, albeit at lower concentration than the free pool fractions. They were more over not present in the so-called translating polysomes (Figure 13B). It is important to consider that the initial pre-90S complex is also fractionated within the 80S monosomal peak according to their sedimentation co-efficient. It is likely the mutational copies that are detected around the monosome fractions correspond to these copies being detected from the initial pre-90S complex. Based on the intensity of band arising within the fractions in two different floral and silique tissues, we observed that the detectable mutated copies were more in maturing fractions than 80S fractions (Figure 13, Appendix Figure 3). This in part shows that proportion of active monosomes or polysomes containing the mutated P-loop fragment is lesser or unlikely.

Moreover, the crystal structure of P-loop region of the eukaryotic ribosome region is shown to interact with N-term region of RPL29 protein (Klinge et al., 2011). Additionally, the P-loop region lies in close proximity to RPL10 although its interaction with P-loop is not verified. Given that P-loop region possess minimum of 3 active residues based on their interaction potential with other proteins (Leshin et al., 2011), it is plausible that the binding of these two proteins on to the ribosomal RNA may not be facilitated as a direct result of the mutation.

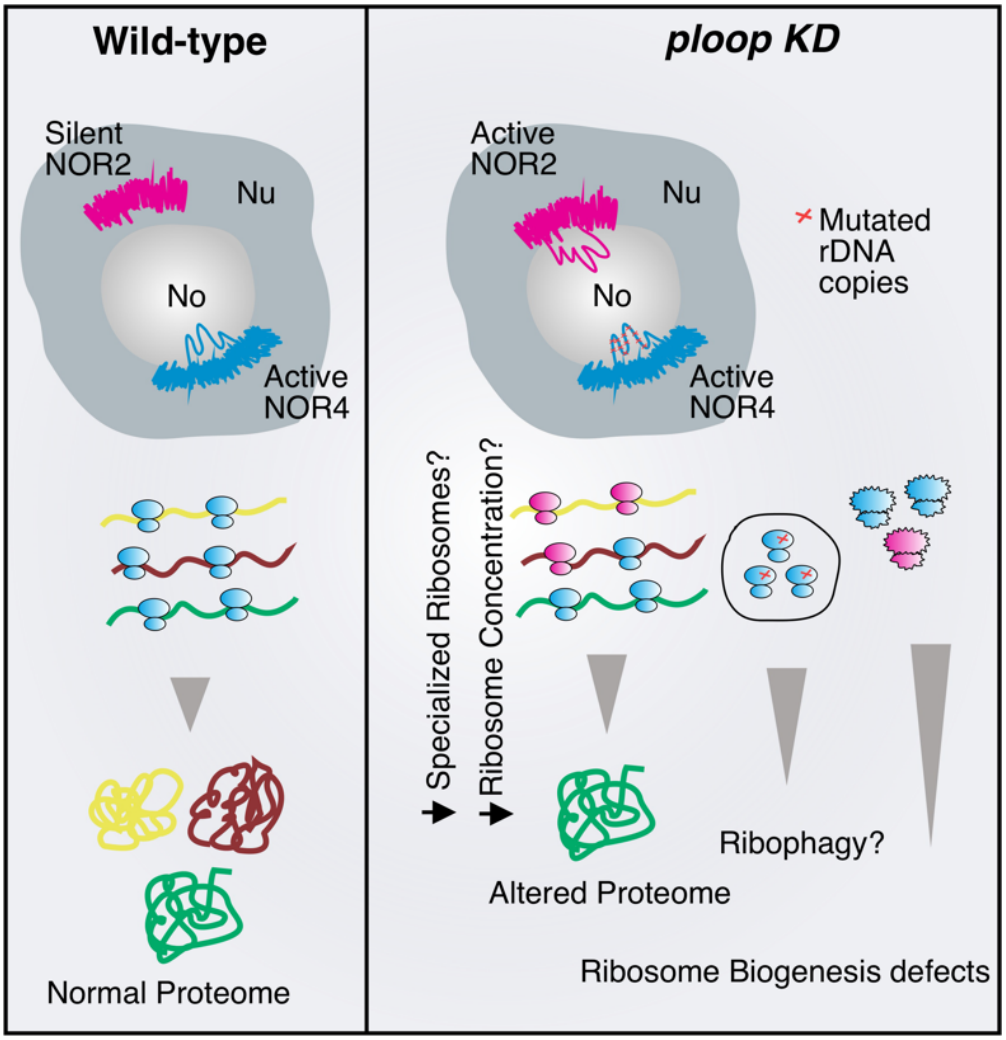

Figure 27. Proposed model of defects in *ploop KD* mutants

This is the proposed model of molecular events leading up to observed morphological defects in *ploop KD* mutants. On the left in wild type, NOR2 (magenta) is silenced while NOR4 (cyan) remains active during the latter seedling growth stages resulting in correct expression of rDNA copies and further normal proteome. On the right in *ploop KD* mutants, the mutation on NOR4 P-loop regions leads to non-functional ribosomes or improperly assembled ribosomes that are

likely subjected to ribophagy. Meanwhile the mutated and intact copies of NOR4 in principle causes reduced functional ribosome pool or disrupted specialized ribosomes required to translate critical mRNAs thus leading to altered proteome. This mutation also leads to de-repression of normally silenced NOR2 thus leading to ectopic NOR2 copies expression which is exacerbated by the associated minor pathway biogenesis defects.

The formation and persistence of immature ribosomal RNAs would likely trigger recycling mechanisms in cell. Consistently, our analysis shows that indeed autophagic turnover rates are high even under control growth conditions (Figure 14B, C). This constitutive autophagy may pose additional stand-alone challenges for the growing cell. The chemical and molecular components of these autophagosomes would shed more light onto the ribophagy mechanisms and the conditions in which they are triggered. If the elevated autophagy levels are indeed due to the defective ribosomes, it would indicate ATG8e ortholog would share the ribophagy cargos as well, making them even more versatile.

6.2 Revised schematics of Arabidopsis pre-rRNA splitting

Based on the primary transcript 35S first cleavage steps, the diagnostic precursors of ITS2-first paths, P-C2 consists within the mature region of 18S and 5.8S thus representing an unusual precursor in which the 5.8S rRNA is entrapped with the small subunits archetypal 18S rRNA. Furthermore, this splitting therefore can lead to large subunit's 25S rRNA without its cognate 5.8S rRNA. Plants with its combined pathways existing in yeast and humans seem to possess ITS2-first pathway at least in RCC under control growth conditions (Figure 16B). The heterogeneity of these precursors is noteworthy since these precursors seem to be derived from an initial cleavage step at C2 site of ITS2 by a putative unknown endonuclease followed by exonucleolytic activity by exosomes (Figure 16C).

Pre-rRNA analysis of a non-lethal *rrp5Δ10* mutant in Arabidopsis showed that despite accumulating 35S over four-fold, this mutant lead to strong production of ITS2-derived precursors (Figure 17A). More importantly, the combined cRT-PCR analysis of RCC and *rrp5Δ10* mutant shows that there are minor variations between these precursors in terms of the exonuclease activity resulting in two marked deterministic sites of C2 and E sites, respectively (Figure 16C, 17F). The precise mechanism governing these differences could be further investigated in exosome deficient rrp6

mutant backgrounds to evaluate if it is indeed exonucleolytically controlled. While the production of ITS2 derived precursors in *rrp5Δ10* mutants is unsurprising due to similar effects on yeast (Venema and Tollervey, 1996) and humans as well (Sloan et al., 2013), the production of ITS2-derived precursor in RCC is particularly interesting. Plant tissues may have evolved to fine-tune these multiple pathways for further optimization in a tissue, growth stage or hormone-dependent manner. In part, a mutant lacking a putative RBF, IRP7 containing ALBA domain has been shown to produce the ITS2-derive P-C2 precursor upon auxin treatment denoting its link between accelerated pre-rRNA synthesis and lack of specific factors thereof (Palm et al., 2019). The overall reduced abundance of this precursor in general may have contributed to its lack of reporting in literature describing RBF mutants as well. The increased specificity and fidelity of cRT-PCR assays might uncover and support the existence of these precursors in more number of mutant studies.

6.3 The dynamics of maturation schemes

In Arabidopsis plants, two pathways for maturing 35S transcript pre-rRNA modeled on yeast and humans is known to co-occur simultaneously (Hang et al., 2014; Weis, Kovacevic, et al., 2015; Tomecki et al., 2017). Pulse labeling and chasing of rRNA maturation is a common feature in Yeast and other mammalian cell lines (Jansen et al., 1991; O'Brien and Wolin, 1994; Baudin-Baillieu et al., 1997; Zanchin et al., 1997; Koš and Tollervey, 2010; Zorbas et al., 2015). While such studies have been discussed to be challenging (Zakrzewska-Placzek et al., 2010; Hang et al., 2018) and scanty in plants, this dissertation shows isotope metabolic labeling can be used in plants for pulsing the ribosomal pre-rRNA synthesis (Figure 18).

Among the longer HMW pre-rRNA, the absence of 45S and $35A^{123}B$ indicated that they are not rate limiting precursors after the initial transcription (Figure 18A). The observed two-fold variations observed between the 35S production in RCC, and seedlings can at least be attributed to two controlling factors: number of RNA Pol I molecules that can regulate the synthesis rate (French et al., 2003), variations in uptake rate of radioactive tracer PO_4 in RCC and seedling tissues (Figure 18C).
Subsequent to 35S pre-rRNA synthesis, detection of both the diagnostic intermediates of 5'ETS-first (32S) and ITS1-first (P-A3) paths marked the the next rate-limiting steps. While their synthesis rates are comparable in RCC, the production rate of 32S is higher

than that of P-A3 in seedlings. This suggests that the ITS1-first pathway can be modulated to suit the cellular demand for ribosome production. For the maturation of 18S rRNA in ITS1-first path, there were no other rate-limiting steps other than the P-A3 marked by the absence of downstream theoretical precursors of P'-A3 and 18S-A3 in both tissue types. However, the 18S rRNA synthesis was ten-fold higher in RCC than seedlings due to its slower production rate of both P-A3 and 18S precursors. Further processing of 5'ETS's diagnostic 32S pre-rRNA results in 27SA2 and 18S-A2 (20S) precursors, the latter of which is short lived even in steady state levels except in mutant conditions (Figure 17A, C) (Weis et al., 2014). Consistently, 18S-A2 were not detectable in pulse analysis of both RCC and seedlings. The non-detectible levels of 27SA2 could be described by the slower processing rates of 32S in general than their accelerated processivity (Figure 18, Figure 28).

Similar to 18S production, the 25S production is marked by a single rate limiting precursor, 27SB which is notably slowest among all the processing rates in RCC. Despite differing rates of processing between RCC and seedlings, 25S production remained similar.

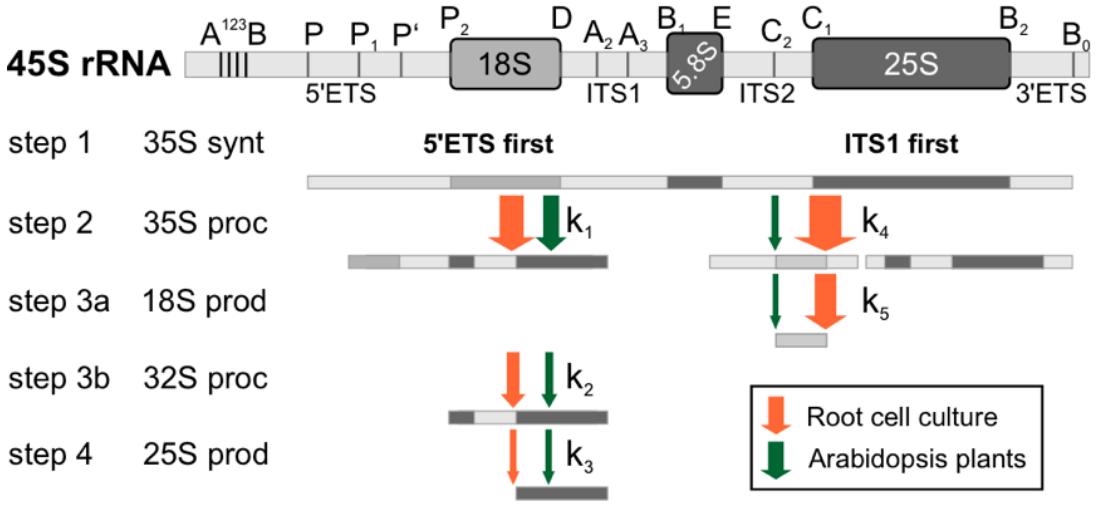

Figure 28. Pre-rRNA maturation dynamics in cell culture and seedlings

The observed kinetic scheme for the 45S rRNA maturation in Arabidopsis root cell culture (orange) and seedlings (green). The different maturation steps (synt, synthesis; proc, processing; and prod, production) and their corresponding intermediates of 5'ETS first and ITS1 first paths are indicated through k_1 to k_5. The variations in rate constants at each step are indicated by the thickness of the arrow in each case. Adapted from Shanmugam et al., 2021)

Taken together, transcription and 25S rRNA synthesis suggests being major rate-limiting factors in plant ribosomal biogenesis. Regarding the pathway features, the small subunit production is faster through the ITS1 mediated pathway in rapidly dividing cells based on their determined rate constants. In seedlings however, these maturation rates are rather comparable. Between the tissue types analyzed, the enhanced 18S production rate in RCC suggests that under high metabolic demand, the rates may be skewed in contrast to presumed slow dividing seedlings possessing synchronized production rates (Figure 28).

6.3.1 RNA maturation schemes are sensitive to heat

Temperature has been reported to affect rRNA synthesis in cell cultures before (Nover et al., 1986). Various pre-rRNA processing modes exist depending on the sensitivity to temperature between 30°C and 42°C. The 35S primary transcript showed dramatic reduction of up to 20-fold under 38°C HS conditions (Figure 23, Table 8). At this same temperature, the downstream of ITS1-first determinate P-A3 precursor possessed a comparable processing rate in both RCC and seedlings before and after HS. The similar HS regimes inflicted reduced P-A3 production rates in seedlings and 27SB processing rates in RCC (Figure 22, 23).

The global sensitivity to pre-rRNA maturation schemes were in turn confirmed for two other model plant species, tomato, and rice. Interestingly, tomato plants exhibited alternative modes arrest of maturation in relation to Arabidopsis through the supposed accumulation of 35SA^{123}B after 36°C. In Rice plantlets, the response is slightly shifted to higher magnitude of HS severity (Figure 21).

Under elevated temperatures, the steady state levels of major pathway's precursors P'-A3 and 18S-A3 in addition to minor pathway's precursor 27SA receded. The absence of P-A3 downstream precursors at HS is coincided by complete decline of P-P1 byproducts (Figure 19). In contrast to major reductions of pre-rRNA levels, the treatment led to production of P-A2 precursors in RCC and their accumulation was slower presumably due to 35S primary transcript's processing rates. Worth mentioning, both P-A3 and P-A2 possessed comparable rates of processing upon return to favorable growth temperature (Figure 23).

6.3.2 Novel precursor formation under heat

The favorable growth temperatures drive the maturation of the initial pre-40S (P-A3) subunit along a well-described series of maturation steps wherein the 5' maturation occurs at successive cleavage sites of P' and P2, followed by the 3' maturation of A3 to A2 resulting in 20S (18S-A2) subunit. High temperature treatment causes the 5' maturation of the P site to stall resulting in lack of steady-state P-P1 fragments. Interestingly, even though P site maturation may remain stalled at 38°C, the A3 to A2 transition at the 3' terminus continues, driving the formation of unusual P-A2 like heterogeneous precursor (Figure 23, 24). Although this putative precursor was postulated before, it has not been supported by experimental evidence in wildtype or mutants (Sikorski et al., 2015). These findings suggest that P to P' cleavage is heat sensitive and that the factor controlling this step remains unknown in plants, whereas in humans, hUtp23 implicated in this step has been characterized before (Bleichert et al., 2006; Wells et al., 2017). Despite this, there was no significant production of P-A2 intermediate at elevated temperatures in Arabidopsis plants (Figure 24B), likely due to steady state levels analyzed in the plants as opposed to dynamic changes analyzed using radiolabeled pre-rRNA in suspension culture. This contrary observation may also be attributed to their tissue-specificity.

6.3.3 A path for the ITS2-first maturation schemes under heat

Given there is a global reduction of upstream precursors under high temperature; major pathway's P-A3, P'-A3 and 18S-A3 and minor pathway's 32S and common precursors 27SA, 27SB, it is significant that P-C2 derived precursors form and rise under these conditions (Figure 19B, C). A similar precursor 24S has been reported to exist in yeast mutants lacking Rrp2 and Rrp5 (Venema and Tollervey, 1996). In Arabidopsis, Rrp5 T-DNA mutation led to lethality (Missbach et al., 2013) and as such did not lead to such 24S production. In this dissertation, the non-lethal *rrp5Δ10* mutant led to similar production of 24S with strong conservation at E site rather than C2 site of ITS2 (Figure 17A, E).

An 18S and 5.8S rRNA-spanning P-C2 transcript is particularly intriguing as it would cause abnormal assembly of pre-rRNA in subunit particles after splitting. Notably after returning to normal temperatures, P-C2 is capable of maturing at a rate comparable to P-A3. The likelihood of such maturation events remains to be

uncovered since large proportion of these precursors are polyadenylated in cRT-PCR assays (Figure 20B, C). Such polyadenylation marks on pre-rRNA have been known to promote degradation of structured RNAs (Sikorski et al., 2015). Moreover, the 3' end of immature 5.8S regions are the target of such polyadenylation machinery (Shanmugam et al., 2017). Endonucleolytic machinery in human cells targets a fraction of mature ribosomal RNA that are described to be polyadenylated (Slomovic et al., 2006). Additionally, the silencing of the components of RNA decay mechanisms has resulted in specific accumulation of adenylated 28S rRNAs in human cells (Slomovic et al., 2010). In Arabidopsis mutant lacking terminal nucleotidyltransferase (*trl*), the elimination of P-P1 fragments through exonucleolytic machinery utilizes polyadenylation priming mechanisms (Sikorski et al., 2015). It is likely that HS-induced P-C2 precursors and P-P1 fragments may undergo similar routes of elimination through the Exo9 complex (Lange et al., 2011; Sikorska et al., 2017). Similar exosome mediated cleavage of non-functional 25S rRNA termed Nonfunctional RNA Decay is based on the selective ubiquitination of ribosomal proteins (Cole et al., 2009; Bassham and MacIntosh, 2017). This model is yet to be tested to determine whether ubiquitination of ribosomal proteins or other factors such as TRAMP or RRP6L-2 are needed for P-C2 degradation.

Summarily, the hypothesis regarding the function of P-C2 might suggest that C2 cleavage at elevated temperatures could act as a mechanism for degrading or disassembling ribosomes resulting from high temperature dependent growth regimes. For cells to avoid the formation of misfolded ribosomal subunits, polyadenylating RNAs (40S subunit) or altering the composition of rRNA (missing 5.8S in 60S subunits) would ensure these fast and efficient removal of pre-ribosomal particles through the existing quality control pathways. Additionally, C2 cleavage may be less susceptible to high temperature than A3 cleavage, which is already inhibited under elevated temperatures, thus resulting in the formation of aberrant P-C2 intermediates (Figure 19, 23).

6.3.4 Fine tuning the maturation schemes based on temperature

At acute growth temperature of 42°C used in this study, the downstream precursors of primary transcript were mainly undetectable due to upstream 35SA^{123}B accumulation. Besides dysfunctional 5'ETS trimming, this temperature also led to

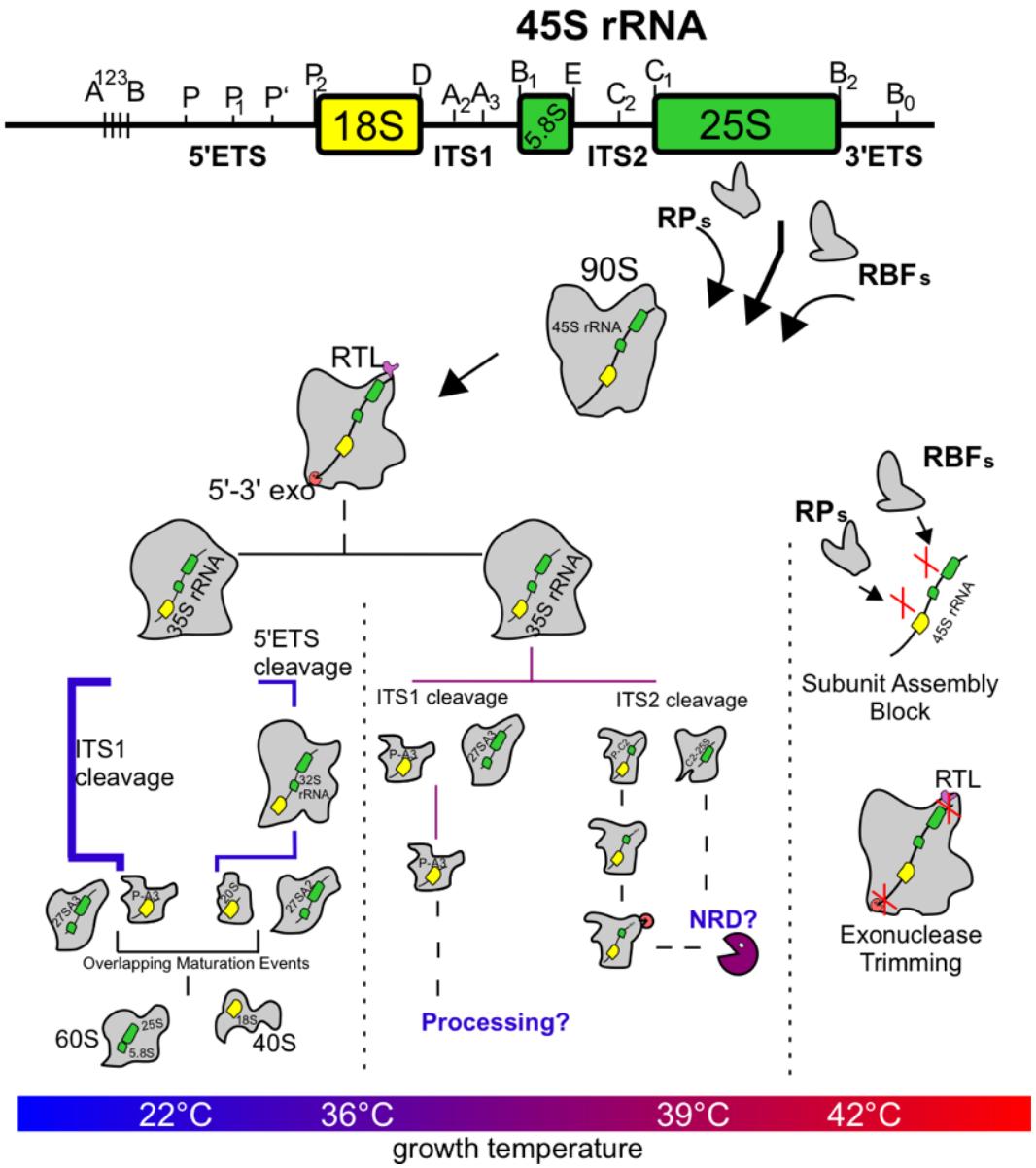

Figure 29. Pre-rRNA maturation paths controlled by temperature

The proposed model for 45S rRNA maturation through moderate to extreme growth temperatures in this study. Under control growth temperature, the 90S complex chiefly undergoes splitting and mature through major and minor path. Under moderately high temperature (36°C-40°C), the maturation scheme switches to ITS2 dependent production of precursor that in principle can lead to functional SSU and without cognate 5.8S in terms of LSU. The fate of this pre-subunit is hence marked for ribosome decay (NRD). At extreme temperature (42°C), all three maturation paths are foregone due to upstream higher order precursor maturation defects due to non-functional exonuclease trimming and possibly due to blockage in subunit assembly. Adapted from Shanmugam et al., 2021.

concurrent failure of 3'ETS trimming resulting in high levels of 35S bands with intact 3'ETS region. This cleavage unlike 5'ETS is mediated by an endonuclease, RTL2 RNase III.

Notably, these temperatures lead to maximal induction of heat shock proteins that traverses from cytoplasm to nucleus to sequester ribosome biogenesis related proteins in granular structures (Cherkasov *et al.*, 2015). Interestingly, the polysome fraction containing pre-rRNA analysis led to absence or bare minimal levels of even the major P-A3 and 27SB precursors likely due to steady state levels analyzed against the precursor levels analyzed after lysate preparation (Figure 25B).

An emerging idea that could potentially play a role in such adaptive mechanism is the phase displacement of whole transcribing pre-rRNAs from the usual fibrillarin center resulting in specialized heat stress granules under these conditions while entrapping ribosomal proteins and biogenesis factors (Frottin et al., 2019). Taken together, this and ITS2-first splitting further goes to show that Arabidopsis pre-rRNA biogenesis is tightly regulated through at least two realms of heat stress response and there may indeed be cross-over response as is the case in 39°C (Figure 29). However, in case of tomato, the formation of P-C2 precursors coincided with the simultaneous appearance 35SA^{123}B precursor through 36°C - 45°C (Figure 21A) pointing to variable schemes in heat stress responses among plant species. The level of P-C2 production in Rice is meagre at 42°C - 45°C (Figure 21B) and its further role in heat stress response remains to be thoroughly investigated owing to its significance in being a model crop plant. Taken together, there is commonality in adaptation responses among plant species in case of pre-rRNA processing with slight variations within. Comparative studies with plant crops grown among variable climatic conditions will lead to broader understanding of ways in which these pathways synchronize to alter the ribosome biogenesis.

7 REFERENCES

Abbasi, N., Kim, H.B., Park, N. il, Kim, H.S., Kim, Y.K., Park, Y. il and Choi, S.B. (2010) APUM23, a nucleolar Puf domain protein, is involved in pre-ribosomal RNA processing and normal growth patterning in Arabidopsis. *Plant Journal*, **64**, 960–976.

Abou-Ellail, M., Cooke, R. and Sáez-Vásquez, J. (2011) Variations on a team: Major and minor variants of arabidopsis thaliana rDNA genes. *Nucleus*, **2**, 294–299.

Andersen, J.S., Lam, Y.W., Leung, A.K.L., Ong, S.-E., Lyon, C.E., Lamond, A.I. and Mann, M. (2005) Nucleolar proteome dynamics. *Nature*, **433**, 77–83.

Azevedo-Favory, J., Gaspin, C., Ayadi, L., et al. (2021) Mapping rRNA 2'-O-methylations and identification of C/D snoRNAs in Arabidopsis thaliana plants. *RNA Biology*, **18**, 1760–1777.

Barrangou, R., Fremaux, C., Deveau, H., Richards, M., Boyaval, P., Moineau, S., Romero, D.A. and Horvath, P. (2007) CRISPR provides acquired resistance against viruses in prokaryotes. *Science*, **315**, 1709–1712.

Bassham, D.C. and MacIntosh, G.C. (2017) Degradation of cytosolic ribosomes by autophagy-related pathways. *Plant Science*, **262**, 169–174.

Baudin-Baillieu, A., Tollervey, D., Cullin, C. and Lacroute, F. (1997) Functional analysis of Rrp7p, an essential yeast protein involved in pre-rRNA processing and ribosome assembly. *Molecular and Cellular Biology*, **17**, 5023–5032.

Bleichert, F., Granneman, S., Osheim, Y.N., Beyer, A.L. and Baserga, S.J. (2006) The PINc domain protein Utp24, a putative nuclease, is required for the early cleavage in 18S rRNA maturation. *Proc Natl Acad Sci U S A*, **103**, 9464–9469.

Bohnsack, K.E. and Bohnsack, M.T. (2019) Uncovering the assembly pathway of human ribosomes and its emerging links to disease. *The EMBO Journal*, **38**, 1–20.

Bolotin, A., Quinquis, B., Sorokin, A. and Ehrlich, S.D. (2005) Clustered regularly interspaced short palindrome repeats (CRISPRs) have spacers of extrachromosomal origin. *Microbiology (Reading)*, **151**, 2551–2561.

Carroll, A.J., Heazlewood, J.L., Ito, J. and Millar, A.H. (2008) Analysis of the Arabidopsis cytosolic ribosome proteome provides detailed insights into its components and their post-translational modification. *Molecular and Cellular Proteomics*, **7**, 347–369.

Casanova-Sáez, R., Candela, H. and Micol, J.L. (2014) Combined haploinsufficiency and purifying selection drive retention of RPL36a paralogs in Arabidopsis. *Scientific Reports*, **4**, 1–7.

Cavanagh, P. and Garrity, A. (2014) "CRISPR Mechanism", CRISPR/Cas9. Available at: https://sites.tufts.edu/crispr/.

Cerqueira, A. v and Lemos, B. (2019) Ribosomal DNA and the Nucleolus as Keystones of Nuclear Architecture, Organization, and Function. *Trends in Genetics*, **35**, 710–723.

Chandrasekhara, C., Mohannath, G., Blevins, T., Pontvianne, F. and Pikaard, C.S. (2016) Chromosome-specific NOR inactivation explains selective rRNA gene silencing and dosage control in arabidopsis. *Genes and Development*, **30**, 177–190.

Chaturvedi, P., Ischebeck, T., Egelhofer, V., Lichtscheidl, I. and Weckwerth, W. (2013) Cell-specific analysis of the tomato pollen proteome from pollen mother cell to mature pollen provides evidence for developmental priming. *J Proteome Res*, **12**, 4892–4903.

Chen, J. and Stark, L.A. (2019) Insights into the Relationship between Nucleolar Stress and the NF-κB Pathway. *Trends Genet*, **35**, 768–780.

Chen, X., Lu, L., Qian, S., Scalf, M., Smith, L.M. and Zhong, X. (2018) Canonical and noncanonical actions of arabidopsis histone deacetylases in ribosomal RNA processing. *Plant Cell*, **30**, 134–152.

Cherkasov, V., Grousl, T., Theer, P., et al. (2015) Systemic control of protein synthesis through sequestration of translation and ribosome biogenesis factors during severe heat stress. *FEBS Letters*, **589**, 3654–3664.

Claypool, J.A., French, S.L., Johzuka, K., Eliason, K., Vu, L., Dodd, J.A., Beyer, A.L. and Nomura, M. (2003) Tor Pathway Regulates Rrn3p-dependent Recruitment of Yeast RNA Polymerase I to the Promoter but Does Not Participate in Alteration of the Number of Active Genes. *Molecular Biology of the Cell*, **15**, 946–956.

Clough, S.J. and Bent, A.F. (1998) Floral dip: A simplified method for Agrobacterium-mediated transformation of Arabidopsis thaliana. *Plant Journal*, **16**, 735–743.

Cole, S.E., LaRiviere, F.J., Merrikh, C.N. and Moore, M.J. (2009) A Convergence of rRNA and mRNA Quality Control Pathways Revealed by Mechanistic Analysis of Nonfunctional rRNA Decay. *Molecular Cell*, **34**, 440–450.

Cong, L., Ran, F.A., Cox, D., et al. (2013) Multiplex genome engineering using CRISPR/Cas systems. *Science*, **339**, 819–823.

Cottilli, P., Belda-Palazón, B., Adkar-Purushothama, C.R., Perreault, J.-P., Schleiff, E., Rodrigo, I., Ferrando, A. and Lisón, P. (2019) Citrus exocortis viroid causes ribosomal stress in tomato plants. *Nucleic Acids Res*, **47**, 8649–8661.

Deltcheva, E., Chylinski, K., Sharma, C.M., Gonzales, K., Chao, Y., Pirzada, Z.A., Eckert, M.R., Vogel, J. and Charpentier, E. (2011) CRISPR RNA maturation by trans-encoded small RNA and host factor RNase III. *Nature*, **471**, 602–607.

Devis, D., Firth, S.M., Liang, Z. and Byrne, M.E. (2015) Dosage sensitivity of RPL9 and concerted evolution of ribosomal protein genes in plants. *Frontiers in Plant Science*, **6**, 1–12.

Earley, K., Lawrence, R.J., Pontes, O., et al. (2006) Erasure of histone acetylation by Arabidopsis HDA6 mediates large-scale gene silencing in nucleolar dominance. *Genes and Development*, **20**, 1283–1293.

Fath, S., Kobor, M.S., Philippi, A., Greenblatt, J. and Tschochner, H. (2004) Dephosphorylation of RNA polymerase I by Fcp1p is required for efficient rRNA synthesis. *J Biol Chem*, **279**, 25251–25259.

Firmino, A.A.P., Gorka, M., Graf, A., Skirycz, A., Martinez-Seidel, F., Zander, K., Kopka, J. and Beine-Golovchuk, O. (2020) Separation and paired proteome profiling of plant chloroplast and cytoplasmic ribosomes. *Plants*, **9**, 1–29.

French, S.L., Osheim, Y.N., Cioci, F., Nomura, M. and Beyer, A.L. (2003) In Exponentially Growing Saccharomyces cerevisiae Cells, rRNA Synthesis Is

Determined by the Summed RNA Polymerase I Loading Rate Rather than by the Number of Active Genes. *Molecular and Cellular Biology*, **23**, 1558–1568.

Frottin, F., Schueder, F., Tiwary, S., et al. (2019) The nucleolus functions as a phase-separated protein quality control compartment. *Science (1979)*, **365**, 342–347.

Galdieri, L., Mehrotra, S., Yu, S. and Vancura, A. (2010) Transcriptional regulation in yeast during diauxic shift and stationary phase. *OMICS*, **14**, 629–638.

Ganot, P., Bortolin, M.L. and Kiss, T. (1997) Site-specific pseudouridine formation in preribosomal RNA is guided by small nucleolar RNAs. *Cell*, **89**, 799–809.

Geerlings, T.H., Vos, J.C. and Raué, H.A. (2000) The final step in the formation of 25S rRNA in Saccharomyces cerevisiae is performed by 5'-->3' exonucleases. *RNA*, **6**, 1698–1703.

Genuth, N.R. and Barna, M. (2018) The discovery of ribosome heterogeneity and its implications for gene regulation and organismal life. *Molecular Cell*, **71**, 364–374.

Ghatak, A., Chaturvedi, P., Bachmann, G., et al. (2020) Physiological and Proteomic Signatures Reveal Mechanisms of Superior Drought Resilience in Pearl Millet Compared to Wheat. *Front Plant Sci*, **11**, 600278.

Giavalisco, P., Wilson, D., Kreitler, T., Lehrach, H., Klose, J., Gobom, J. and Fucini, P. (2005) High heterogeneity within the ribosomal proteins of the Arabidopsis thaliana 80S ribosome. *Plant Molecular Biology*, **57**, 577–591.

Grandi, P., Rybin, V., Baßler, J., et al. (2002) 90S pre-ribosomes include the 35S pre-rRNA, the U3 snoRNP, and 40S subunit processing factors but predominantly lack 60S synthesis factors. *Molecular Cell*, **10**, 105–115.

Greber, B.J. (2016) Mechanistic insight into eukaryotic 60S ribosomal subunit biogenesis by cryo-electron microscopy. *Rna*, **22**, 1643–1662.

Hang, R., Liu, C., Ahmad, A., Zhang, Y., Lu, F. and Cao, X. (2014) Arabidopsis protein arginine methyltransferase 3 is required for ribosome biogenesis by affecting precursor ribosomal RNA processing. *Proc Natl Acad Sci U S A*, **111**, 16190–16195.

Hang, R., Wang, Z., Deng, X., Liu, C., Yan, B., Yang, C., Song, X., Mo, B. and Cao, X. (2018) *Ribosomal RNA Biogenesis and Its Response to Chilling Stress in Oryza sativa*,.

Held, W.A., Mizushima, S. and Nomura, M. (1973) Reconstitution of Escherichia coli 30 S ribosomal subunits from purified molecular components. *J Biol Chem*, **248**, 5720–5730.

Henras, A.K., Plisson-Chastang, C., O'Donohue, M.F., Chakraborty, A. and Gleizes, P.E. (2015) An overview of pre-ribosomal RNA processing in eukaryotes. *Wiley Interdisciplinary Reviews: RNA*, **6**, 225–242.

Hong, S.W. and Vierling, E. (2001) Hsp101 is necessary for heat tolerance but dispensable for development and germination in the absence of stress. *Plant Journal*, **27**, 25–35.

Horiguchi, G., Mollá-Morales, A., Pérez-Pérez, J.M., Kojima, K., Robles, P., Ponce, M.R., Micol, J.L. and Tsukaya, H. (2011) Differential contributions of ribosomal protein genes to arabidopsis thaliana leaf development. *Plant Journal*, **65**, 724–736.

Horn, D.M., Mason, S.L. and Karbstein, K. (2011) Rcl1 protein, a novel nuclease for 18 S ribosomal RNA production. *J Biol Chem*, **286**, 34082–34087.

Huang, C.K., Shen, Y.L., Huang, L.F., Wu, S.J., Yeh, C.H. and Lu, C.A. (2016) The DEAD-box RNA helicase AtRH7/PRH75 participates in pre-rRNA processing, plant development and cold tolerance in arabidopsis. *Plant and Cell Physiology*, **57**, 174–191.

Ito, T., Kim, G.T. and Shinozaki, K. (2000) Disruption of an Arabidopsis cytoplasmic ribosomal protein S13-homologous gene by transposon-mediated mutagenesis causes aberrant growth and development. *Plant Journal*, **22**, 257–264.

Jansen, R.P., Hurt, E.C., Kern, H., Lehtonen, H., Carmo-Fonseca, M., Lapeyre, B. and Tollervey, D. (1991) Evolutionary conservation of the human nucleolar protein fibrillarin and its functional expression in yeast. *Journal of Cell Biology*, **113**, 715–729.

Jones, H.S., Kawauchi, J., Braglia, P., Alen, C.M., Kent, N.A. and Proudfoot, N.J. (2007) RNA polymerase I in yeast transcribes dynamic nucleosomal rDNA. *Nature Structural & Molecular Biology*, **14**, 123–130.

Kannan, K., Tsvetanova, B., Chuang, R.Y., et al. (2016) One step engineering of the small-subunit ribosomal RNA using CRISPR/Cas9. *Scientific Reports*, **6**, 1–10.

Kiss-László, Z., Henry, Y., Bachellerie, J.P., Caizergues-Ferrer, M. and Kiss, T. (1996) Site-specific ribose methylation of preribosomal RNA: A novel function for small nucleolar RNAs. *Cell*, **85**, 1077–1088.

Klinge, S., Voigts-Hoffmann, F., Leibundgut, M., Arpagaus, S. and Ban, N. (2011) Crystal structure of the eukaryotic 60S ribosomal subunit in complex with initiation factor 6. *Science (1979)*, **334**, 941–948.

Kong, R., Zhang, L., Hu, L., Peng, Q., Han, W., Du, X. and Ke, Y. (2011) hALP, A Novel Transcriptional U Three Protein (t-UTP), Activates RNA Polymerase I Transcription by Binding and Acetylating the Upstream Binding Factor (UBF) *. *Journal of Biological Chemistry*, **286**, 7139–7148.

Koningsbruggen, S. van, Gierliński, M., Schofield, P., Martin, D., Barton, G.J., Ariyurek, Y., Dunnen, J.T. den and Lamond, A.I. (2010) High-resolution whole-genome sequencing reveals that specific chromatin domains from most human chromosomes associate with nucleoli. *Molecular Biology of the Cell*, **21**, 3735–3748.

Koš, M. and Tollervey, D. (2010) Yeast Pre-rRNA Processing and Modification Occur Cotranscriptionally. *Molecular Cell*, **37**, 809–820.

Kos-Braun, I.C., Jung, I. and Koš, M. (2017) Tor1 and CK2 kinases control a switch between alternative ribosome biogenesis pathways in a growth-dependent manner. *PLoS Biology*, **15**.

Kovacevic, J., Palm, D., Jooss, D., Bublak, D., Simm, S. and Schleiff, E. (2019) Co-orthologues of ribosome biogenesis factors in A. thaliana are differentially regulated by transcription factors. *Plant Cell Reports*, **38**, 937–949.

Kufel, J., Dichtl, B. and Tollervey, D. (1999) Yeast Rnt1p is required for cleavage of the pre-ribosomal RNA in the 3' ETS but not the 5' ETS. *RNA*, **5**, 909–917.

La Cruz, J. de, Karbstein, K. and Woolford, J.L. (2015) Functions of ribosomal proteins in assembly of eukaryotic ribosomes in vivo. *Annual Review of Biochemistry*, **84**, 93–129.

Lange, H., Sement, F.M. and Gagliardi, D. (2011) MTR4, a putative RNA helicase and exosome co-factor, is required for proper rRNA biogenesis and development in Arabidopsis thaliana. *Plant Journal*, **68**, 51–63.

Langmead, B. and Salzberg, S.L. (2012) Fast gapped-read alignment with Bowtie 2. *Nat Methods*, **9**, 357–359.

Larkindale, J., Hall, J.D., Knight, M.R. and Vierling, E. (2005) Heat stress phenotypes of Arabidopsis mutants implicate multiple signaling pathways in the acquisition of thermotolerance. *Plant Physiology*, **138**, 882–897.

Learned, R.M., Cordes, S. and Tjian, R. (1985) Purification and characterization of a transcription factor that confers promoter specificity to human RNA polymerase I. *Molecular and Cellular Biology*, **5**, 1358–1369.

Leitch, A.R., Mosgoller, W., Shi, M. and Heslop-Harrison, J.S. (1992) Different patterns of rDNA organization at interphase in nuclei of wheat and rye. *Journal of Cell Science*, **101**, 751–757.

Leshin, J.A., Heselpoth, R., Belew, A.T. and Dinman, J.D. (2011) High throughput structural analysis of yeast ribosomes using hSHAPE. *RNA Biology*, **8**, 478–487.

Lewicki, B.T.U., Margus, T., Remme, J. and Nierhaus, K.H. (1993) Coupling of rRNA Transcription and Ribosomal Assembly in Vivo: Formation of Active Ribosomal Subunits in Escherichia coli Requires Transcription of rRNA Genes by Host RNA Polymerase which Cannot be Replaced by Bacteriophage T7 RNA Polymerase. *Journal of Molecular Biology*, **231**, 581–593.

Li, K., Zhou, X., Sun, X., et al. (2021) Coordination between MIDASIN 1-mediated ribosome biogenesis and auxin modulates plant development. *Journal of Experimental Botany*, **72**, 2501–2513.

Lijsebettens, M. van, Block, M. de, Bauw, G., Villarroel, R. and Montagu, M. van (1994) Plant Development By. , **13**, 3378–3388.

Lillie, S.H. and Pringle, J.R. (1980) Reserve carbohydrate metabolism in Saccharomyces cerevisiae: responses to nutrient limitation. *J Bacteriol*, **143**, 1384–1394.

Lindström, M.S., Jurada, D., Bursac, S., Orsolic, I., Bartek, J. and Volarevic, S. (2018) Nucleolus as an emerging hub in maintenance of genome stability and cancer pathogenesis. *Oncogene*, **37**, 2351–2366.

Liu, C., Wu, Q., Liu, W., Gu, Z., Wang, W., Xu, P., Ma, H. and Ge, X. (2017) Poly (ADP-ribose) polymerases regulate cell division and development in Arabidopsis roots. *Journal of Integrative Plant Biology*, **59**, 459–474.

Lopez, F.B., Fort, A., Tadini, L., et al. (2021) Gene dosage compensation of rRNA transcript levels in Arabidopsis thaliana lines with reduced ribosomal gene copy number. *Plant Cell*, **33**, 1135–1150.

Lygerou, Z., Allmang, C., Tollervey, D. and Séraphin, B. (1996) Accurate processing of a eukaryotic precursor ribosomal RNA by ribonuclease MRP in vitro. *Science*, **272**, 268–270.

Maekawa, S., Ishida, T. and Yanagisawa, S. (2018) Reduced expression of APUM24, encoding a novel rRNA processing factor, induces sugar-dependent nucleolar stress and altered sugar responses in arabidopsis thaliana. *Plant Cell*, **30**, 209–227.

Mali, P., Yang, L., Esvelt, K.M., Aach, J., Guell, M., DiCarlo, J.E., Norville, J.E. and Church, G.M. (2013) RNA-guided human genome engineering via Cas9. *Science*, **339**, 823–826.

Manuelidis, L. and Borden, J. (1988) Reproducible compartmentalization of individual chromosome domains in human CNS cells revealed by in situ hybridization and three-dimensional reconstruction. *Chromosoma*, **96**, 397–410.

Marraffini, L.A. and Sontheimer, E.J. (2008) CRISPR interference limits horizontal gene transfer in staphylococci by targeting DNA. *Science*, **322**, 1843–1845.

Martinez-Seidel, F., Beine-Golovchuk, O., Hsieh, Y.C. and Kopka, J. (2020) Systematic review of plant ribosome heterogeneity and specialization. *Frontiers in Plant Science*, **11**, 1–23.

Melnikov, S., Ben-Shem, A., Garreau De Loubresse, N., Jenner, L., Yusupova, G. and Yusupov, M. (2012) One core, two shells: Bacterial and eukaryotic ribosomes. *Nature Structural and Molecular Biology*, **19**, 560–567.

Miller, O.L. and Beatty, B.R. (1969) Visualization of nucleolar genes. *Science (1979)*, **164**, 955–957.

Missbach, S., Weis, B.L., Martin, R., Simm, S., Bohnsack, M.T. and Schleiff, E. (2013) 40S Ribosome Biogenesis Co-Factors Are Essential for Gametophyte and Embryo Development. *PLoS ONE*, **8**, 1–19.

Mojica, F.J.M., Díez-Villaseñor, C., García-Martínez, J. and Soria, E. (2005) Intervening sequences of regularly spaced prokaryotic repeats derive from foreign genetic elements. *J Mol Evol*, **60**, 174–182.

Mullineux, S.T. and Lafontaine, D.L.J. (2012) Mapping the cleavage sites on mammalian pre-rRNAs: Where do we stand? *Biochimie*, **94**, 1521–1532.

Nissan, T.A., Baßler, J., Petfalski, E., Tollervey, D. and Hurt, E. (2002) 60S pre-ribosome formation viewed from assembly in the nucleolus until export to the cytoplasm. *The EMBO Journal*, **21**, 5539–5547.

Nissen, P., Hansen, J., Ban, N., Moore, P.B. and Steitz, T.A. (2000) The Structural Basis of Ribosome Activity in Peptide Bond Synthesis. *Science (1979)*, **289**, 920–930.

Nomura, M. (1973) Assembly of Bacterial Ribosomes. *Science (1979)*, **179**, 864–873.

Norris, K., Hopes, T. and Aspden, J.L. (2021) Ribosome heterogeneity and specialization in development. *Wiley Interdisciplinary Reviews: RNA*, **12**, 1–23.

Nover, L., Munsche, D., Neumann, D., Ohme, K. and Scharf, K. -D (1986) Control of ribosome biosynthesis in plant cell cultures under heat-shock conditions: Ribosomal RNA. *European Journal of Biochemistry*, **160**, 297–304.

Nürenberg-Goloub, E. and Tampé, R. (2019) Ribosome recycling in mRNA translation, quality control, and homeostasis. *Biological Chemistry*.

O'Brien, C.A. and Wolin, S.L. (1994) A possible role for the 60-kD Ro autoantigen in a discard pathway for defective 5S rRNA precursors. *Genes and Development*, **8**, 2891–2903.

Oeffinger, M., Zenklusen, D., Ferguson, A., Wei, K.E., Hage, A. el, Tollervey, D., Chait, B.T., Singer, R.H. and Rout, M.P. (2009) Rrp17p is a eukaryotic exonuclease required for 5' end processing of Pre-60S ribosomal RNA. *Mol Cell*, **36**, 768–781.

Palm, D. (2017) *Identification and characterization of ribosome biogenesis factors in plants*. Goethe Universität Frankfurt am Main.

Palm, D., Streit, D., Shanmugam, T., Weis, B.L., Ruprecht, M., Simm, S. and Schleiff, E. (2019) Plant-specific ribosome biogenesis factors in Arabidopsis thaliana with essential function in rRNA processing. *Nucleic Acids Research*, **47**, 1880–1895.

Paoletti, A.C., Parmely, T.J., Tomomori-Sato, C., Sato, S., Zhu, D., Conaway, R.C., Conaway, J.W., Florens, L. and Washburn, M.P. (2006) Quantitative proteomic analysis of distinct mammalian Mediator complexes using normalized spectral abundance factors. *Proc Natl Acad Sci U S A*, **103**, 18928–18933.

Philippi, A., Steinbauer, R., Reiter, A., Fath, S., Leger-Silvestre, I., Milkereit, P., Griesenbeck, J. and Tschochner, H. (2010) TOR-dependent reduction in the expression level of Rrn3p lowers the activity of the yeast RNA Pol I machinery, but does not account for the strong inhibition of rRNA production. *Nucleic Acids Res*, **38**, 5315–5326.

Picart-Picolo, A., Grob, S., Picault, N., et al. (2020) Large tandem duplications affect gene expression, 3D organization, and plant-pathogen response. *Genome Research*, **30**, 1583–1592.

Pontvianne, F., Abou-Ellail, M., Douet, J., et al. (2010) Nucleolin is required for DNA methylation state and the expression of rRNA gene variants in Arabidopsis thaliana. *PLoS Genetics*, **6**, 1–13.

Pontvianne, F., Carpentier, M.C., Durut, N., et al. (2016) Identification of Nucleolus-Associated Chromatin Domains Reveals a Role for the Nucleolus in 3D Organization of the A. thaliana Genome. *Cell Reports*, **16**, 1574–1587.

Röhl, R. and Nierhaus, K.H. (1982) Assembly map of the large subunit (50S) of Escherichia coli ribosomes. *Proc Natl Acad Sci U S A*, **79**, 729–733.

Rosado, A., Li, R., Ven, W. van de, Hsu, E. and Raikhel, N. v. (2012) Arabidopsis ribosomal proteins control developmental programs through translational regulation of auxin response factors. *Proc Natl Acad Sci U S A*, **109**, 19537–19544.

Rosado, A., Sohn, E.J., Drakakaki, G., Pan, S., Swidergal, A., Xiong, Y., Kang, B.H., Bressan, R.A. and Raikhela, N. v. (2010) Auxin-mediated ribosomal biogenesis regulates vacuolar trafficking in Arabidopsis. *Plant Cell*, **22**, 143–158.

Sambrook, J. and Russell, D.W. (2001) *Molecular Cloning: A Laboratory Manual*, Cold Spring Harbor Press.

Sanchez, J.C., Ollodart, A., Large, C.R.L., et al. (2019) Phenotypic and genotypic consequences of CRISPR/ Cas9 editing of the replication origins in the rDNA of saccharomyces cerevisiae. *Genetics*, **213**, 229–249.

Schindelin, J., Arganda-Carreras, I., Frise, E., et al. (2012) Fiji: An open-source platform for biological-image analysis. *Nature Methods*, **9**, 676–682.

Schneider, D.A., Michel, A., Sikes, M.L., Vu, L., Dodd, J.A., Salgia, S., Osheim, Y.N., Beyer, A.L. and Nomura, M. (2007) Transcription Elongation by RNA Polymerase I Is Linked to Efficient rRNA Processing and Ribosome Assembly. *Molecular Cell*, **26**, 217–229.

Schroll, F. (2019) *rRNA biogenese Modifikation durch schaltbare RNAs*. Goethe Universität-Frankfurt am Main.

Shanmugam, T., Abbasi, N., Kim, H.S., et al. (2017) An Arabidopsis divergent pumilio protein, APUM24, is essential for embryogenesis and required for faithful pre-rRNA processing. *Plant Journal*, **92**, 1092–1105.

Shanmugam, T., Streit, D., Schroll, F., Kovacevic, J. and Schleiff, E. (2021) Dynamics and thermal sensitivity of rRNA maturation paths in plants. *Journal of Experimental Botany*, **72**, 7626–7644.

Sikorska, N., Zuber, H., Gobert, A., Lange, H. and Gagliardi, D. (2017) RNA degradation by the plant RNA exosome involves both phosphorolytic and hydrolytic activities. *Nature Communications*, **8**, 2162.

Sikorski, P.J., Zuber, H., Philippe, L., Sement, F.M., Canaday, J., Kufel, J., Gagliardi, D. and Lange, H. (2015) Distinct 18S rRNA precursors are targets of the exosome complex, the exoribonuclease RRP6L2 and the terminal nucleotidyltransferase TRL in Arabidopsis thaliana. *Plant Journal*, **83**, 991–1004.

Sims, J., Sestini, G., Elgert, C., Haeseler, A. von and Schlögelhofer, P. (2021) Sequencing of the Arabidopsis NOR2 reveals its distinct organization and tissue-specific rRNA ribosomal variants. *Nature Communications*, **12**, 1–13.

Sloan, K.E., Mattijssen, S., Lebaron, S., Tollervey, D., Pruijn, G.J.M. and Watkins, N.J. (2013) Both endonucleolytic and exonucleolytic cleavage mediate ITS1 removal during human ribosomal RNA processing. *Journal of Cell Biology*, **200**, 577–588.

Sloan, K.E., Warda, A.S., Sharma, S., Entian, K.D., Lafontaine, D.L.J. and Bohnsack, M.T. (2017) Tuning the ribosome: The influence of rRNA modification on eukaryotic ribosome biogenesis and function. *RNA Biology*, **14**, 1138–1152.

Slomovic, S., Fremder, E., Staals, R.H.G., Pruijn, G.J.M. and Schuster, G. (2010) Addition of poly(A) and poly(A)-rich tails during RNA degradation in the cytoplasm of human cells. *Proc Natl Acad Sci U S A*, **107**, 7407–7412.

Slomovic, S., Laufer, D., Geiger, D. and Schuster, G. (2006) Polyadenylation of ribosomal RNA in human cells. *Nucleic Acids Research*, **34**, 2966–2975.

Sluis, M. van and McStay, B. (2019) Nucleolar DNA Double-Strand Break Responses Underpinning rDNA Genomic Stability. *Trends in Genetics*, **35**, 743–753.

Streit, D. and Schleiff, E. (2021) The Arabidopsis 2′-O-Ribose-Methylation and Pseudouridylation Landscape of rRNA in Comparison to Human and Yeast. *Frontiers in Plant Science*, **12**, 1–19.

Streit, D., Shanmugam, T., Garbelyanski, A., Simm, S. and Schleiff, E. (2020) The existence and localization of nuclear snoRNAs in arabidopsis thaliana revisited. *Plants*, **9**, 1–18.

Sun, L., Xu, Y., Bai, S., et al. (2019) Transcriptome-wide analysis of pseudouridylation of mRNA and non-coding RNAs in Arabidopsis. *Journal of Experimental Botany*, **70**, 5089–5600.

Tomecki, R., Sikorski, P.J. and Zakrzewska-Placzek, M. (2017) Comparison of preribosomal RNA processing pathways in yeast, plant and human cells – focus on coordinated action of endo- and exoribonucleases. *FEBS Letters*, **591**, 1801–1850.

Urban, J., Soulard, A., Huber, A., et al. (2007) Sch9 is a major target of TORC1 in Saccharomyces cerevisiae. *Mol Cell*, **26**, 663–674.

Veith, T., Martin, R., Wurm, J.P., et al. (2012) Structural and functional analysis of the archaeal endonuclease Nob1. *Nucleic Acids Res*, **40**, 3259–3274.

Venema, J. and Tollervey, D. (1996) RRP5 is required for formation of both 18S and 5.8S rRNA in yeast. *EMBO Journal*, **15**, 5701–5714.

Wang, R., Zhao, J., Jia, M., et al. (2018) Balance between cytosolic and chloroplast translation affects leaf variegation. *Plant Physiology*, **176**, 804–818.

Warner, J.R. (1999) The economics of ribosome biosynthesis in yeast. *Trends in Biochemical Sciences*, **24**, 437–440.

Weber, E., Engler, C., Gruetzner, R., Werner, S. and Marillonnet, S. (2011) A modular cloning system for standardized assembly of multigene constructs. *PLoS ONE*, **6**.

Weis, B.L. (2015) *Pre-rRNA processing in A . thaliana and the role of 60S ribosome biogenesis factors.* Goethe Universität Frankfurt am Main.

Weis, B.L., Kovacevic, J., Missbach, S. and Schleiff, E. (2015) Plant-Specific Features of Ribosome Biogenesis. *Trends in Plant Science*, **20**, 729–740.

Weis, B.L., Missbach, S., Marzi, J., Bohnsack, M.T. and Schleiff, E. (2014) The 60S associated ribosome biogenesis factor LSG1-2 is required for 40S maturation in Arabidopsis thaliana. *Plant Journal*, **80**, 1043–1056.

Weis, B.L., Palm, D., Missbach, S., Bohnsack, M.T. and Schleiff, E. (2015) atBRX1-1 and atBRX1-2 are involved in an alternative rRNA processing pathway in Arabidopsis thaliana. *Rna*, **21**, 415–425.

Wells, G.R., Weichmann, F., Sloan, K.E., Colvin, D., Watkins, N.J. and Schneider, C. (2017) The ribosome biogenesis factor yUtp23/hUTP23 coordinates key interactions in the yeast and human pre-40S particle and hUTP23 contains an essential PIN domain. *Nucleic Acids Research*, **45**, 4796–4809.

Werner-Washburne, M., Braun, E., Johnston, G.C. and Singer, R.A. (1993) Stationary phase in the yeast Saccharomyces cerevisiae. *Microbiol Rev*, **57**, 383–401.

Wilm, A., Aw, P.P.K., Bertrand, D., et al. (2012) LoFreq: a sequence-quality aware, ultra-sensitive variant caller for uncovering cell-population heterogeneity from high-throughput sequencing datasets. *Nucleic Acids Res*, **40**, 11189–11201.

Wilson, D.N. and Nierhaus, K.H. (2007) The Weird and Wonderful World of Bacterial Ribosome Regulation. *Critical Reviews in Biochemistry and Molecular Biology*, **42**, 187–219.

Wittner, M., Hamperl, S., Stöckl, U., Seufert, W., Tschochner, H., Milkereit, P. and Griesenbeck, J. (2011) Establishment and maintenance of alternative chromatin states at a multicopy gene locus. *Cell*, **145**, 543–554.

Woolford, J.L. and Baserga, S.J. (2013) Ribosome biogenesis in the yeast Saccharomyces cerevisiae. *Genetics*, **195**, 643–681.

Wu, S., Wang, Y., Wang, J., Li, X., Li, J. and Ye, K. (2021) Profiling of RNA ribose methylation in Arabidopsis thaliana. *Nucleic Acids Research*, **49**, 4104–4119.

Xue, S. and Barna, M. (2012) Specialized ribosomes: A new frontier in gene regulation and organismal biology. *Nature Reviews Molecular Cell Biology*, **13**, 355–369.

Yusupova, G. and Yusupov, M. (2017) Crystal structure of eukaryotic ribosome and its complexes with inhibitors. *Philosophical Transactions of the Royal Society B: Biological Sciences*, **372**.

Zakrzewska-Placzek, M., Souret, F.F., Sobczyk, G.J., Green, P.J. and Kufel, J. (2010) Arabidopsis thaliana XRN2 is required for primary cleavage in the pre-ribosomal RNA. *Nucleic Acids Research*, **38**, 4487–4502.

Zanchin, N.I., Roberts, P., DeSilva, A., Sherman, F. and Goldfarb, D.S. (1997) Saccharomyces cerevisiae Nip7p is required for efficient 60S ribosome subunit biogenesis. *Molecular and Cellular Biology*, **17**, 5001–5015.

Zhang, L., Liu, X., Gaikwad, K., et al. (2017) Mutations in eIF5b confer thermosensitive and pleiotropic phenotypes via translation defects in Arabidopsis thaliana. *Plant Cell*, **29**, 1952–1969.

Zhang, S., Ghatak, A., Bazargani, M.M., Bajaj, P., Varshney, R.K., Chaturvedi, P., Jiang, D. and Weckwerth, W. (2021) Spatial distribution of proteins and metabolites in developing wheat grain and their differential regulatory response during the grain filling process. *Plant J*, **107**, 669–687.

Zhang, Y., Malzahn, A.A., Sretenovic, S. and Qi, Y. (2019) The emerging and uncultivated potential of CRISPR technology in plant science. *Nature Plants*, **5**, 778–794.

Zhou, X., Liao, W.J., Liao, J.M., Liao, P. and Lu, H. (2015) Ribosomal proteins: Functions beyond the ribosome. *Journal of Molecular Cell Biology*, **7**, 92–104.

Zhu, X., Xu, Y., Yu, S., et al. (2014) An efficient genotyping method for genome-modified animals and human cells generated with CRISPR/Cas9 system. *Scientific Reports*, **4**, 1–8.

Zorbas, C., Nicolas, E., Wacheul, L., Huvelle, E., Heurgué-Hamard, V. and Lafontaine, D.L.J. (2015) The human 18S rRNA base methyltransferases DIMT1L and WBSCR22-TRMT112 but not rRNA modification are required for ribosome biogenesis. *Molecular Biology of the Cell*, **26**, 2080–2095.

Zsögön, A., Szakonyi, D., Shi, X. and Byrne, M.E. (2014) Ribosomal protein RPL27a promotes female gametophyte development in a dose-dependent manner. *Plant Physiology*, **165**, 1133–1143.

8. APPENDIX

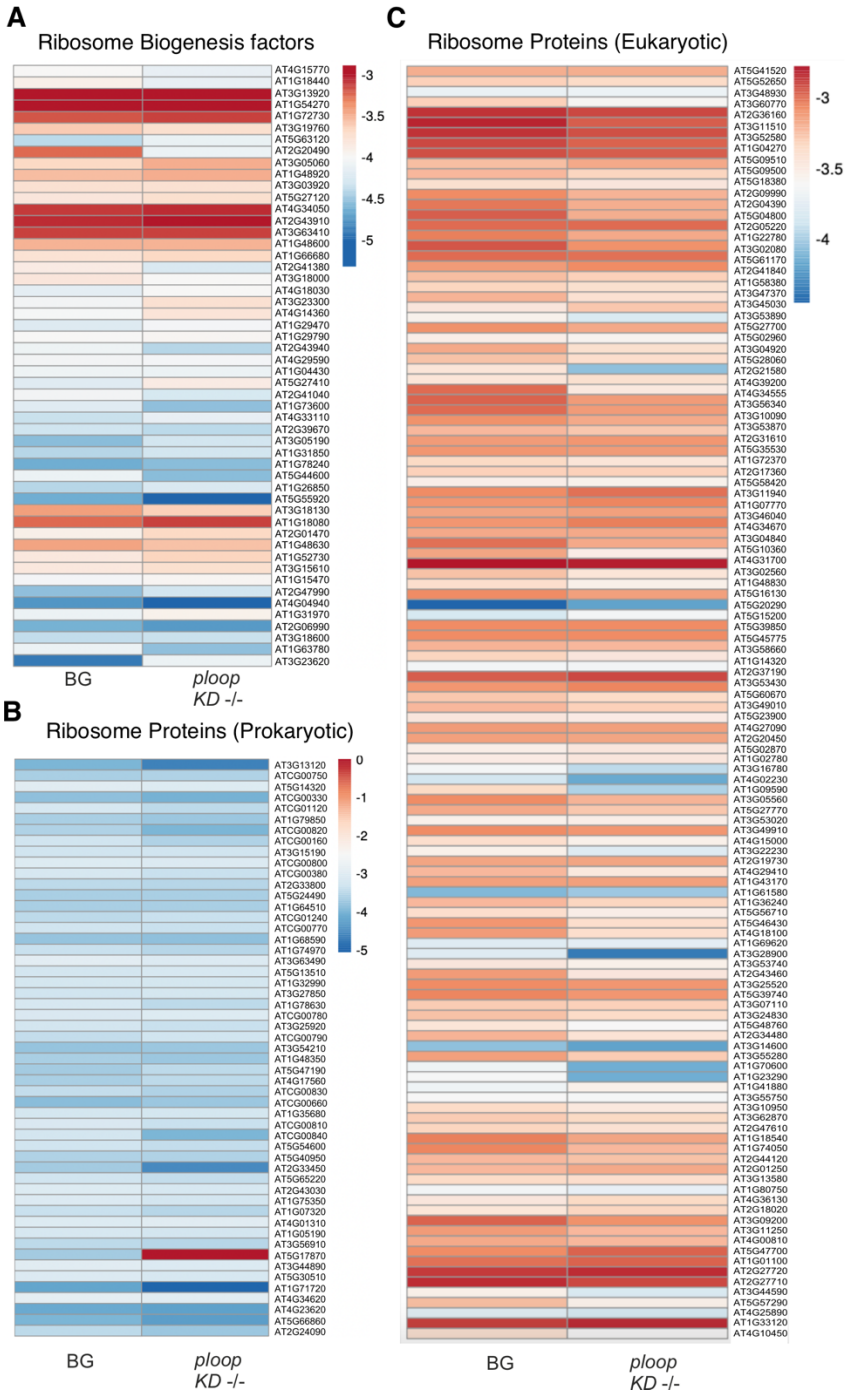

Appendix Figure 1. Differential abundance of proteins measured in mass-spectrometric analysis of BG and *ploop KD* -/- mutants denoted by their respective heat maps in gene ontological category of ribosome biogenesis-related (**A**), prokaryotic origin ribosomal proteins (**B**) and eukaryotic origin ribosomal proteins (**C**). Colors in all panels allude to relative increase (red) or decrease (blue).

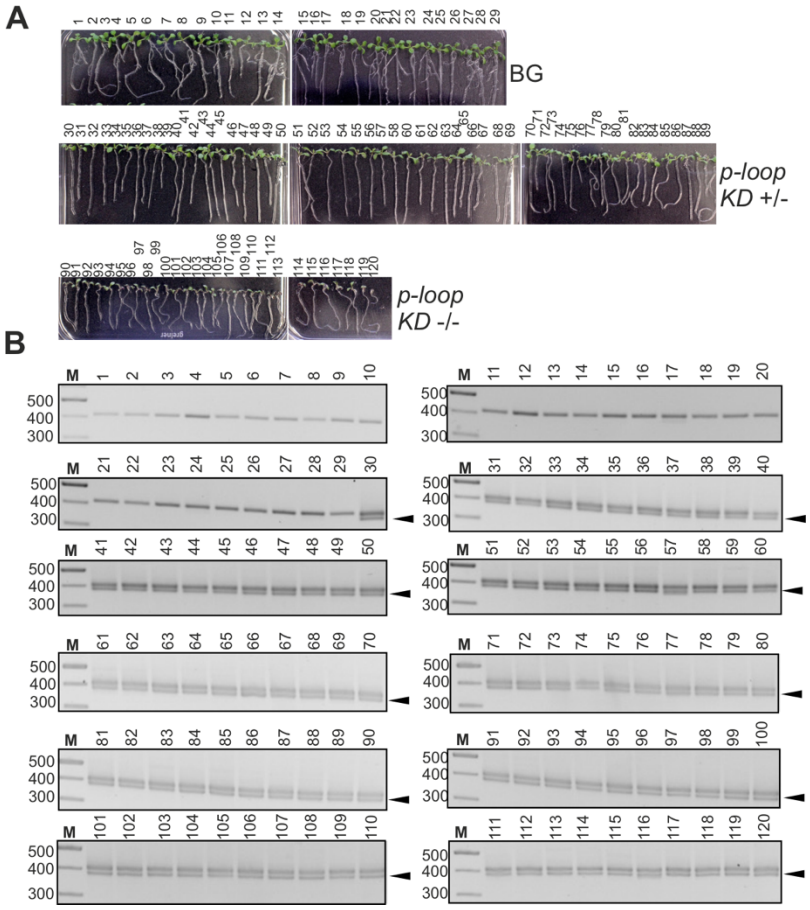

Appendix Figure 2. Phenotypic segregation analysis and mutational allele determination on 120 *ploop KD* +/- progeny plantlets. **A.** The randomized 120 progenies segregated phenotypically in 1:2:1 ratio as BG, KD +/- and KD -/- like seedlings. **B.** PCR conducted on genomic DNA of panel A seedlings with mutation-specific forward and 25S specific reverse oligonucleotide PCR and the amplicons resolved on 2.5% TTE gel. Note the absence of mutational band on BG progenies.

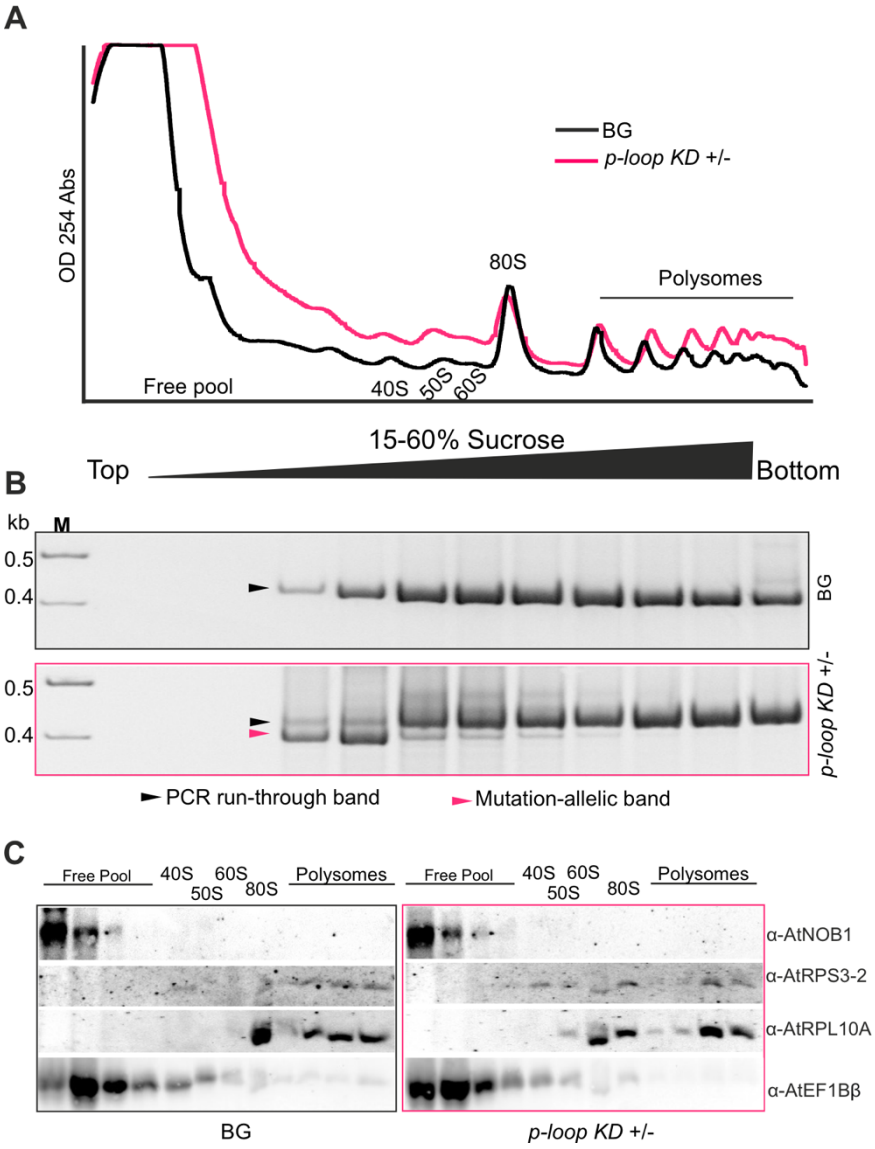

Appendix Figure 3. Analysis of mutational copies distribution in ribosomal complexes of BG and *ploop KD* +/- mutant silique tissues. **A.** Absorbance profile at 254 nm of silique tissues from BG (black line) and *ploop KD* +/- (magenta line) plotted with time of detection from top to bottom subsequent to sucrose-density gradient centrifugation. **B.** The RNA from the according fractions at panel A of both genotypes purified, reverse transcribed with 25S rRNA-specific oligo and the PCR products with mutation specific forward oligo and 25S-specific reverse oligo resolved in 12% Native PAGE gel. The black arrow denotes PCR-run through product and the magenta arrow indicates mutated rRNA product. **C.** The protein from the fractions at panel A of both genotypes were resolved on 10% SDS-PAGE and blotted with indicated antibodies.

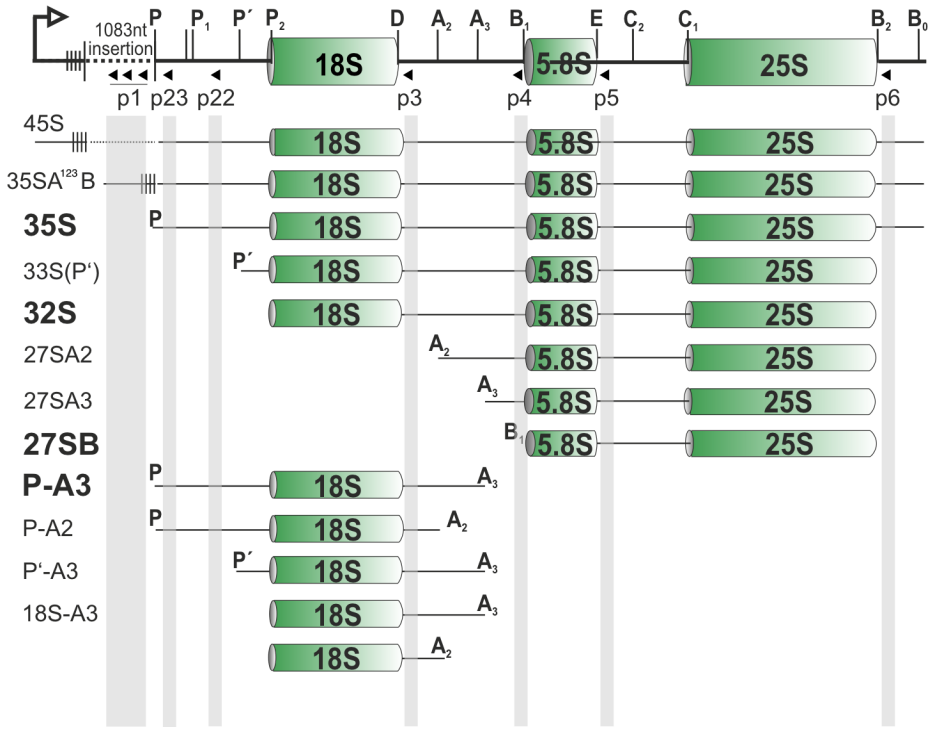

Appendix Figure 4. Arabidopsis high molecular weight precursor rRNAs identified so far in wildtype control growth and mutant conditions. The complementary oligos (p1, p23, p22, p3, p4, p5, and p6) are the probes used in this study and the corresponding precursors detected are inferred here by vertical grey bars. Adapted from Shanmugam et al., 2021.

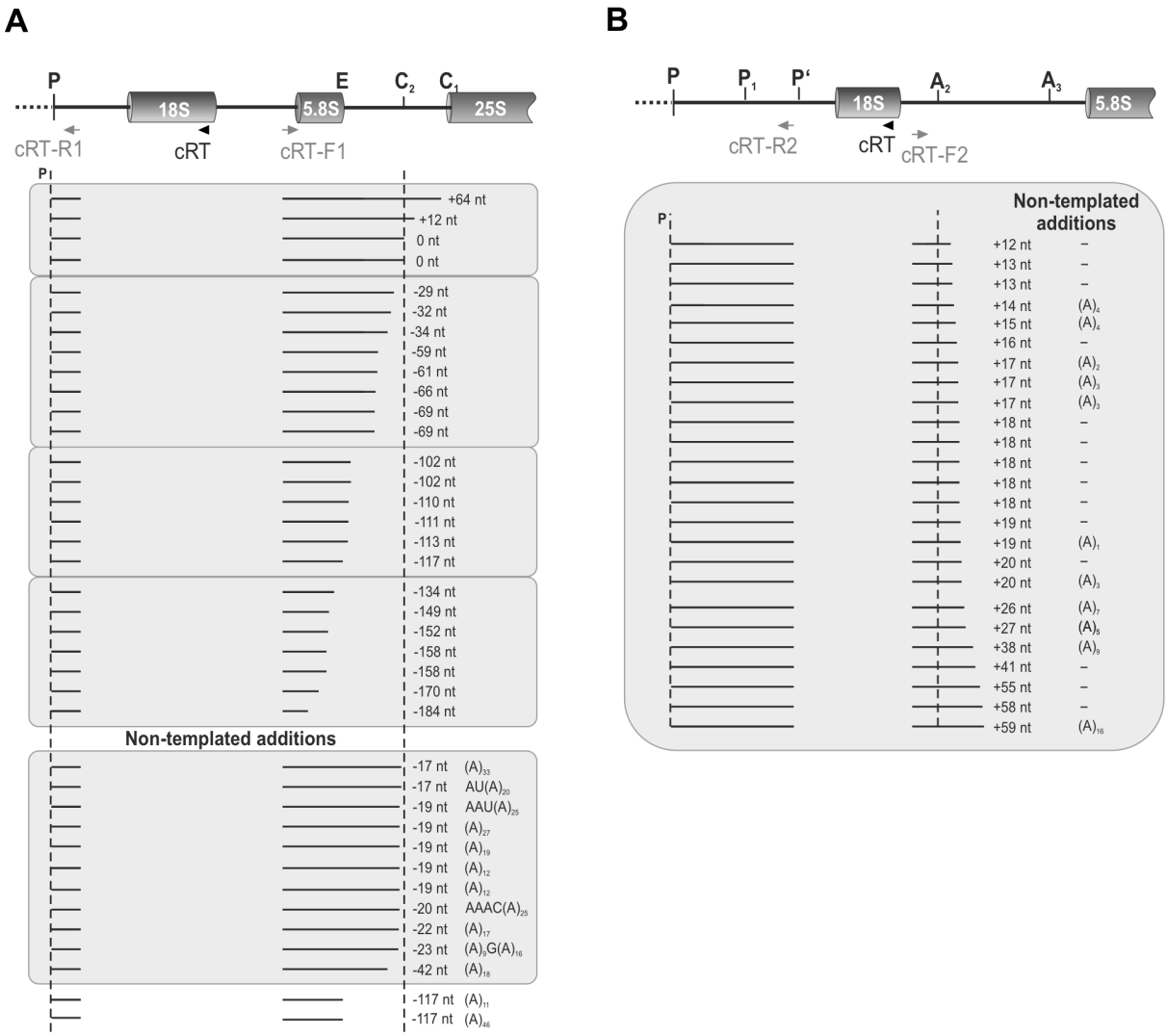

Appendix Figure 5. The precise summary of heterogeneous ends of cRT-PCR assays conducted on Figure 20 (**A**) and Figure 24 (**B**) using the indicated oligos. The non-templated additions are given below in **A** and, to the right in **B**. Adapted from Shanmugam et al., 2021.

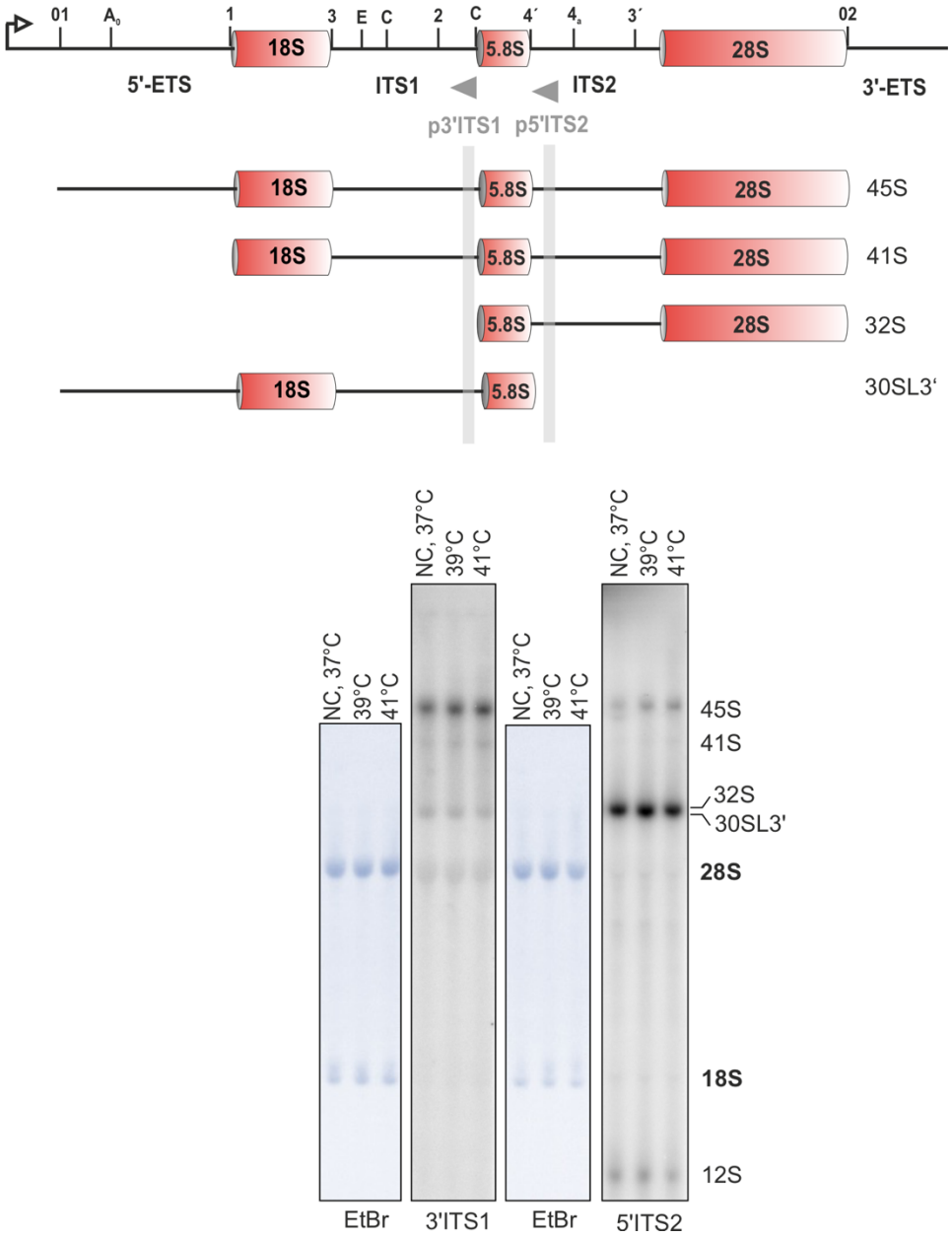

Appendix Figure 6. Heat stress assays performed on HeLa cell lines. The coding region of primary transcript rRNA with the conserved sites are indicated. p3'ITS1 and p5'ITS2 (Sloan et al) are the probes used for the northern hybridization with purified RNAs from non-treated control, NC; and temperature stressed cells (39°C and 41°C) for 3 h duration. (Courtesy: Dr. Frank McNicoll, GU-Frankfurt

PUBLICATIONS

Part of thesis is published as follows:

Shanmugam T, Streit D, Schroll F, Kovacevic J, Schleiff E. (2021) Dynamics and thermal sensitivity of rRNA maturation paths in plants. *J. Exp. Bot*. 72(21):7626-7644

Palm D, Streit D, **Shanmugam T**, Weis BL, Ruprecht M, Simm S, Schleiff E. (2019) Plant-specific ribosome biogenesis factors in Arabidopsis thaliana with essential functions in rRNA processing. *Nuc. Acids. Res*. 47(4):1880-1895

Part of thesis in preparation:

Shanmugam T, Chaturvedi P, Streit D, Ghatak A, Bergelt T, Simm S, Weckwerth W, Schleiff E. (2022) Low dose ribosomal DNA P-loop mutation affects development and enforces autophagy in Arabidopsis.

Other publications:

Streit D, **Shanmugam T**, Garbelyanski A, Simm S, Schleiff E. (2020) The existence and localization of nucleolar snoRNAs in Arabidopsis thaliana revisited. *Plants*. 9, 1016

ERKLÄRUNG

Ich erkläre hiermit, dass ich mich bisher keiner Doktorprüfung unterzogen habe.

Frankfurt am Main, den ....

EIDESSTATTLICHE VERSICHERUNG

Ich erkläre hiermit an Eides Statt, dass ich die vorgelegte Dissertation über

"Mutational analysis of ribosomal DNA and maturation-scheme analysis of ribosomal RNA in *A. thaliana*"

selbständig angefertigt und mich anderer Hilfsmittel als der in ihr angegebenen nicht bedient habe, insbesondere, dass alle Entlehnungen aus anderen Schriften mit Angabe der betreffenden Schrift gekennzeichnet sind.

Ich versichere, die Grundsätze der guten wissenschaftlichen Praxis beachtet, und nicht die Hilfe einer kommerziellen Promotionsvermittlung in Anspruch genommen zu haben.

Frankfurt am Main, den ....